INSTITUTE of
HYDROLOGY

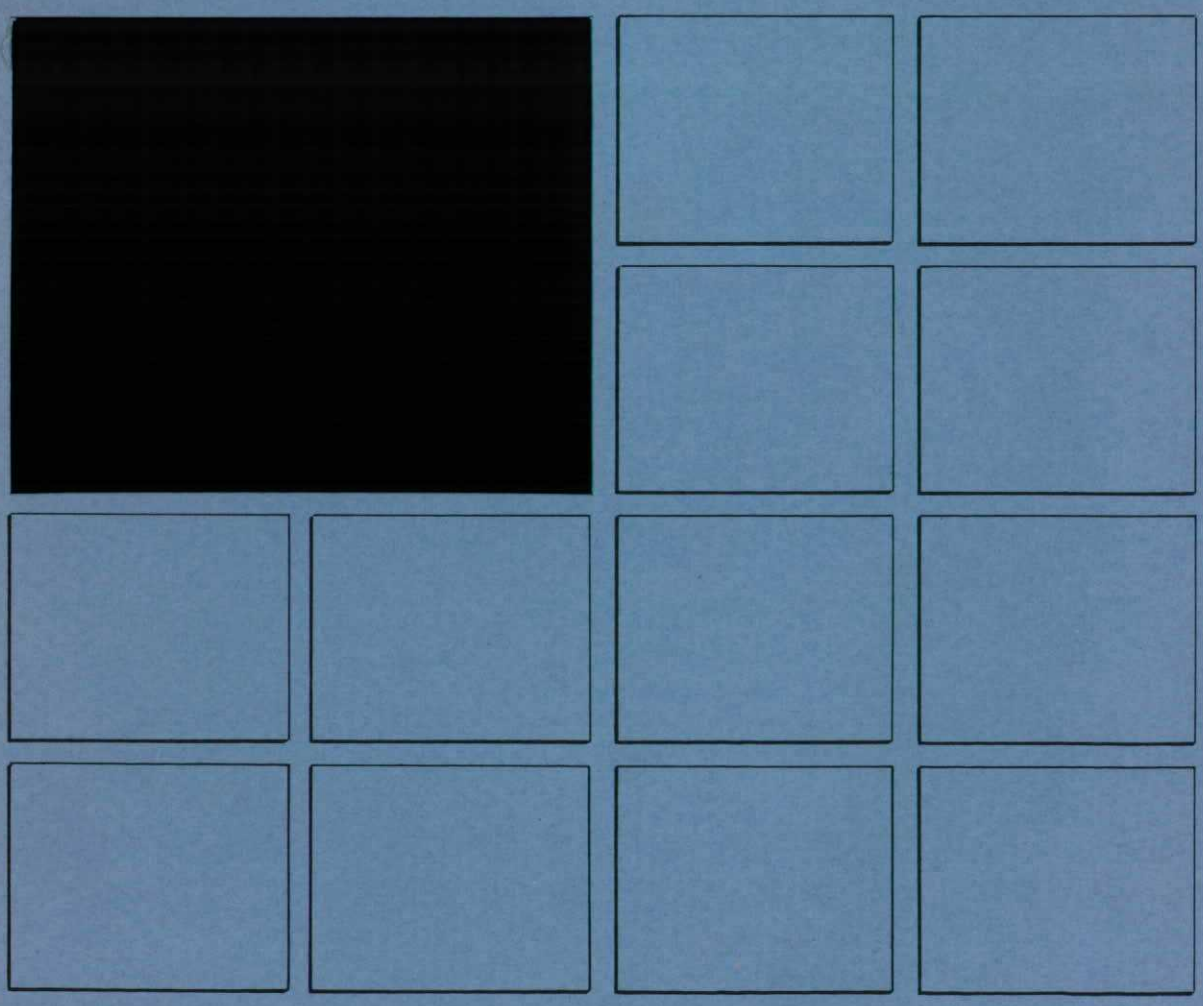

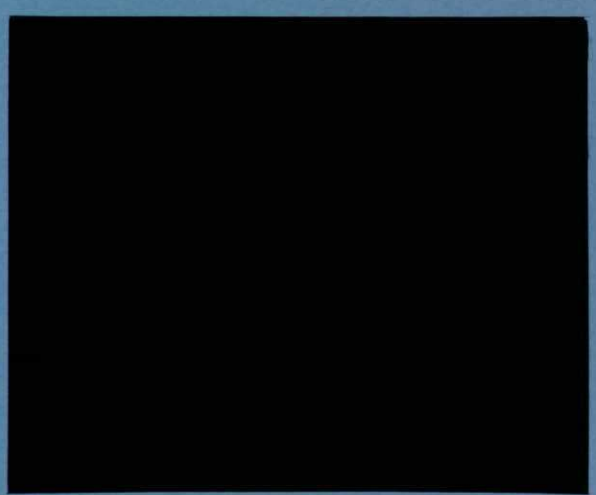

MEASUREMENT AND PREDICTION OF ACTUAL EVAPORATION FROM SPARSE DRYLAND CROPS.

An interim report on Phase I of ODA project 149.

J.S. Wallace, *et. al.*

Evaporation from Sparse Dryland Crops

How much water moves out of the soil, up through vegetation and back into the atmosphere is a key question for plant physiologists interested in crop production, since crop water use is closely linked with yield.

In arid parts of the world where water is a major limiting factor in expanding agricultural productivity, finding the answer can be crucial.

The Institute of Hydrology (IH) has recently started a project to study the detailed processes of evaporation from sparse dryland barley crops, typical of those grown in many low rainfall areas of Africa and the Middle East. In this type of vegetation much of the rainfall is 'lost' as direct evaporation from the soil and conventional methods of calculating crop water use are often very inaccurate. The principal aim of the study is to make detailed measurements of plant, soil and total evaporation and to use these to develop models which will give more accurate predictions of sparse crop evaporation.

A pair of solar-powered automatic weather stations continuously record sunshine, temperature, humidity, windspeed and rainfall.

Evaporation from barley plants is measured using a porometer. This only gives part of the total crop water use since water also evaporates from the soil between the rows.

The 'HYDRA', a new instrument developed at the Institute of Hydrology, U.K., which directly measures the total evaporation from the barley crop. The device works by making high frequency measurements of the amount of water vapour moving away from the crop.

The project is in Syria at the ICARDA research station (International Center for Agricultural Research in the Dry Areas) near Aleppo where experiments on crop productivity should benefit from the precise and frequent measurements of evaporation rate that the study can provide.

One of the main instruments used is the Institute of Hydrology's new evaporation measuring device called the 'Hydra' The instrument is composed of a sonic anemometer, a new electronic instrument that measures vertical wind speeds very rapidly, and an infra-red hygrometer, which measures humidity in the air with a beam of infra-red light. The third component, a thermocouple, gauges fluctuations in air temperature. These sensors are linked to a microprocessor to analyse the measurements as they are made. One feature which is very important for environmental research is the ability to run under battery power - very attractive for both hydrological and agricultural research applications.

Testing the Hydra's direct measurement of evaporation in Syria is only part of the joint study between ICARDA and IH. A second goal is to predict evaporation. Weather data, recorded hourly using an automatic weather station, will be fed into an equation which breaks down evaporation into its components. Water loss from the plants and soil can then be predicted more exactly, since the equation includes a value for soil 'resistance' to evaporation and a value representing the degree to which plant stomata hamper evaporation. A model which quantifies the amounts of water used by the plants and lost as soil evaporation should be a useful tool in helping to assess different crop management practices which attempt to make more efficient use of the limited soil water supply.

Institute of Hydrology Wallingford Oxfordshire OX10 8BB UK
Telephone Wallingford (STD 0491) 38800 Telegrams Hycycle Wallingford Telex 849365 Hydrol G

The Institute of Hydrology is a component establishment of the Natural Environment Research Council

Interim report on Phase I of ODA project 149:-

"MEASUREMENT AND PREDICTION OF ACTUAL EVAPORATION FROM SPARSE DRYLAND CROPS"

by

J.S. Wallace, W.J. Shuttleworth, J.H.C. Gash, C.J. Moore, H.R. Oliver, S.A. Oliver

Institute of Hydrology, Wallingford, Oxon, U.K.

J.D.H. Keatinge, M. Salem, H. Jokhadar and N. Chapanian

International Centre for Agricultural Research in the Dry Areas (ICARDA), P.O. Box 5466, Aleppo, Syria

Report No. OD149/1, January 1985.

Institute of Hydrology
Maclean Building
Crowmarsh Gifford
Wallingford
Oxon
OX10 8BB

CONTENTS

ACKNOWLEDGEMENTS

We would like to acknowledge the financial support of the Overseas Development Administration. A great many of the staff of our collaborative Institute, ICARDA, have assisted in the establishment of the work; these include the Director General Dr M A Nour, the Deptuy Director General, Dr P Goldsworthy, the Farming Systems Programs Leader, Dr P. Cooper and many of the assistant staff of the Farming Systems Program. At the Institute of Hydrology, Steve Edwards and Kevin Black have contributed greatly to the development of the automatic data recording systems and the associated microcomputer software. We are pleased to have the opportunity to thank all the staff of ICARDA and the Institute of Hydrology who have contributed to the project during its first year.

2. SUMMARY

This study was set up to improve our understanding of the detailed processes of evaporation from sparse dryland crops; an area where there is considerable uncertainty about the applicability of conventional evaporation formulae. The overall approach is to make detailed measurements of plant, soil and total evaporation in sparse dryland crops and to use these measurements to develop models which can predict evaporation from these types of vegetation. This report describes the first phase of the project which had the objectives of installing the equipment at the experimental site at ICARDA in Northern Syria, obtaining preliminary results from each experimental system and the formulation of a theoretical description of evaporation from sparse crops.

During the first season measurements were made in a barley crop which, because of below average rainfall, only achieved a maximum ground cover of ca 50%, thereby providing an excellent substrate to test our experimental techniques. Total crop evaporation was measured using a neutron probe and results compared with the more detailed (hourly) values obtained using an eddy correlation device (the 'Hydra'). The Hydra results were found to be in error (ca. 30% too low) towards the end of the crop season. These errors in the Hydra data were shown (theoreticaly) to be attributable to temperature drifts in the humidity and vertical windspeed sensors and also to high frequency flux losses. The discovery of these faults in the Hydra were very timely as the instrument is currently undergoing a comprehensive redesign prior to commercialization. The next phase of the project will contain a rigorous testing program for the new Hydra to see if the redevelopments have been successful.

Direct measurements of leaf stomatal conductance, made using a porometer, and subsequent calculations of transpiration gave results which were consistent with the high degree of water stress. Afternoon leaf conductances were very low (< 2 mm s^{-1}), however, the conductance of the ear was much higher ($3 - 4$ mm s^{-1}), suggesting that the stomata in the ear were kept preferentially open, possibly to maintain photosynthesis and the development of the grains. More measurements of stomatal conductance are required at different stages of the crop season, to further examine the relationships between crop conductance and weather and soil variables.

Soil evaporation was measured directly, using a small lysimeter, after harvest. Preliminary results showed good agreement with evaporation measured using the neutron probe, over a period of up to 6 days. It seems feasible that this method can therefore be used to measure direct evaporation from the soil between the crop rows in the next phase of the project.

A theoretical description of the energy partition of sparse crops is presented, which describes evaporation in terms of the controlling resistances associated with the plants, and with the soil (or water) in which they are growing. The model provides a simple but physically plausible description of the transition between bare soil and a closed canopy. Although the aerodynamic transfer resistances for incomplete canopies have, as yet, no experimental justification, typical values, appropriate to a specimen agricultural crop and soil, are shown to have limited sensitivity in the model. Processes which require further study if the equation is to be used to calculate evaporation throughout a crop season are also discussed.

To calculate the separate components of evaporation which originate from the plants and the soil, it is necessary to know the amount of net radiation intercepted by the plants and, hence, the remainder which falls on the soil. Miniature tube net radiometers were used to measure net radiation interception and preliminary results showed that near harvest only 30-50% of the incident net radiation was intercepted by the plants. There was also a marked diurnal variation in radiation interception due to the changing solar angle.

The flux of sensible heat in the soil can form a significant part of the surface energy balance in sparse crops. Accurate predicton of crop evaporation therefore requires some measure (and/or model) of soil heat flux. Small heat flux plates were used to measure soil heat flux and the results obtained indicated that, even in very dry soil, there were days when nearly 10% of the incident net radiation was used to heat the soil. There also appears to be a good relationship between the daily input of heat to the soil and the rise in soil temperature. However, more measurements are required in wetter soils, where soil heat fluxes could be even larger than the values already obtained.

In summary, substantial progress has been made during the first phase of the project both in evaluating techniques and in formulating a theoretical description of sparse crop evaporation. The next phase of the project should concentrate on the following:-

(i) Testing the redesigned Hydra.

(ii) Making measurements of leaf area, crop height, plant and soil surface conductances, net radiation interception and soil heat flux throughout the crop season.

(iii) Estimation of the aerodynamic resistance within and above the crop canopy.

(iv) Testing/validation of the sparse crop model.

3. INTRODUCTION

Low and erratic rainfall is one of the main factors limiting crop production in dryland regions. However, there is substantial potential for yield improvement through the development of more efficient strategies for utilizing the limited soil water reserves. These changes in crop management will be better understood, and therefore should be more generally applicable, if the processes of evaporation from sparse dryland crops are more fully examined.

Much of the past research on evaporation processes has concentrated on temperate areas where the ground is covered with uniform vegetation. As a result substantial information exists about the rates of evaporation and associated surface and aerodynamic resistances of many common land surfaces, for example, grassland, forests and temperate cereals. However, much less is known about the evaporation and surface resistances of crops in dryland regions which for much (or all) of the crop season do not completely cover the ground. Although evaporation can be calculated (for example, using the Penman-Monteith equation) for uniform vegetation giving complete ground cover, there is considerable uncertainty about the use of such evaporation formulae for incomplete canopies. The overall aim of the study is, therefore, to make detailed measurements of plant, soil and total evaporation in sparse dryland crops and to use these measurements to develop models which will give more accurate predictions of evaporation from these types of vegetation.

The specific aims of the first phase of the project were:-

(i) To transfer equipment to and install it at the field site.
(ii) To evaluate the experimental techniques by obtaining some preliminary results for each system.
(iii) To formulate a theoretical description of sparse crop evaporation within which the field measurements could eventually be combined.

This report describes the progress made during the first field season, with descriptions of the different experimental systems used and examples of the data obtained from them.

4. SITE, CROP AND SEASON

(a) Site and sowing

The site selected for the first seasons work was at Tel Hadya (35° 55' N, 36° 55' E), the main experimental farm of the International Center for Agricultural Research in the Dry Areas (ICARDA), in Northern Syria. The soil at Tel Hadya is described as Vertic (calcic) Luvisol, a full soil profile description is given in Cooper et al (1981). The site has a Mediterranean type climate with an annual average rainfall of 342 mm. Further details of the climate are given by Smith and Harris (1981) and Dennett, Keatinge and Rodgers (1983).

The experimental field measured ca 500 x 250 m with the longer side in an East-West orientation; which provided the best fetch for the micro-meteorological instruments during the prevaling (westerly) winds (see Appendix I).

The barley (Hordeum vulgare L. cv Arabi aswad) crop studied was sown at a rate of 45 kg ha^{-1} on 3 November 1983 by broadcasting the seed and then ploughing with a ducksfoot cultivator. This formed ridges along the field (running East-West) about 45 cm apart; a planting method which mimicked the normal agricultural practice of the surrounding region. Germination occurred on 13 November 1984 and the crop received no husbandry other than being sprayed twice to control broadleaf weeds (at the end of January and the beginning of March). The crop was harvested on the 8th May 1984.

(b) Crop development

The green and dead leaf area indices of barley and weeds were measured at intervals of 1 to 3 weeks throughout the crop season. On each sampling occasions five 0.45 x 0.45 m quadrats were harvested and the total projected green and dead areas of barley and weeds were measured using a leaf area meter (Hayashi Denkoh AAM-7). The results of this sampling are shown in Figure 1. The barley reached a maximum green leaf area index of about 1.3 at the beginning of March 1984. From mid-March onwards the rate of senesence increased markedly, so that by the 17 April, of a total green area index of 0.5, only 6% of this was leaves, 64% was stem and 30% was ears. During

January there was a significant growth of broadleaf weeds which were irradicated by spraying.

Above ground total dry matter of barley (TDM) was also measured on the same samples used to determine leaf area index. Figure 2 shows that the rate of dry matter production increased steadily after crop emergence, reaching a saximum of about 50 kg ha^{-1} d^{-1} at the end of February. The dry matter production rate during March (20 kg ha^{-1} d^{-1}) was less than half of that achieved during February, but it returned to a rate of 50 kg ha^{-1} d^{-1} during April when the ear emerged.

Crop cover was also estimated on the same days when leaf area index and dry matter were measured. This was done by photographing ten randomly located 0.45 x 0.45 m quadrats which were placed across the crop rows. The photogrphs were taken from a height of 2 m, using an automatic camera (Canon AE1-Program) with a 50 mm lens; high speed colour slide film (200 or 400 ASA) was used to minimize any blurring due to leaf movement etc. The developed slides were analysed by projecting them onto a grid 30 x 15, and the 450 intersections inspected to see if they hit a green or dead leaf or soil. Figure 3(a) shows the values of crop cover obtained in this way during the 1983/84 season. The pattern of green area cover is similar to that for leaf area index (Figure 1) with a maximum ground cover of about 50% during March. Note that as the green area cover decreased during April the amount of soil exposed remained fairly constant, because the dead plant material still shaded the ground.

Crop height measurements were not started until 6 March by which time the crop was 0.36 m tall, Figure 3(b). Maximum height, 0.55 m, was achieved by 1 April.

At harvest, crop productivity was assessed from a random sample of 25 single metre rows (Table I). The low total dry matter production and grain yield are consistent with the below average rainfall received during the growing season (see Table 2); (note, the grain yield is still three times the Syrian national barley yield). Even though the grain yield is only a fraction of that obtained in barley crops grown in temperate climates, their mean weight per grain is similar (Gallagher, Biscoe and Scott 1975). This implies that even in such severely droughted crops such as the one studied here, the mean weight per grain is fairly stable and hence total grain yield is determined by the grain number per unit ground area.

(c) Weather during the crop season

Table 2 gives a summary of the weather conditions at Tel Hadya during the crop season (November 1983 to May 1984). During November high temperatures and substantial rainfall ensured good germination and rapid early crop development. From December to March rainfall fell well short of average, so that conditions of increasingly severe drought developed during the last two months of the season.

5. MEASUREMENTS OF EVAPORATION

This section describes the four different techniques used to measure evaporation.

(a) Neutron probe

Changes in soil moisture content were measured using an Institute of Hydrology neutron probe (Bell, 1976). Eight access tubes were installed to a depth of 180 cm immediately after planting and monitored regularly through the season at 15 cm depth intervals. Moisture changes in the 0-15 cm horizon were determined gravimetrically using a volumetric soil sampler. Total crop evaporation was calculated for each period from the change in total moisture in the 180 cm profile, plus any precipitation which occurred, between the reading dates. In this experiment runoff and drainage did not occur and were therefore ignored in computing evaporation.

Figure 4 shows the seasonal variation in the mean daily rate of total crop evaporation, E_c. During November and early December E_c was about 75% of that indicated by the class A pan, E_o. Lack of rain during the latter latter half of December depressed E_c to only 25% of E_o. From January onwards E_o increased rapidly, whereas E_c remained fairly constant, at just over 1 mm d^{-1}, until just before harvest. Figure 5 shows the cumulative crop and pan evaporation and cumulative rainfall between sowing and harvest. Clearly, crop evaporation was limited by rainfall, and not atmospheric evaporative demand.

(b) The Hydra

The 'Hydra' is the name of an eddy correlation device for measuring evaporation, which has been recently developed at the Institute of Hydrology (see Shuttleworth et al 1982, 1984 and Lloyd et al 1984). Although the Hydra has been shown to work satisfactorily in temperate and tropical climates, it has not yet been rigorously tested in a semi-arid dryland climate over sparse dryland crops. The use of the Hydra in the current study was therefore the first field trial of the device in this type of environment.

Before the Hydras were sited the experimental field was surveyed to assess its slope, since Wallace et al (1984) have shown that significant errors can arise if the Hydra is set vertically on sloping land. The field was found to have a slight south facing slope, with a maximum slope of 1.9° along an axis 168° from magnetic north. Two Hydras were set up perpendicular to this slope at the eastern end of the field (Figure A1). This arrangement gave maximum fetch for the widest range of wind directions centred around the prevailing westerly wind direction. Further details of the estimated acceptable wind directions, effective fetch and associated measurement errors are given in Appendix 1.

Hourly measurements of sensible and latent heat fluxes from the crop were recorded from 4 April to 28 May, however, the data are not continuous due to periods when the Hydras were wet due to rain or dew, or when the wind was blowing in an unacceptable direction. Figure 6 shows two examples of the values of sensible (H) and latent (E) heat fluxes measured using one of the Hydras before and after the crop was harvested. Before harvest (18 April 1984) the sensible heat flux was about a third of the incident net radiation. Less energy was used in evaporation and the total evaporation for the day was 1.6 mm. These figures are representative of a crop under water stress, since the potential evaporation (Penman 1948) for this day was 5.8 mm. Although the potential evaporation was only slightly more on 12 May 1984 (6.4 mm), after the crop was harvested, (Figure 6b) the sensible heat flux was twice that on 18 April and evaporation was reduced to only 8% of net radiation; giving a total evaporation of 0.4 mm for the day.

In order to check the values of H and E given by the Hydra they were compared with the available energy, $(R_n - G)$. Figure 7 shows a typical

example of the cumulative values of available energy, $\Sigma(R_n-G)$ and sensible and latent heat, $\Sigma(H+E)$, on 18 April 1984. The Hydra fluxes $\Sigma(H+E)$ fell increasingly short of $\Sigma(R_n-G)$, so that over the whole day $\Sigma(H+E)$ was only 66% of $\Sigma(R_n-G)$. The ratio $\Sigma(H+E)/\Sigma(R_n-G)$ is referred to as the flux recovery ratio, and Figure 8 shows that this was fairly consistent throughout the period that the Hydras were working. Clearly there was some error in the Hydras (or the instruments used to measure R_n and G) which was generating ≈ 30% short fall in the energy balance.

Several possible explanations of the gap in the energy balance have been investigated theoretically. Table 3 summarizes the four most probable contenders and indicates the approximate size of the error in each case. Firstly it was found that (see Appendix II) there is a very real possibility that fluxes calculated using the on-line Hydra software can be contaminated by false fluxes caused by correlated drifts in the sensors. The environmental conditions in Syria generated rather large drifts in the outputs of the Hydras hygrometer and vertical (sonic) anemometer because of the large daily temperature cycle and the high radiation loading on the sensors. The on-line Hydra software continuously calculates a 'running mean' temperature and humidity. Fluctuations in these quantities about these means are correlated with simultaneous fluctuations in vertical windspeed. When the temperatures of the Hydra sensors are changing rapidly, the computed runnings means can deviate significantly from their true values such that this difference is interpreted by the computer as a real fluctuation, which in turn, generates the calculation of 'pseudo' fluxes. Detailed simulations of this phenomenon are given in Appendix II which illustrates the effect, but concludes that it is difficult to give a precise quantitative assessment of the size of the sensor drift flux contamination without further knowledge of the temperature and humidity frequency distributions. However, from our purely theoretical computations to date, we can tentatively suggest that the effect could generate an unerestimate in E and H of the order of 5%.

The second possible source of error in the hydra data is due to the instrument not recording some of the energy fluxes which are carried in high

frequency eddies. Ideally, the Hydra would be capable of measuring and subsequently analysing, signals corresponding to the whole frequency range of atmospheric turbulence in the form of temperature, humidity and wind velocity fluctuations. In practice the Hydra cannot respond perfectly to all the frequencies encountered in the atmosphere, because of the finite time constants of the sensors, their size, separation and sampling rate. Other factors also affect the frequency response of the Hydra (e.g. height of exposure, windspeed and atmospheric stability) and these have been combined in a model (see Appendix III) to calculate the amount of 'flux loss' in different conditions. Figure 9 illustrates the amount of flux loss expected when using the Hydra in Syria. A range of values for the flux losses in E and H are given in Figure 9(a) because in unstable conditions the turbulent spectra are poorly defined at low frequencies (see Kaimal et al 1972). In typical unstable atmospheric conditions, which occur during the day, the flux loss is similar for sensible and latent heat, being between 5 and 10% irrespective of windspeed. At night, when the atmosphere is usually stable, flux losses are much higher; 25 - 40% depending on windspeed. However, since absolute fluxes of H and E are smaller at night, the absolute error incurred during the night contributes little to the total error in E and H over a whole (24 hour) day.

Figure 10 illustrates that when the Hydra data are corrected for sensor temperature drifts and high frequency flux loss, total daily evaporation agrees fairly well with that deduced from the soil moisture balance. Detailed comparison is difficult since the soil moisture data gives an average evaporation rate over several weeks. However, the Hydra data are well distributed about the mean soil moisture evaporation figure and also show a realistic response following the rainfall event on 15-16 April 1984.

For completeness Table 3 also shows possible errors in net radiation and soil heat flux. The figures quoted are based on literature reports of the overestimation of net radiation when making measurements over a hot surface (Idso and Cooley 1971) and calculations of the error in soil heat flux (see Leuning et al 1982) due to their location 1-2 cms below the soil surface. Further details of the instruments used to measure net radiation and soil heat flux and the data obtained from them are given later in section 6 of this report.

(c) Porometers

The transpiration component of the total crop evaporation was estimated using two types of porometer. On the 7, 14 and 21 of March 1984, before ear emergence, the stomatal conductance of the leaves and stems were measured using an automatic diffusion porometer (AP II, Delta-T Devices, Cambridge). On each day measurements were made at 2 h intervals between dawn and dusk on the stem and the adaxial and abaxial surfaces of all the green leaves. During each measurement period the stomatal conductances of five samples of each leaf and the stem were taken using separate, randomly selected, plants. On 28 March and 4 April, after the ear had emerged, measurements of the conductance of the ear was also measured using a null-balance diffusion porometer of the type described by Beardsell, Jarvis and Davidson (1972).

Figure 11 shows an example of the stomatal conductances of the adaxial and abaxial leaf surfaces. The adaxial leaf surfaces had the highest conductances, nearly three times those observed on the abaxial leaf surfaces. In this highly water stressed barley crop, the plants tended to display their leaves with their abaxial surfaces preferentially exposed. This behaviour would tend to decrease the effective total crop conductance and hence reduce transpiration. The total stomatal conductance of the leaves is obtained from the sum of the conductances of the adaxial and abaxial surfaces. Figure 12 shows the variation is total stomatal conductance of the four different leaves, the stem and the ear on 28 March 1984. Leaf conductances were low and decreased continuously during the day, an indication of a highly water stressed crop. The oldest leaves tended to have the lowest conductances, however, the leaf below the flag leaf was the one with the highest conductances. The conductance of the stem was very low and close to zero from midday onwards. Although the conductance of the ear decreased in parallel with the leaf conductances during the morning, its conductance increased again in the afternoon, so that it became the most actively transpiring organ in the crop at that time. It is tempting to suggest that the stomata in the ear were being kept preferentially open so as to allow photosynthesis and the development of the grains.

Figure 13 shows the amount of green area in the individual plant organs on 25 March 1984. The ear and flag leaf only made a small contribution to the total green area, the bulk being contained in the leaves lower down the plants. The stems made a large contribution to the total green area, so that

their contribution to the total canopy conductance was not insignificant even though their stomatal conductances were very low (see Figure 12). Total canopy conductance was calculated by multiplying together the stomatal conductances and green areas of the individual plant organs and then adding these up.

Figure 14(a) shows the variation in the total canopy conductance of the plants during 28 March 1984. Canopy conductance decreased rapidly during the day, however, even the maximum conductance 2 mm s^{-1} is very low and characteristic of crops under severe water stress (e.g. see Wallace et al 1981). The values of canopy conductance shown in figure 14(a) were used in the Penman-Monteith equation (Monteith 1965) to calculate transpiration. The necessary aerodynamic conductances were calculated from crop height and windspeed (see Wallace et al 1984) and the other weather variables required were obtained using an automatic weather station (see Section 6 of this report). Figure 14(b) shows that transpiration increased to a maximum just before midday and then decreased throughout the afternoon; the total transpiration for the day was 1.0 mm. At this time of the season the mean daily total crop evaporation rate derived from the soil moisture balance (see figure 4) was about 1.2 mm, which suggests that the soil evaporation was about 0.2 mm on 28 March. Figure 14(a) also shows the potential rate of evaporation, again calculated using the Penman-Monteith equation, but using an infinite surface conductance (i.e. no physiological restriction to evaporation). This illustrates the high degree of control the plants had over their water loss, since without this evaporation would have been about 5 times that calculated with the measured canopy conductances.

(d) Soil lysimeter

In order to compare the values of transpiration obtained using the porometers with total crop evaporation measurements made using the Hydra and neutron probe, it is necessary to have an independent measure of soil evaporation. In an attempt to do this a small soil lysimeter was constructed. The lysimeter was made by hammering a steel tube (20 x 20 cm in cross-section and 15 cm deep) into the soil between two crop rows. The soil around this was removed and the 'undisturbed' soil monolith removed by hammering a flat steel plate horizontally across the bottom of the tube. When the tube and soil had been raised above the ground the flat steel plate was replaced with a perforated based which was securely attached to the

lysimeter. In another part of the field a hole was carefully dug between the crop rows and lined with an aluminium box. The lysimeter was then lowered into this box to complete the installation. The installation of the soil lysimeter was not completed until after the crop was harvested, however, it was weighed daily for a period of two weeks in order to make some assessment of its feasibility. The balance used to weigh the lysimeter had a capacity of 12 kg ± 1g, which gave an equivalent resolution of the lysimeter of 0.025 mm.

Figure 15 shows a comparison of the results obtained using the soil lysimeter with those derived from the soil moisture balance. Since the plants had been harvested, both techniques should have been measuring the same soil evaporation. For about the first 6 days after the soil lysimeter had been installed, the agreement between the soil lysimeter and the soil moisture balance was fairly good, bearing in mind the extremely low rates of evaporation involved. After 6 days the rate of evaporation given by the soil lysimeter decreased, however, no measurements of soil moisture were available to check this. This short test of the soil lysimeter does give results which are similar to those reported by Shawcroft and Gardener (1983), where soil lysimeters were used under a corn crop (Zea Mays L.). The results obtained in the present study are therefore encouraging enough to warrant further use of small soil lysimeters in the next phase of the project.

6. PREDICTION OF EVAPORATION

This section describes the methods used to calculate or predict evaporation. Also included are descriptions of the experimental systems which were used to provide the input variables for these calculations.

(a) Evaporation equations

There are a great many equations available for calculating evaporation; almost as many as their are situations in which evaporation needs to be calculated. However, we choose to restrict our efforts to the use of the more physically based equations, a summary of which is given in Table 4. The Penman (1948) formula, which strictly applies to well watered short grass, has long been accepted as a standard method of calculating potential evaporation, E_p. However, in many situations, particularly where the vegetation is not 'adequately supplied' with water, this formula does not give a very good guide to actual crop evaporation. To obtain actual evaporation many workers multiply E_p by a 'crop factor' (see Doorenbos and Pruitt 1977). This may provide reasonably accurate estimates of actual evaporation if locally derived crop factors are used, however, the method is not generally applicable to crops which have an inadequate water supply (eg See Wallace et al 1981).

The Penman-Monteith formula (Table 4) has become increasingly accepted as a method for calculating evaporation from crops which have a different surface conductance than 'short-grass' and/or are not adequately supplied with water (eg see Roberts et al 1980; Aston 1984). However, this formula only applies to vegetation which completely covers the ground and where there is no soil evaporation. Because of the lack of a generalized, physically based model for describing evaporation from sparse crops we have attempted to reinterpret the approach of Shuttleworth (1976, 1978 and 1979) and have developed a model which can simultaneously describe evaporation from sparse plants and the soil (or water) in which they are growing (Table 4). Details of the derivation of the model are given in Appendix IV, however, some of the salient features of the approach are reproduced here. Figure 16 shows a schematic representation of the energy partition of sparse crops. Soil evaporation, λE_s, traverses the soil surface resistance r_s^s and the aerodynamic resistance r_a^s where it joins the crop component of evaporation

λE_c. The total evaporation, λE, then moves into the atmosphere via the remaining aerodynamic resistance, r_a^a. λE_s and λE_c can be described using combination equations, ie

$$\lambda E_s = \frac{\Delta A_s + \rho c_p D_o / r_a^s}{\Delta + \gamma(1 + r_s^s / r_a^s)} \qquad (1)$$

$$\lambda E_c = \frac{\Delta (A - A_s) + \rho c_p D_o / r_a^c}{\Delta + \gamma(1 + r_s^c / r_a^c)} \qquad (2)$$

The total evaporation from the crop, λE, is the sum of these two, and it can be shown (see Appendix IV) that this is described by a combination equation of the form

$$\lambda E = C_c PM_c + C_s PM_s \qquad (3)$$

where PM_c and PM_s are terms each similar to the Penman-Monteith combination equations which would apply to evaporation from a closed canopy and from bare soil respectively. They have the form

$$PM_c = \frac{\Delta A + [\rho c_p D - \Delta r_a^c A_s]/(r_a^a + r_a^c)}{\Delta + \gamma [1 + r_s^c / r_a^a + r_a^c)]} \qquad (4)$$

$$PM_S = \frac{\Delta A + [\rho c_p D - \Delta r_a^s (A - A_s)]/(r_a^a + r_a^s)}{\Delta + \gamma [1 + r_s^s / (r_a^a + r_a^s)]} \qquad (5)$$

The coefficients C_c and C_s are given by the expressions

$$C_c = \left[1 + \frac{R_c R_a}{R_s (R_c + R_a)}\right]^{-1} \qquad (6)$$

$$\text{and} \quad C_s = \left[1 + \frac{R_s R_a}{R_c(R_s + R_a)}\right]^{-1} \tag{7}$$

$$\text{where} \quad R_a = (\Delta + \gamma) r_a^a \tag{8}$$

$$R_s = (\Delta + \gamma) r_a^s + \gamma\ r_s^s \tag{9}$$

$$R_c = (\Delta + \gamma) r_a^c + \gamma\ r_s^c \tag{10}$$

An example of the response of the sparse crop model is shown in Figure 17, where evaporation is calculated for crops of different density growing in soils of different wetness. The total evaporation rate of sparse crops is significantly altered by the condition (i.e. surface resistance, r_s^s of the soil substrate (Figure 17a). The contribution to total evaporation made by plants is also sensitive to r_s^s, and can easily exceed the fraction of energy intercepted by the canopy when leaf area index is low (< 2) and soil surface resistance high (Figure 17b). In this situation some of the energy incident on the soil is transferred as sensible heat to the canopy and utilized their for transpiration.

Another interesting feature of the model is its limited sensitivity to the parameterization of aerodynamic resistance, which for sparse crops is a poorly understood area of micrometeorology. To use the model to describe the variation in plant and soil evaporation through a crop season would require substantial measurements or submodels of crop height, leaf area, stomatal and soil conductance, net radiation interception and soil heat flux. However, the principal aim of the model is to provide a theoretical framework through which such measurements or submodels can be combined to calculate plant and soil evaporation.

(b) Automatic Weather Stations

All of the formulae for calculating evaporation shown in Table 4 require weather data, either daily (Penman) or hourly (Penman-Monteith, Shuttleworth-Wallace). In order to provide this information two automatic weather

stations (Strangeways 1972) were installed just after sowing (9 November 1983) and run continuously until after harvest (22 May 1984). Seven weather variables, solar and net radiation, wind speed and direction, dry and wet bulb temperatures and rainfall were recorded every 10 minutes. The wet and dry bulb thermometer assembly was modified to allow the thermometers to be continuously aspirated using a small 12 volt fan. The recording system was completely solid state (Monolog Systems, Computing Techniques, Billingshurst, England) and data stores were changed weekly and transferred onto floppy disc (5¼") using a microcomputer (Commodore 4032). The micro computer was also programmed to produce an hourly summary of the weather data and a daily total value of potential evaporation (Penman 1948). Table 5 gives an example of this summary for 16 April 1984. Hourly weather data can also be plotted directly from the data discs, Figure 18 shows an example of this from 12 May 1984.

(c) Net radiation interception

To calculate the separate components of evaporation which originate from the plants and the soil, it is necessary to know the amount of net radiation intercepted by the plants and, hence, the remainder which falls on the soil. Net radiation interception was measured using miniature tube net radiometers, 380 mm long x 11 mm wide (Delta-T devices, Cambridge, UK). Tube radiometers lack perfect spherical symmetry, so their output varies with the orientation of the solar beam. For this reason the tube radiometers were only used for comparative measurements of net radiaion above and below the crop. Eight tube net radiometers were located below the crop so that they crossed two crop rows (see, Figure 19), this gave a measure of the average net radiation at the soil surface. Another tube net radiometer was placed 1.2 m above the crop and at the same orientation as those below the crop. Absolute values of net radiation above the crop were recorded using a dome net radiometer (Type DRN/301; Didcot Instrument Company, Abingdon, UK). The outputs from each of the radiometers were integrated and each logged hourly using a solid state recording system similar to that used in the automatic weather stations (i.e. Monolog Systems; Computing Techniques, Billingshurst, UK). Measurements were taken continuously from 19 April 1984 (before harvest) to 21 May 1984 (after harvest).

Figure 20 shows an example of the fraction of above crop net radiation reaching the soil, just before harvest. The values shown are hourly means from three bright sunny days (1, 5 and 6 May), which have been corrected for

the effects of having the below crop net radiometers close to the ground (see Idso and Cooley 1971, 1972). These correction factors were derived for each hour of the day from measurements of net radiation just above the soil and at 1.2 m made after the crop was harvested. The fraction of net radiation reaching the soil, R_n^s/R_n, (Figure 20), increased during the morning to about 0.7. In the afternoon R_n^s/R_n decreased to about 0.5. A simplified view of net radiation interception is shown in Figure 21. Following Ross (1981, page 351) we describe the net radiation at the soil surface R_n^s as a function above crop net radiation, R_n and leaf area index, L, viz

$$R_n^s = R_n \exp(-KL). \qquad (11)$$

K is the extinction coefficient given by

$$K = K_{min}/\sin\beta , \qquad (12)$$

where K_{min} is the minimum value of K which occurs when the solar angle, β, is 90°. This relationship has been found to apply to net radiation during daylight hours, since R_n is then primarily determined by direct solar radiation. Figure 22 shows the values of K calculated using equation (11) and the data shown in Figure 20, with a leaf area index (green and dead plant material) of 1.3 (see Figure 1). Also shown is the 'theoretical' change in K during the day, given by the measured value of K at solar noon (0.178) divided by the solar angle, β (equation 12). Although the midday values of K are very low (ca 0.2), they are similar to values found in other erectophile row crops (see, for example, Baldocchi, Verma and Rosenberg 1983). The theoretical and measured responses of K shown in Figure 22 are similar during the morning, however, there is significant disagreement in the afternoon. Calculations were made to see if this was due to the existence of discreet crop rows (McCaughey and Davies 1974). This analysis suggests that the rows had no significant effect on the diurnal pattern of net radiation interception. If it did R_n^s/R_n would have a minimum value at solar noon (when the solar azimuth is 90° to the crop rows), with maxima in the morning and evening. This would produce a maximum extinction coefficient at noon and

minumum in the morning and evening, exactly the opposite of what was observed (Figure 22). When the crop rows are not East - West they can significantly affect the diurnal pattern of radiation interception (see McCaughey and Davies 1974).

Since the theoretical change in K during the day (equation 12) is based solely on allowing for the change in optical path length through the crop, this is considered to be the dominant mechanism affecting net radiation interception. The afternoon discrepancy between the measured values of K and those predicted by equation (12) remains unexplained. Two phenomena which cannot account for this are leaf curl during afternoon water stress and variation in tube net radiometer sensitivity with solar azimuth. Leaf curl would increase light penetration (and R_n^s/R_n) during the afternoon and hence decrease K. During calibration experiments we found that the output of the tube net radiometers in direct radiation depended on their orientation with respect to the solar beam. For a fixed value of radiation at a given solar zenith angle, the tube net radiometers give a maximum output when the solar beam is perpendicular to the axis of the radiometer (and a minimum when solar beam parallel to the axis of the radiometer). Given the orientation of the instruments in the present study (Figure 19) this means that the net radiometers would be less sensitive to direct radiation in the afternoon. However, since there is more diffuse radiation below the crop, which is <u>not</u> uni-directional, measurements of R_n will be reduced proportionately more than R_n^s and hence the apparent ratios of R_n^s/R_n will be larger in the afternoon. This, in turn, would decrease the apparent extinction coefficient K.

(d) Soil heat flux

In sparse crops the flux of sensible heat in the soil can form a substantial part of the surface energy balance. Accurate prediction of crop evaporation therefore requires some measure (or model) of soil heat flux. This section describes the method used to measure soil heat flux and gives some example results. Also presented is a technique for predicting soil heat flux from soil temperature.

Soil heat flux was measured using eight small heat flux plates (25 mm diameter x 2.6 mm deep; Thornthwaite Associates, New Jersey, USA) located 1-2 cms below the soil surface (see Figure 23). Soil temperature was also measured using platinum resistance thermometers, 'on' the row (at a depth of 16 cm) and 'off' the row (at a depth of 10 cm). The signals from the flux plates were integrated and logged along with the soil temperatures at hourly intervals using a solid state logging system similar to that used in the automatic weather stations (Monolog Systems, Computing techiques, Billingshurst, UK). Measurements were made continuously between the 8 April 1984 and 22 May 1984.

Figure 24 shows examples of the change in soil heat flux and temperature on three days. On 13 April 1984 the heat flux into the soil reached a maximum of ≈ 50 W m^{-2} around midday; the rise in soil temperature (at 16 cm) on this day was 3.6 deg K. Five days later (18 April) greater insolation led to a higher soil heat flux and a greater rise in soil temperature, 5.4 deg. K. After harvest (12 May 1984) high insolation gave an even greater flux of heat into the soil, up to 100 W m^{-2} at midday. Also soil temperatures were higher by 7 deg. K) and the diurnal rise in soil temperature greater (6.1 deg. K) than in mid-April. \ Figure 25 shows the relationship between the rise in soil temperature during the day and the cumulative flux of heat into the soil (e.g. the area under the positive portion of the curves in Figure 24(b)). The relationship could be interpreted as linear, with no difference in slope before and after harvest. This means that from simple measurements of soil maximum and minimum temperatures it may be possible to calculate the total positive flux of heat into the soil. It is, of course, likely that the form of the relationship between soil temperature rise and heat flux will change as the thermal properties of the soil change, with for example soil wetness. The extent of this effect will be studied in future phases of the project.

CONCLUDING REMARKS AND FUTURE PLANS

The principal objectives of the first phase of the project were substantially met. Despite administrative difficulties, all of the equipment necessary for setting up the project were successfully imported and installed at the experimental site in Syria. Most of the techniques required in the study were also tested and either proved satisfactory or revealed shortcomings which could be dealt with before the second phase of the project.

A good example of this is the discovery that the Hydra measurements obtained over a sparse crop in the hot, dry Mediterranean climate were seriously in error. It should be noted that these faults in the Hydra's performance were not previously known, and it was only through the use of the instrument in Syria that they became apparent. Once discovered, the data from Syria provided the stimulation to rigorously examine the hardware and software of the whole Hydra system. This re-evaluation of the Hydra was also very timely since the instrument was already under a program of redesign prior to commercialization. The practical outcome of this work is that redevelopments of the Hydra are currently in progress, which should minimize most of the errors found in Syria. However, the next phase of the project will involve a rigorous test of the new Hydra system, to see how successful the redevelopments have been.

A second area of major progrss was in the formulation of a theoretical description of evaporation from sparse crops. This is a significant advance since it provides a means of calculating evaporation from sparse crops using a physically based model which employs a consistent approach to the plant and soil components. The model highlights a major gap in our current knowledge, i.e. the quantitative response of within canopy aerodynamic transfer to crop density. However, evaporation calculations made using the model were shown to have limited sensitivity to the parameterization of aerodynamic resistance. Future work will attempt to assess if this prediction is correct.

The use of the model to describe the variation in soil and plant evaporation throughout a crop season would require measurements (and/or models) of leaf area, crop height, stomatal and soil resistances, net radiation interception and soil heat flux. The next phase of the project

will attempt to make measurements of these quantities, and where appropriate develop models of them, for a range of conditions throughout the crop season. These measurements will then be combined in the sparse crop model and the predicted values of total, plant and soil evaporation compared with measurements made using the Hydra, porometers, and interrow soil lysimeters respectively.

Another area of study which the project could be extended to cover in the future is in the relationships between crop water use and yield. Having developed methods to measure and calculate both total crop water use and transpiration this information could be combined with measurements of dry matter production and yield to provide a stronger link with the more agricultural aspects of crop growth.

A final objective of the project, both current and future, is the transfer of technical skills and knowledge to the indigeneous staff of our collaborative institute in Syria. By working closely with them throughout the project, it is hoped that the work will be of more lasting benefit to the agriculture of that region.

8. REFERENCES

Aston, A.R. 1984. Evaporation from eucalypts growing in a weighing lysimeter: A test of the combination equations. Agric. For. Meteorol. 31, 241-249.

Baldocchi, D.D., Verma, S.B. and Rosenberg, N.J., 1983. Microclimate in the soybean canopy. Agric. Meteorol., 28: 321-337.

Beardsell, M.F., Jarvis, P.G. and Davidson, B. (1972) A null-balance diffusion porometer suitable for use with leaves of many shapes. J. Appl. Ecol. vol. 9, 677-690.

Bell, J.P. 1976. Neutron probe practice. NERC, Instite of Hydrology, Wallingford. Report No.19, 65 pp.

Cooper, P.J.M., Allan, A.Y., Harmsen, K., Keatinge, J.D.H., Nygaard, D., Saxena, N. and Islam, R. 1981. Soil water and nutrient research 1979-80. ICARDA Project Report 3, International Centre for Agricultural Research in the Dry Areas, Aleppo, Syria, 191 pp.

Dennett, M.D., Rodgers, J.A. and Keatinge, J.D.H. 1983. Simulation of a rainfall record for the site of a new agricultural development: An example for Northern Syria. Agric. Meteorol. 29, 247-258.

Doorenbos, J. and Pruitt, W.O., 1977. Crop water requirements. FAO Irrigation and Drainage Pap. 24, Rome, 144 pp.

Gallagher, J.N., Biscoe, P.V. and Scott, R.K. 1975. Barley and its environment. V. Stability of grain weight. Journal of Applied Ecology 12, 319-336.

Gash, J.H.C., 1985. Some estimates of the effective fetch of micrometeorological evaporation measurements, made with a simple diffusion equation. Submitted to Boundary Layer Meteorol.

Idso, S.B. and Cooley, K.R. 1971. The vertical location of net radiometers I. The effects of the underlying air layer. J. Meteorol. Soc. of Japan 49, 343-349.

Idso, S.B. and Cooley, K.R. 1972. The vertical location of net radiometers. II The effects of the net radiometers shadow. J. Meteorol. Soc. of Japan 50, 49-58.

Kaimal, J.C., Wyngaard, J.C., Izumi, Y. and Cote, O.R. 1972. Spectral characteristics of surface-layer turbulence. Quart. J.R. Met. Soc. 98, 563-589.

Leuning, R., Denmead, O.T., Long, A.R.G. and Ohtaki, E. 1982. Effects of heat and water vapor transport on eddy covariance measurements of CO_2 fluxes. Boundary Layer Meteorology 23, 209-222.

Lloyd, C.R., Shuttleworth, W.J., Gash, J.H.C. and Turner, M. 1984. A microprocessor system for eddy correlation. Agric. For. Meteorol., 33, 67-80.

McCaughey, J.H. and Davies, J.A. 1974. Diurnal variation in net radiation depletion within a corn crop. Boundary-layer Meteorol., 5, 505-511

Monteith, J.L., 1965. Evaporation and environment. In: State and movement of water in living organisms, Symp. Soc. Exp. Biol. 19th., pp. 205-234.

Penman, H.L. (1948) Natural evaporation from open water, bare soil and grass. Proc. Roy. Soc. Lond. A. vol. 193, 120-146.

Roberts, J., Pymar, C.F., Wallace, J.S. and Pitman, R.M., 1980. Seasonal changes in leaf area, stomatal and canopy conductances and transpiration from bracken below a forest canopy. J. Appl. Ecol., 17: 409-422.

Ross, J. 1981 The radiation regime and architecture of plant stands. Tasks for vegetation sciences 3: (ed. Helmut Leith). Dr W. Junk Publishers. The Hague pp 391.

Shawcroft, R.W. and Gardner, H.R., 1983. Direct evaporation from soil under a row crop canopy. Agric. Meteorol., 28: 229-238.

Shuttleworth, W.J., 1976. A simplified one-dimensional theoretical description of the vegetation-atmosphere interaction. Boundary-Layer Meteorol., 10, 273-302.

Shuttleworth, W.J., 1978. A simplified one-dimensional theoretical description of the vegetation-atmoshere interaction. Boundary-Layer Meteorol., 14, 3-27.

Shuttleworth, W.J., 1979. Below canopy fluxes in a simplified one dimensional theoretical description of the vegetation-atmosphere interaction. Boundary-layer Meteorol., 17, 315-331.

Shuttleworth, W.J., McNeil, D.D. and Moore, C.J., 1982. A switched continuous-wave sonic anemometer for measuring surface heat fluxes. Boundary-Layer Meteorol., 23: 425-448.

Shuttleworth, W.J., Gash, J.H.C., Lloyd, C.R., Moore, C.J., Roberts, J., Marques, A. de O., Fisch, G., Silva, V. de P., Ribeiro, M.N.G., Molion, L.C.B., de Sa, L.D.A., Nobre, C.A., Cabral, O.M.R., Patel, S.R. and de Moraes, J.C., 1984. Eddy-correlation measurements of energy partition for Amazonian forest. Q.J.R. Meteorol. Soc., 110, 1143-1162.

Smith, R.C.G. and Harris, H.C. 1981. Environmental resources and restraints to agricultural production in a mediterranean-type environment. In Soil Water and Nitrogen in Mediterranean-type environments. Developments in Plant and soil sciences Vol 1 (ed. J.L. Monteith and C. Webb), p 31-57. Dr W Junk, The Hague.

Strangeways, I.C. (1972) Automatic Weather Stations for network operation. Weather, 27, 403-408.

Wallace, J.S., Batchelor, C.H. and Hodnett, M.G., 1981. Crop evaporation and surface conductance calculated using soil moisture data from central India. Agric. Meteorol., 25: 83-96.

Wallace, J.S., Lloyd, C.R., Roberts, J. and Shuttleworth, W.J., 1984. A comprison of methods for estimating aerodynamic resistance of heather (Calluna vulgaris (L.) Hull) in the field. Agric. For. Meteorol., 32: 289-305.

TABLE 1. The productivity of barley (C.V. Arabi Aswad) grown at Tel Hadya, Northern Syria during the 1983/84 season and harvested on 7 May 1984.

	Mean	S.D.
*Total Dry Matter at harvest ($Kg\ ha^{-1}$)	2,360	(± 210)
Grain dry weight ($Kg\ ha^{-1}$)	1,140	(± 95)
Harvest Index	0.48	(± 0.01)
Number of ears per m^2	238	(± 26)
Number of grains per ear	15.1	(± 2.4)
Mean weight per grain (mg)	31.7	(± 0.7)

(*Above ground plant organs only)

TABLE 2 Weather at Tel Hadya during the 1983/84 crop season.

	November	December	January	February	March	April	May
Rainfall (mm)	71.5	18.6	49.3	11.8	31.1	38.8	0.0
Solar Radiation (MJ m^{-2} d^{-1})	8.9	8.6	7.1	13.6	16.5	20.0	26.6
Mean temperature (°C)	19.5	14.3	12.3	15.2	18.2	21.0	30.1
Relative humidity (%)	74	73	78	66	66	68	47
Wind Speed at 2m (m s^{-1})	1.7	*NA	1.9	2.2	2.6	2.5	3.3
Class A pan evaporation (mm)	1.6	1.3	1.0	1.8	2.8	4.0	8.6

(* data not available for whole month)

TABLE 3 Summary of the possible sources of error and their magnitude, which could contribute to the 30% shortfall in the energy balance.

POSSIBLE SOURCES OF ERROR	APPROXIMATE SIZE
(a) Temperature sensitivity of the humidity and vertical windspeed sensors.	- 5% in E + H
(b) High frequency flux loss due to sensor response, size, separation and sampling rate.	- 5 to 10% in E + H
(c) Overestimate of net radiation due to hot soil surface.	+ 5 to 10% in Rn
(d) Underestimate of soil heat flux due to heat storage in soil.	- 5 to 10% in G

TABLE 4. A summary of the formulae used to calculate evaporation

FORMULA	EQUATION	COMMENTS
PENMAN	$Ep = \frac{\Delta R_n + \gamma\ (e_s-e)f(u)}{\Delta + \gamma}$	POTENTIAL EVAPORATION
PENMAN X CROP FACTOR	$E_a = K_c \times E_p$	ACTUAL CROP EVAPORATION
PENMAN-MONTEITH	$E_a = \frac{\Delta R_n + \rho\ C_p(e_s-e)/r_a}{\Delta + \gamma(1 + r_s/r_a)}$	ACTUAL CROP EVAPORATION
SHUTTLEWORTH-WALLACE	$E_a = C_c\ PM_c + C_s\ PM_s$	ACTUAL EVAPORATION FROM PLANTS AND SOIL

TABLE 5. Hourly summary of weather data produced by the automatic weather stations and microcomputer processing system

HOUR FROM	SOLAR WATTS/M**2	NET	DEP DEGS	TEMP C	SPEED M/S	DIRN DEG	RAIN MM	ASP BAT VOLTS	GOOD SCANS	
00.00	- 2.	- 5.	+ .07	+ 9.1	.5	136.	.0	12.63	6	16-APR-1984
01.00	- 4.	- 7.	+ .14	+ 9.6	.8	151.	1.0	12.60	6	16-APR-1984
02.00	- 4.	- 11.	+ .17	+ 9.7	1.4	140.	.5	12.60	6	16-APR-1984
03.00	+ 15.	- 0.	+ .20	+ 9.7	1.1	133.	.0	12.60	6	16-APR-1984
04.00	+ 70.	+ 38.	+ .41	+10.3	1.7	155.	.0	12.67	6	16-APR-1984
05.00	+ 252.	+189.	+ .76	+11.6	1.6	185.	.0	13.16	6	16-APR-1984
06.00	+ 290.	+219.	+ 1.53	+13.1	1.7	270.	.0	13.52	6	16-APR-1984
07.00	+ 375.	+283.	+ 2.04	+14.3	2.0	255.	.0	13.63	6	16-APR-1984
08.00	+ 531.	+407.	+ 2.76	+15.5	1.7	195.	.5	13.84	6	16-APR-1984
09.00	+ 741.	+569.	+ 3.63	+16.8	1.9	191.	.0	13.87	6	16-APR-1984
10.00	+ 368.	+265.	+ 2.85	+15.4	3.9	140.	.0	13.41	6	16-APR-1984
11.00	+ 108.	+ 61.	+ 1.52	+12.8	1.8	128.	1.5	13.15	6	16-APR-1984
12.00	+ 41.	+ 19.	+ .50	+11.8	1.4	332.	5.0	13.03	6	16-APR-1984
13.00	+ 112.	+ 72.	+ 1.02	+12.1	1.4	320.	.5	13.10	6	16-APR-1984
14.00	+ 47.	+ 23.	+ .90	+11.7	2.1	283.	.5	13.08	6	16-APR-1984
15.00	+ 14.	- 3.	+ .48	+11.3	1.3	266.	1.0	12.98	6	16-APR-1984
16.00	- 3.	- 22.	+ .38	+11.1	.5	235.	.5	12.95	6	16-APR-1984
17.00	- 4.	- 22.	+ .12	+10.2	.6	169.	.0	12.84	6	16-APR-1984
18.00	- 3.	- 11.	+ .09	+10.5	.3	31.	.0	12.82	6	16-APR-1984
19.00	- 2.	- 11.	+ .07	+10.6	.6	176.	.5	12.84	6	16-APR-1984
20.00	- 2.	- 12.	+ .05	+10.4	.6	159.	.5	12.81	6	16-APR-1984
21.00	- 2.	- 12.	+ .04	+10.2	.7	162.	.0	12.80	6	16-APR-1984
22.00	- 2.	- 10.	+ .06	+10.3	.2	148.	.0	12.75	6	16-APR-1984
23.00	- 2.	- 11.	+ .06	+10.3	.1	136.	.0	12.71	6	16-APR-1984
10.52	7.18		.83	11.6	1.2	179	12	SOLAR & NET IN MJ/M**2		

DAILY CALCULATIONS BASED ON
24 HOURS OF DATA FOR 16-APR-1984

PENMAN ESTIMATE OF POTENTIAL EVAPORATION FOR DAY IS 1.34 MM

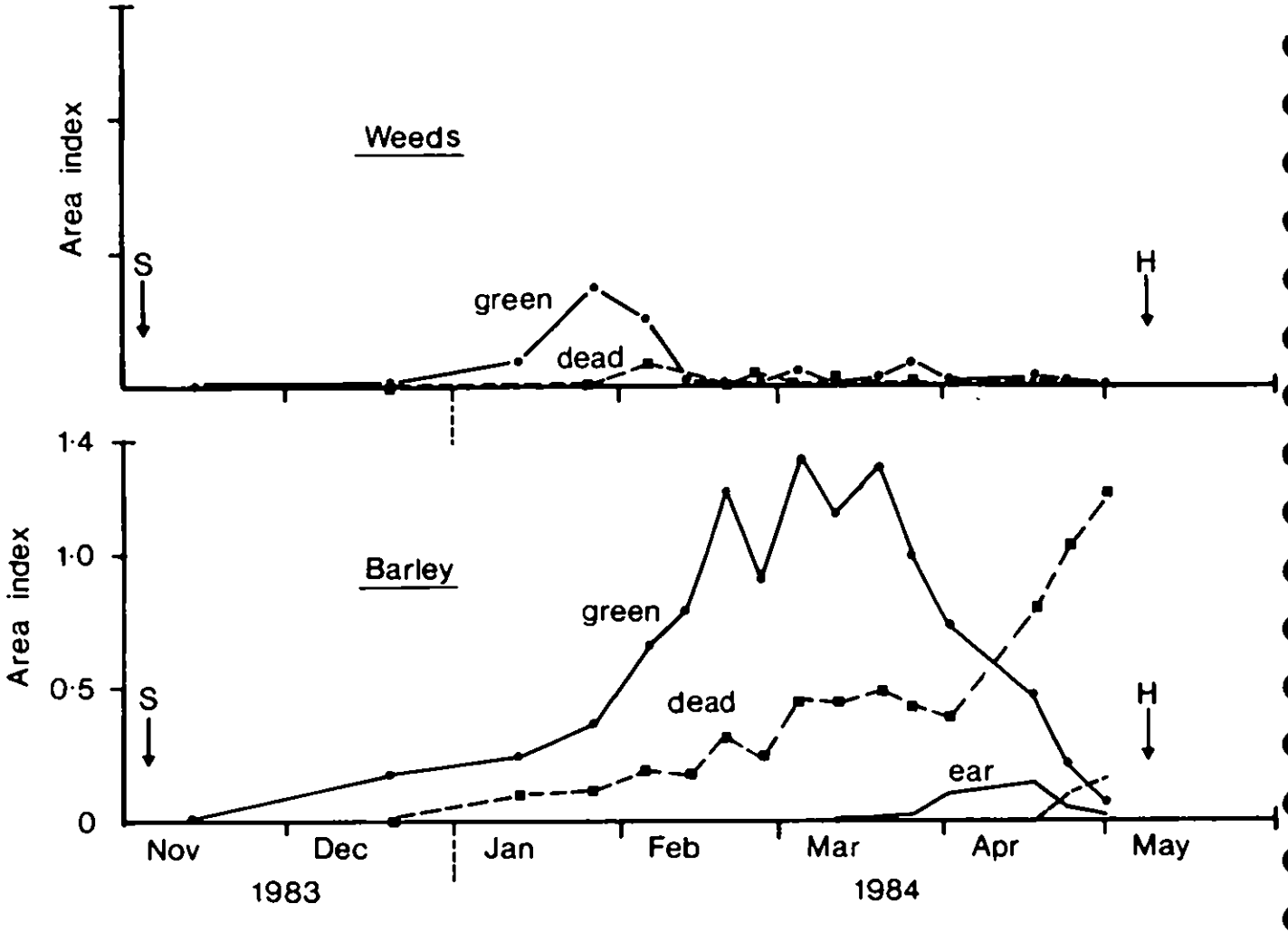

Figure 1. The green and dead area indices of barley and weeds at Tel Hadya 1983/84 season. Sowing (S) and harvest (H) dates are also shown.

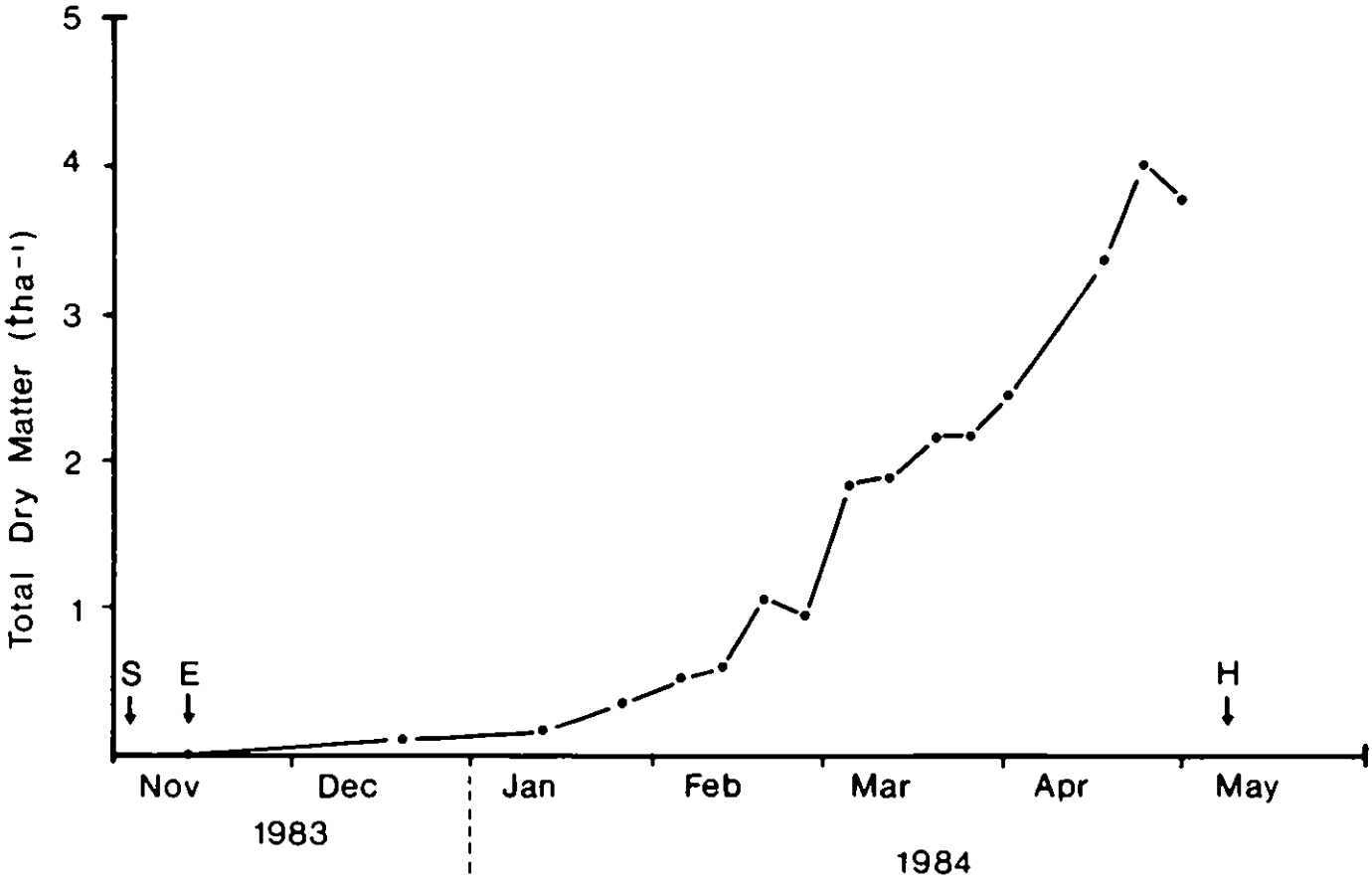

Figure 2. Above ground dry matter production of barley at Tel Hadya 1983/84 season. Sowing (S), emergence (E) and harvest (H) dates are also shown.

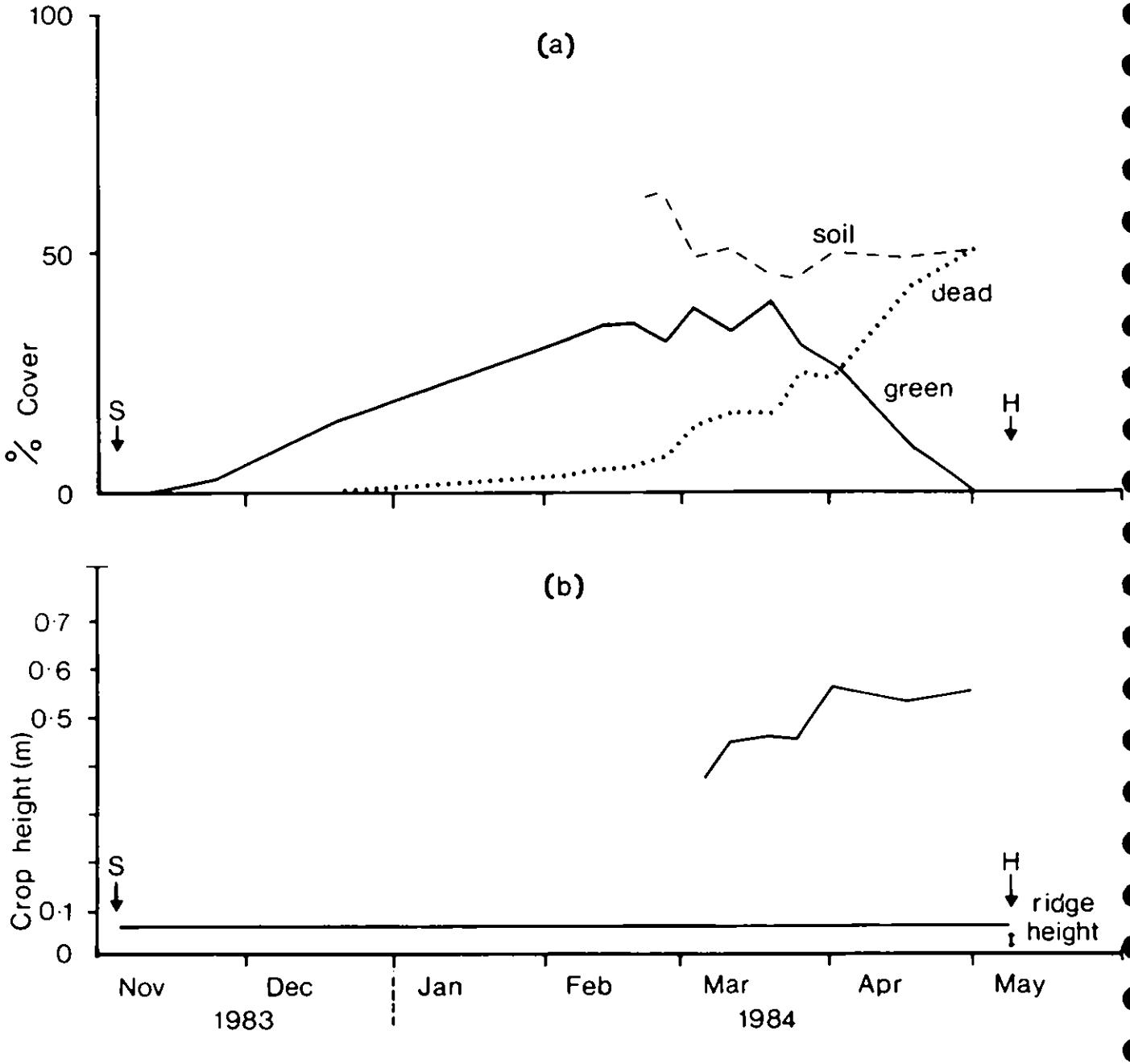

Figure 3. (a) % ground cover of barley and (b) crop height at Tel Hadya 1983/84 season. Sowing (S) and harvest (H) dates are also indicated.

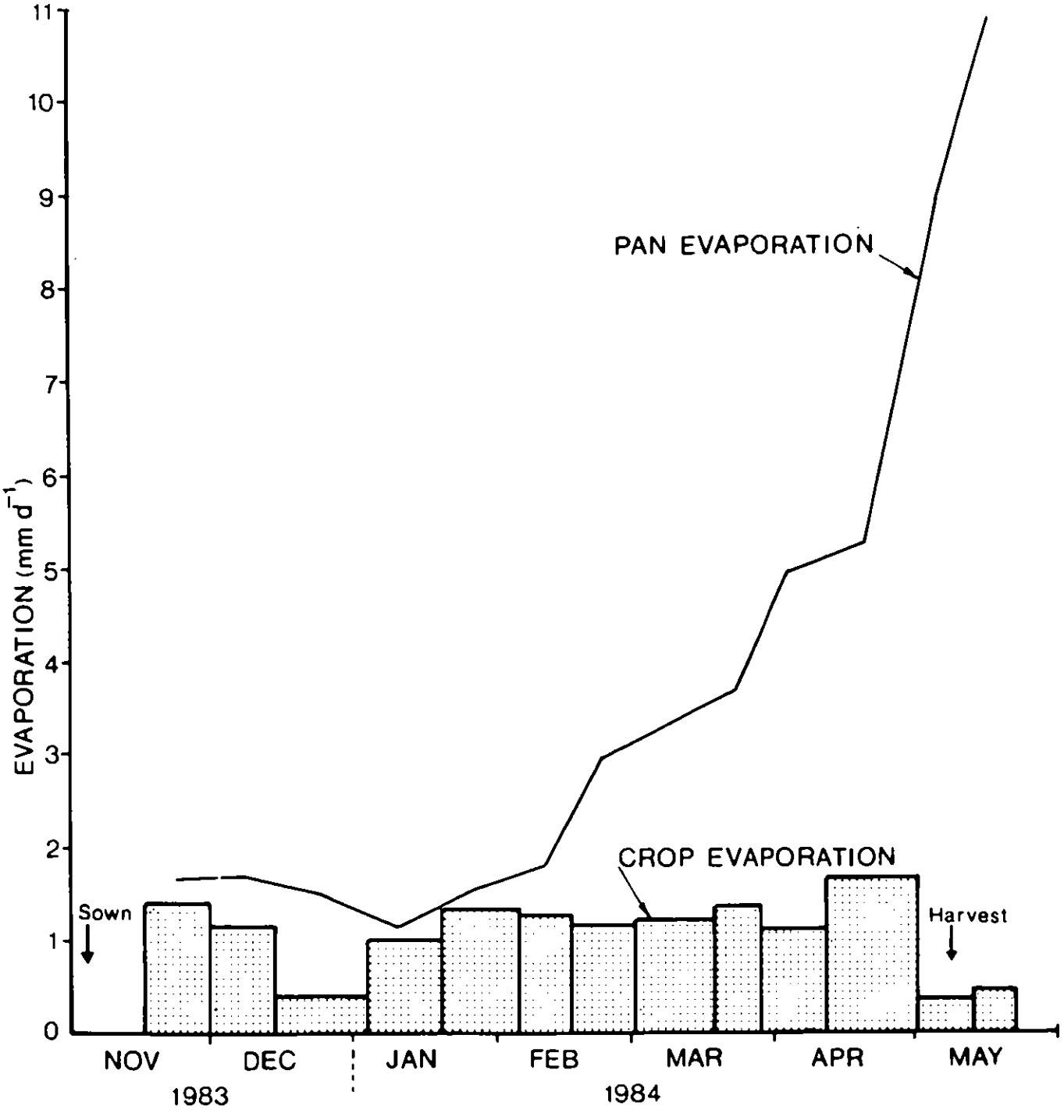

Figure 4. The variation in total crop evaporation during the 1983/84 season. Class A pan evaporation is also shown for comparison.

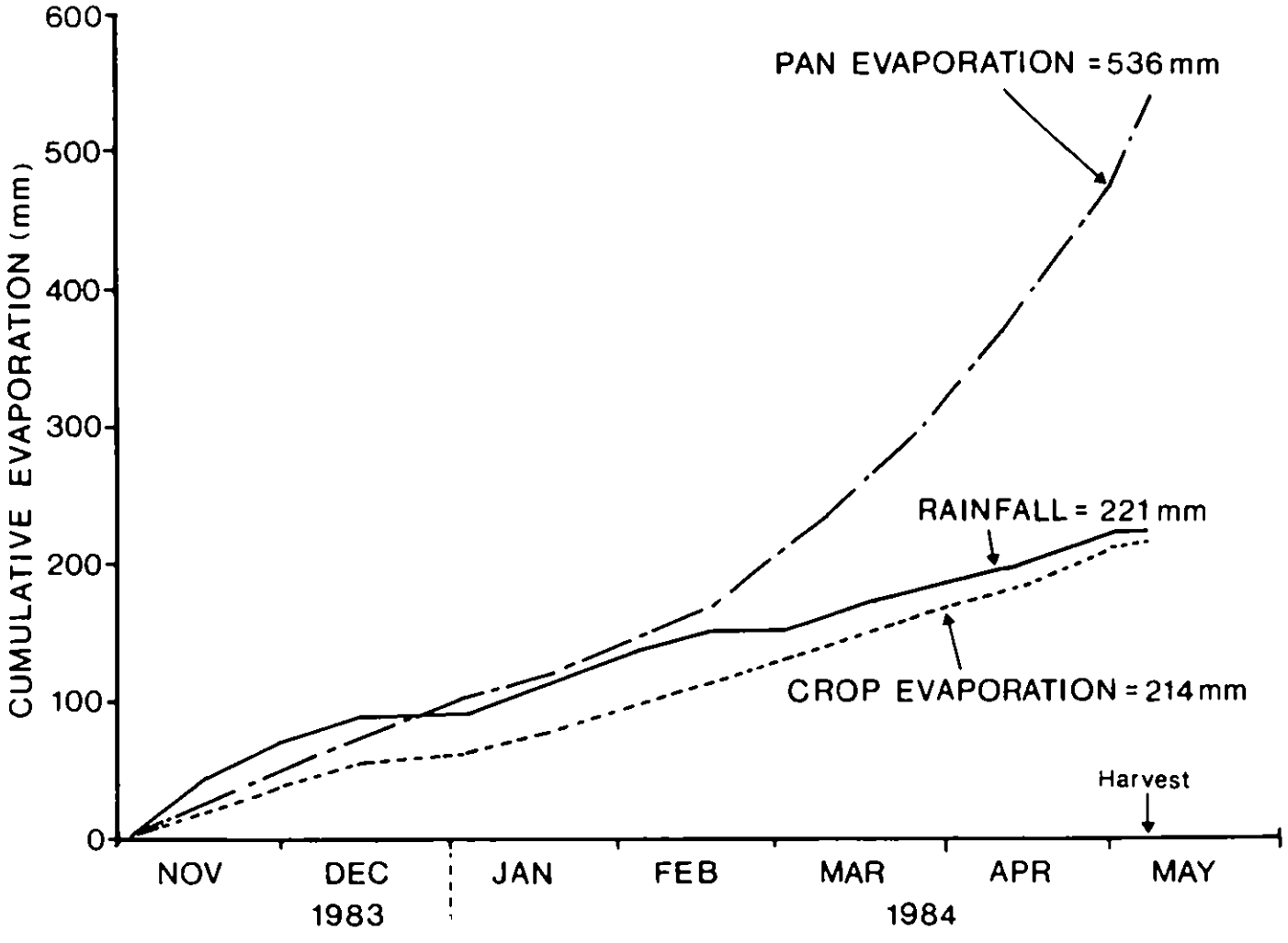

Figure 5. Cumulative crop evaporation, rainfall and pan evaporation between sowing and harvest.

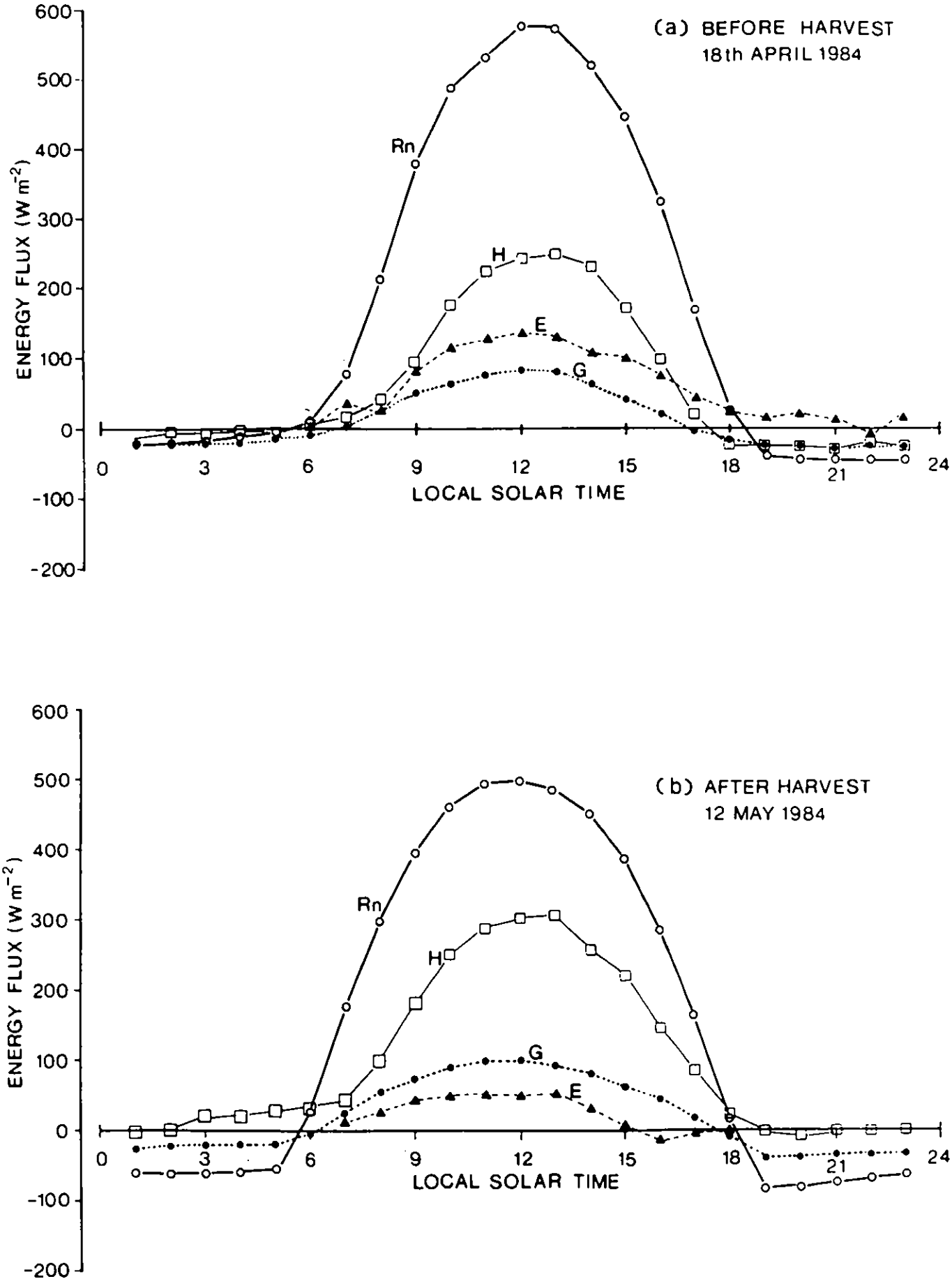

Figure 6. The diurnal variation in sensible (H) and latent (E) heat fluxes as measured by the Hydra on two days (a) before and (b) after harvest. Concurrent values of net radiation (R_n) and soil heat flux (G) are also shown.

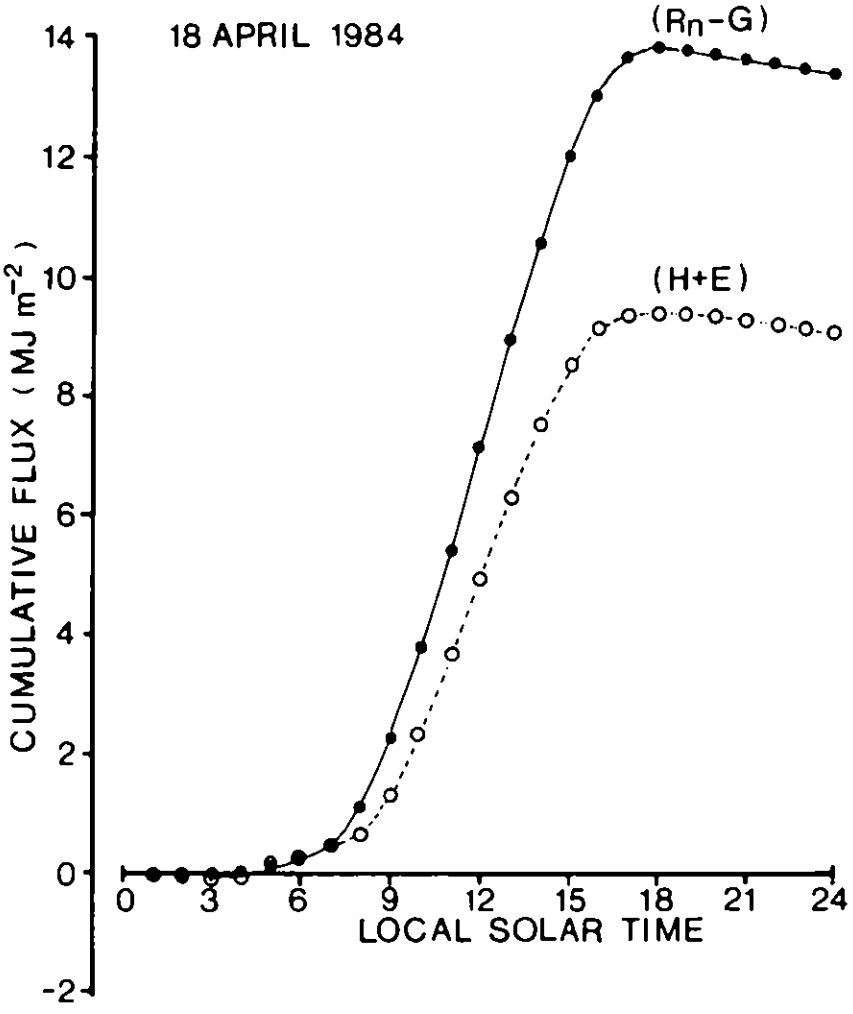

Figure 7. A comparison of the cumulative flux of available energy (R_n-G) with the cumulative sum of the sensible and latent heat fluxes (H + E) measured by the Hydra on 18 April 1984.

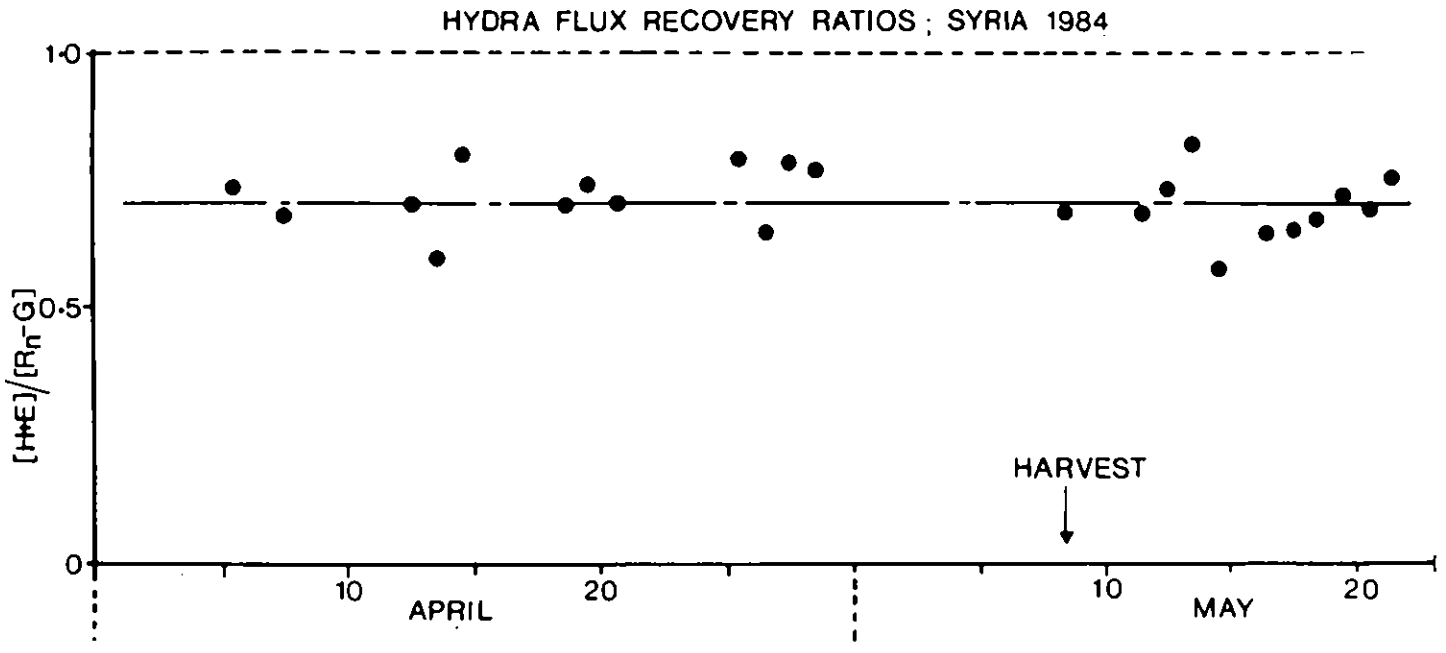

Figure 8. Daily values of the Hydra flux recovery ratio, $(H + E)/(R_n - G)$, obtained before and after harvest.

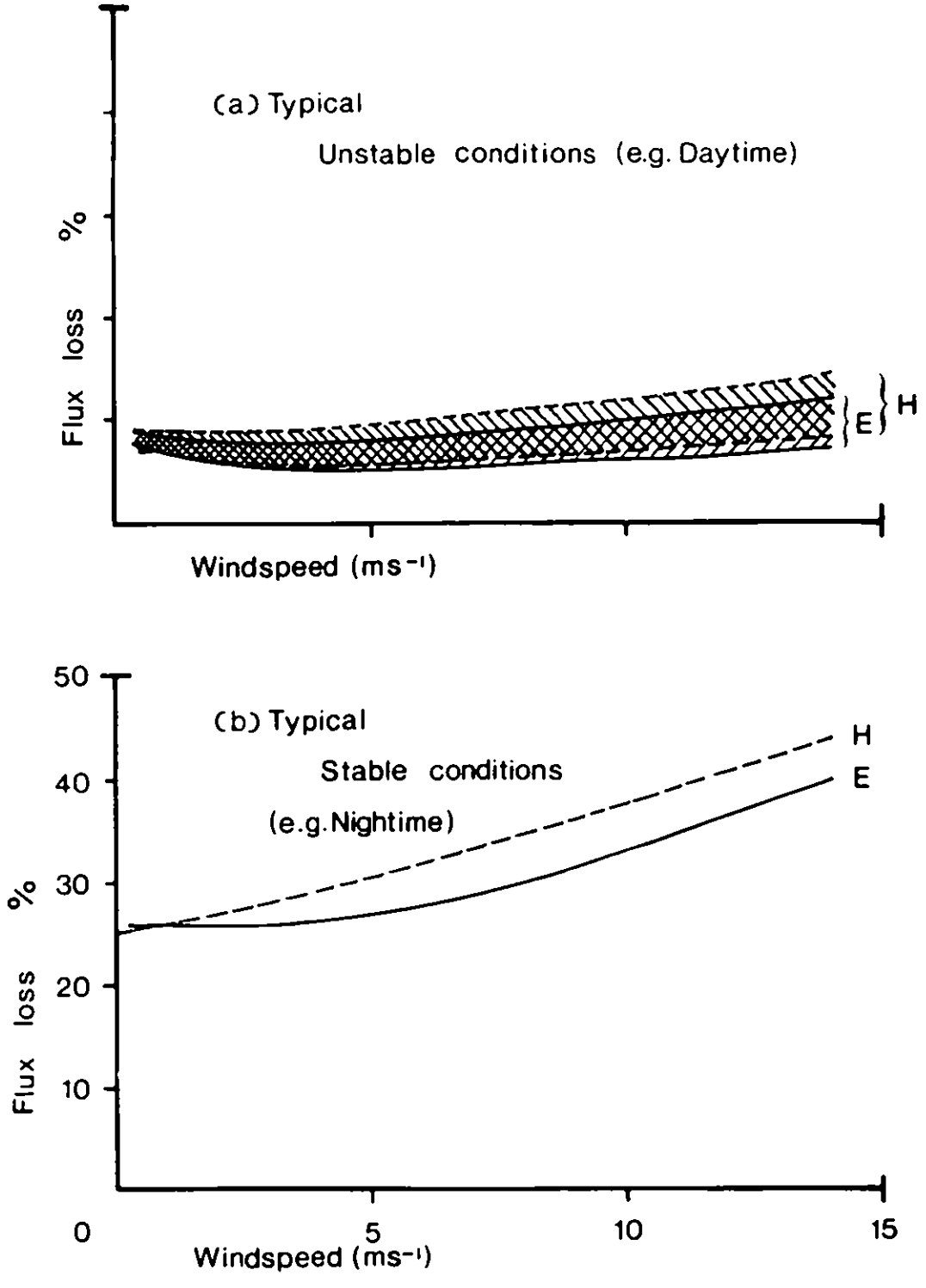

Figure 9. Predicted high frequency flux loss in (a) Unstable (z/L = - 1) and (b) stable (z/L = + 1) conditions using the Hydra at a height of 3.45 m above a crop 0.53 m high.

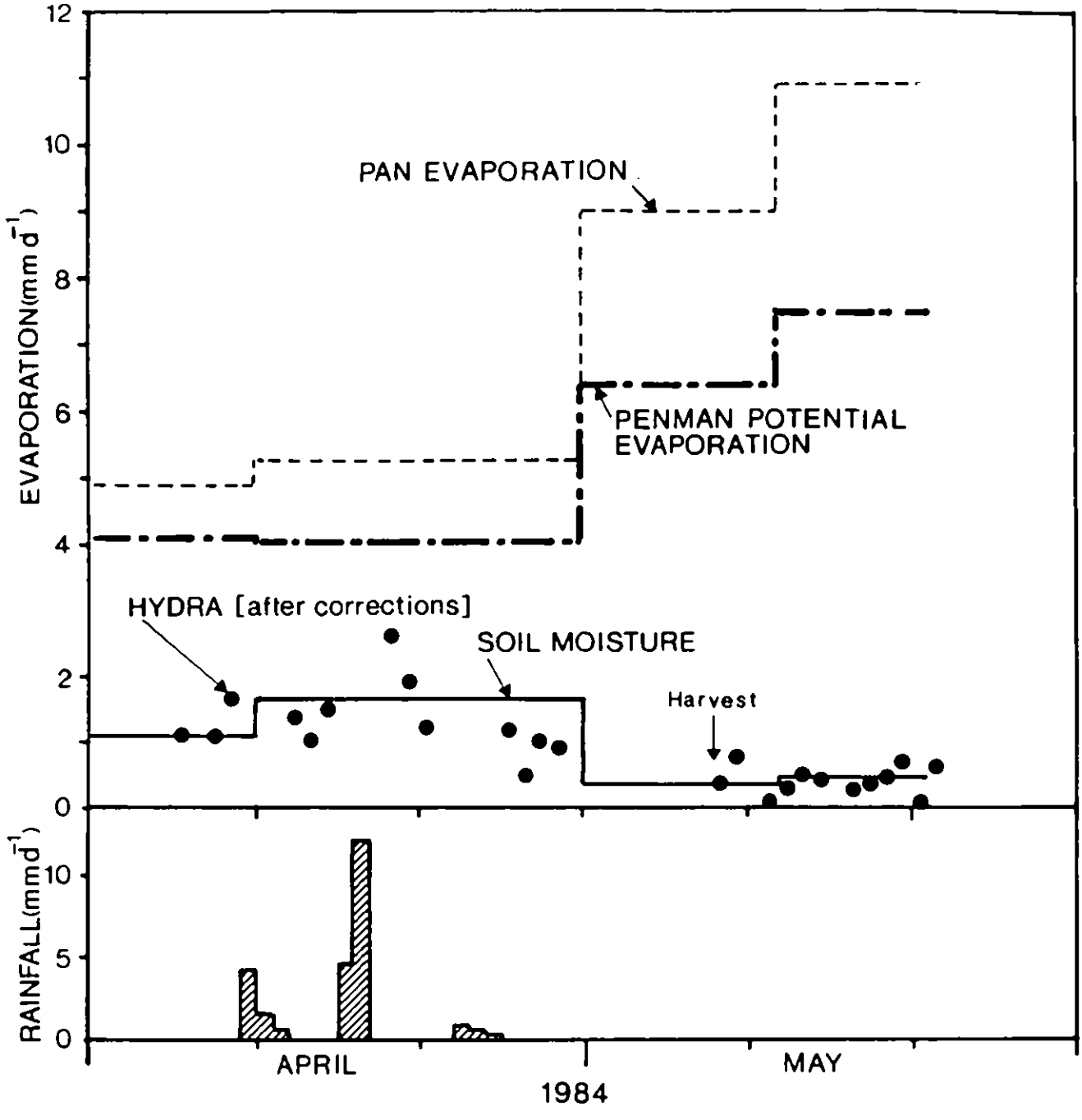

Figure 10. A comparison of daily evaporation measured by the Hydra (corrected for temperature drift and high frequency flux loss) and evaporation deduced from the soil moisture balance. Rainfall, class A pan and Penman potential evaporation are also shown for comparison.

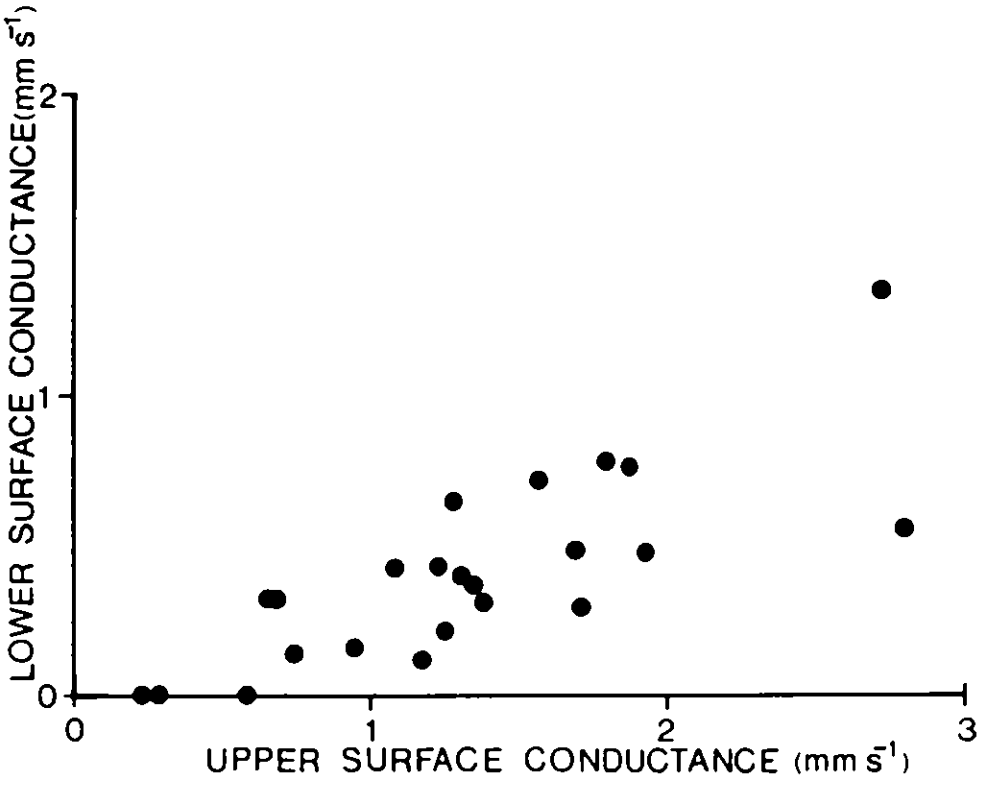

Figure 11. A plot of the stomatal conductances of the adaxial and abaxial surfaces of barley leaves. Data are from 28 March 1984.

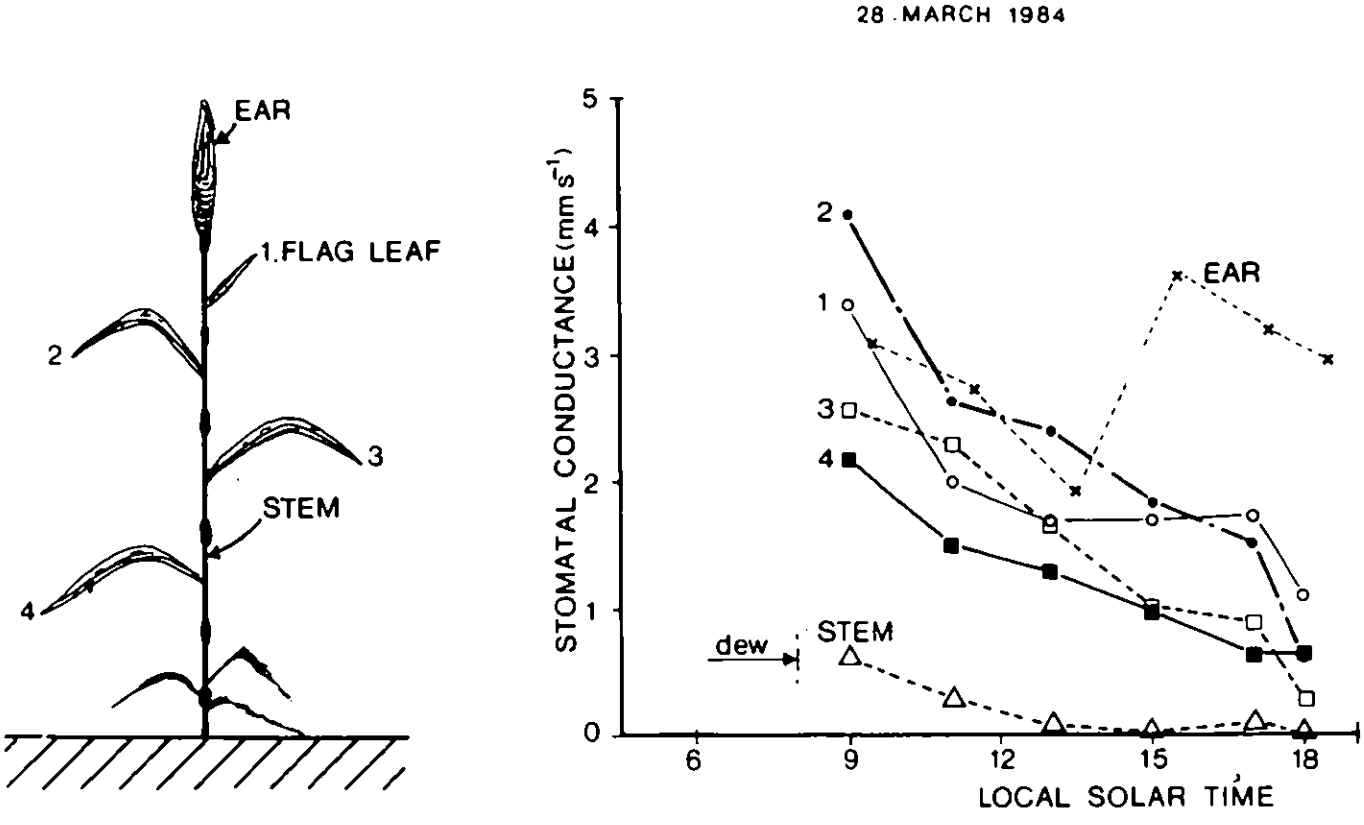

Figure 12. Diurnal variation in the stomatal conductance of the leaves, stem and ear on 28 March 1984.

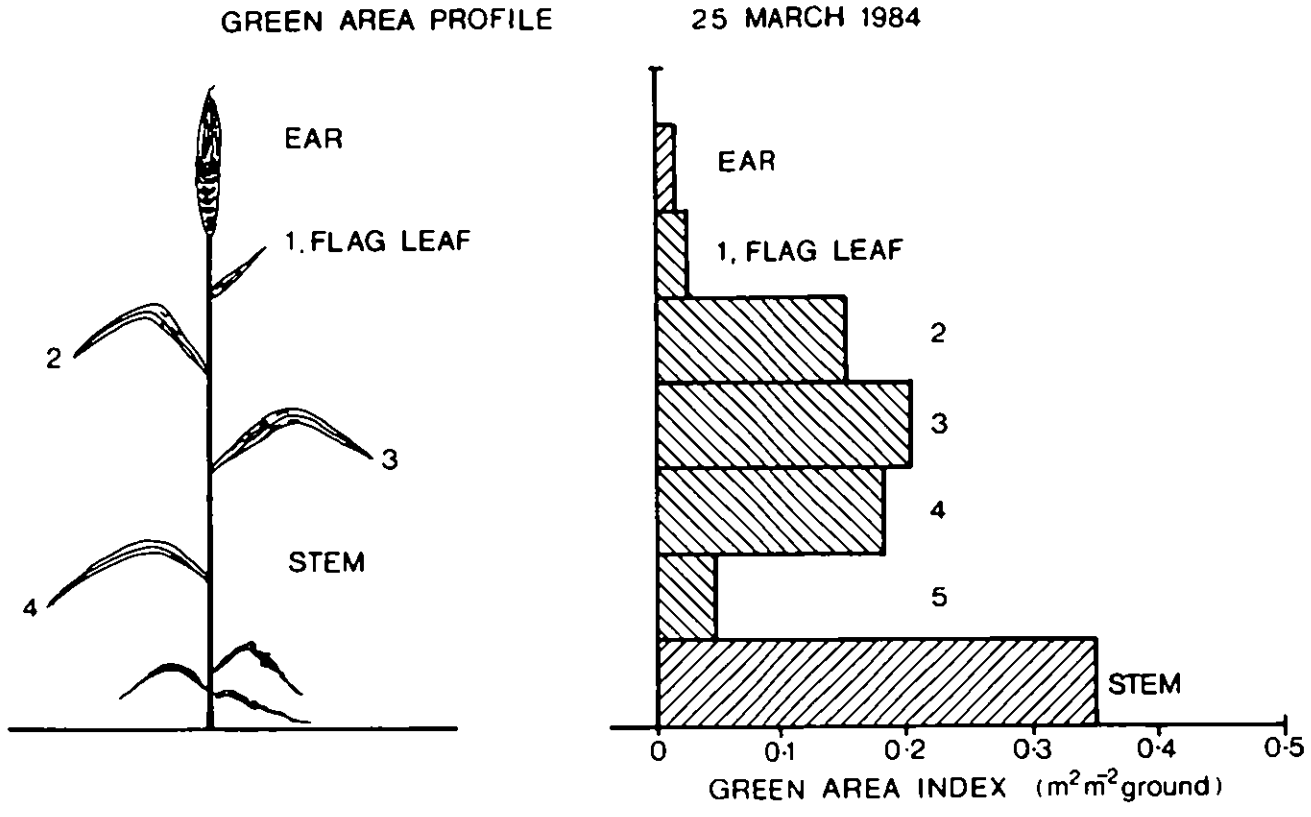

Figure 13. The projected green area index of the ears, leaves and stems on 25 March 1984.

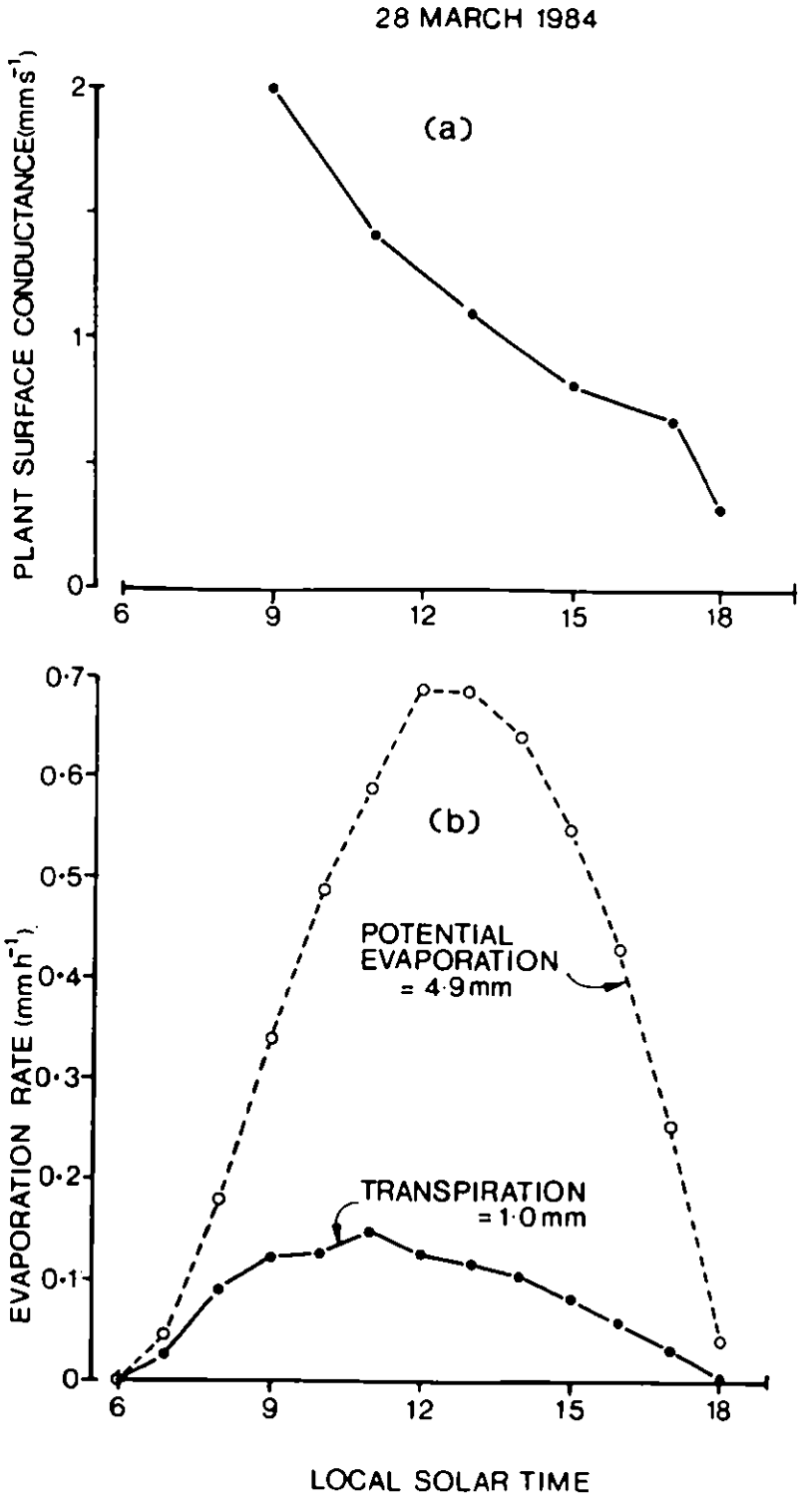

Figure 14. Diurnal variation in (a) plant surface conductance and (b) actual and potential transpiration on 28 March 1984.

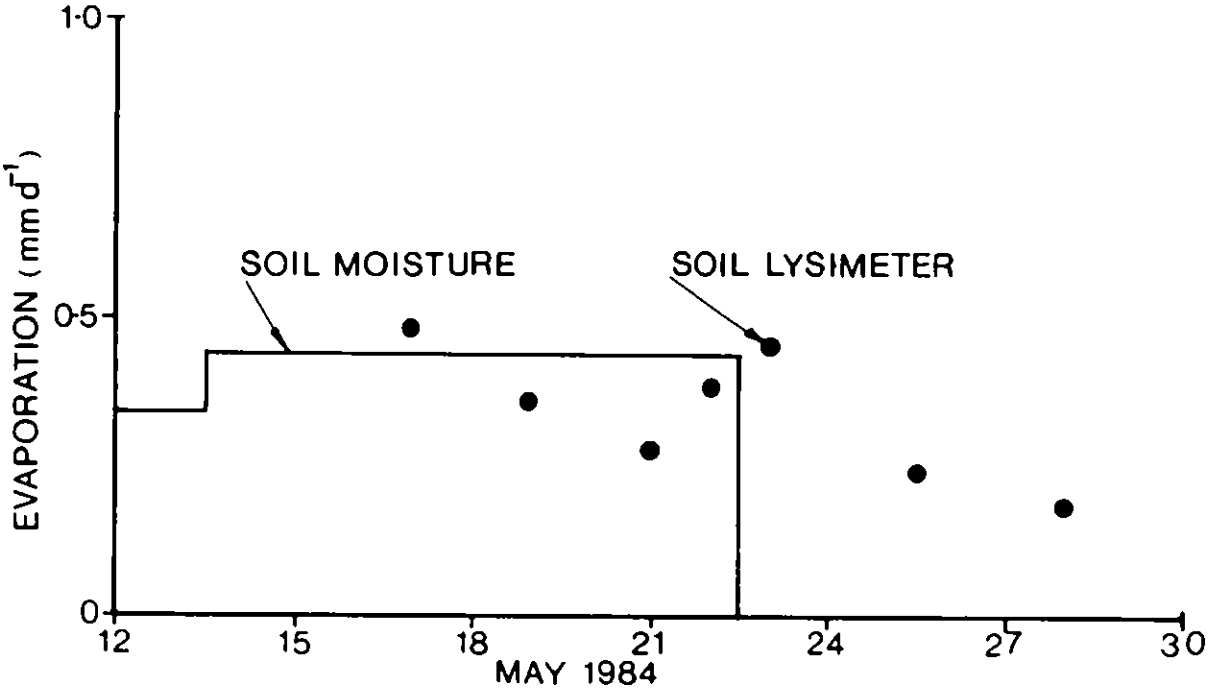

Figure 15. A comparison of soil evaporation (a) measured using a small soil lysimeter and (b) calculated from the change in soil moisture content during May 1984.

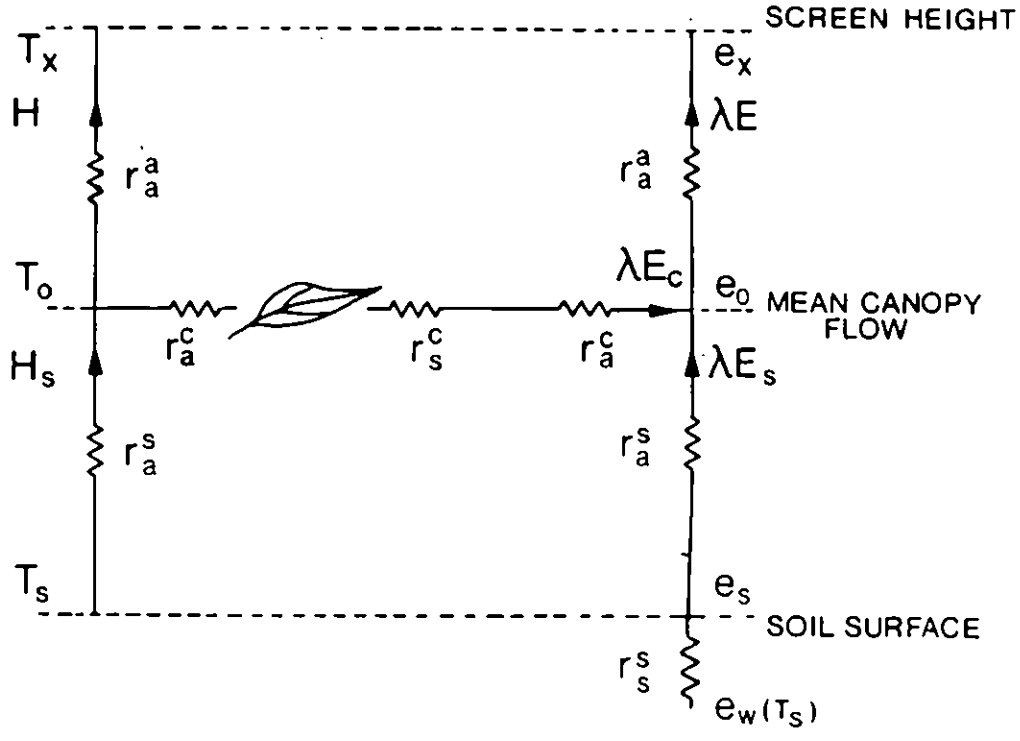

Figure 16. Schematic diagram of the one dimensional description of energy partition for sparse crops. The nomenclature used is given in Appendix IV.

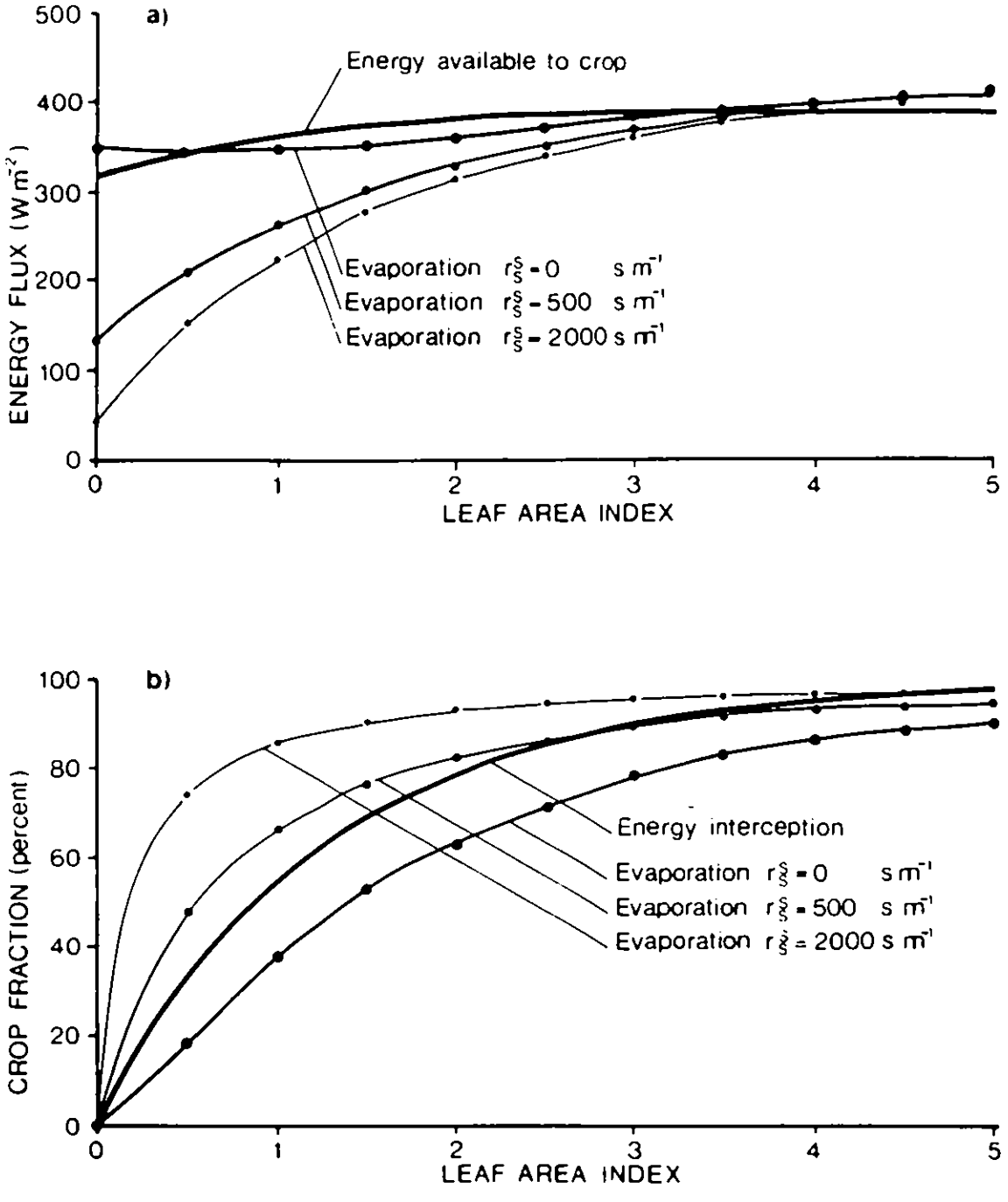

Figure 17(a) Computed total crop evaporation rates expressed as a function of leaf area index for the model and conditions described in the text, with substrate surface resistances of 0,500 and 2000 s m^{-1}, compared with the energy available to the crop.

(b) Fraction of total evaporation originating from the plants expressed as a function of leaf area index computed for the model and conditions described in the text with substrate surface resistances of 0,500 and 2000 s m^{-1}. (R_n, T_x, u, D, C,n, r_{ST}, r_b, x, h and z_o' held constant)

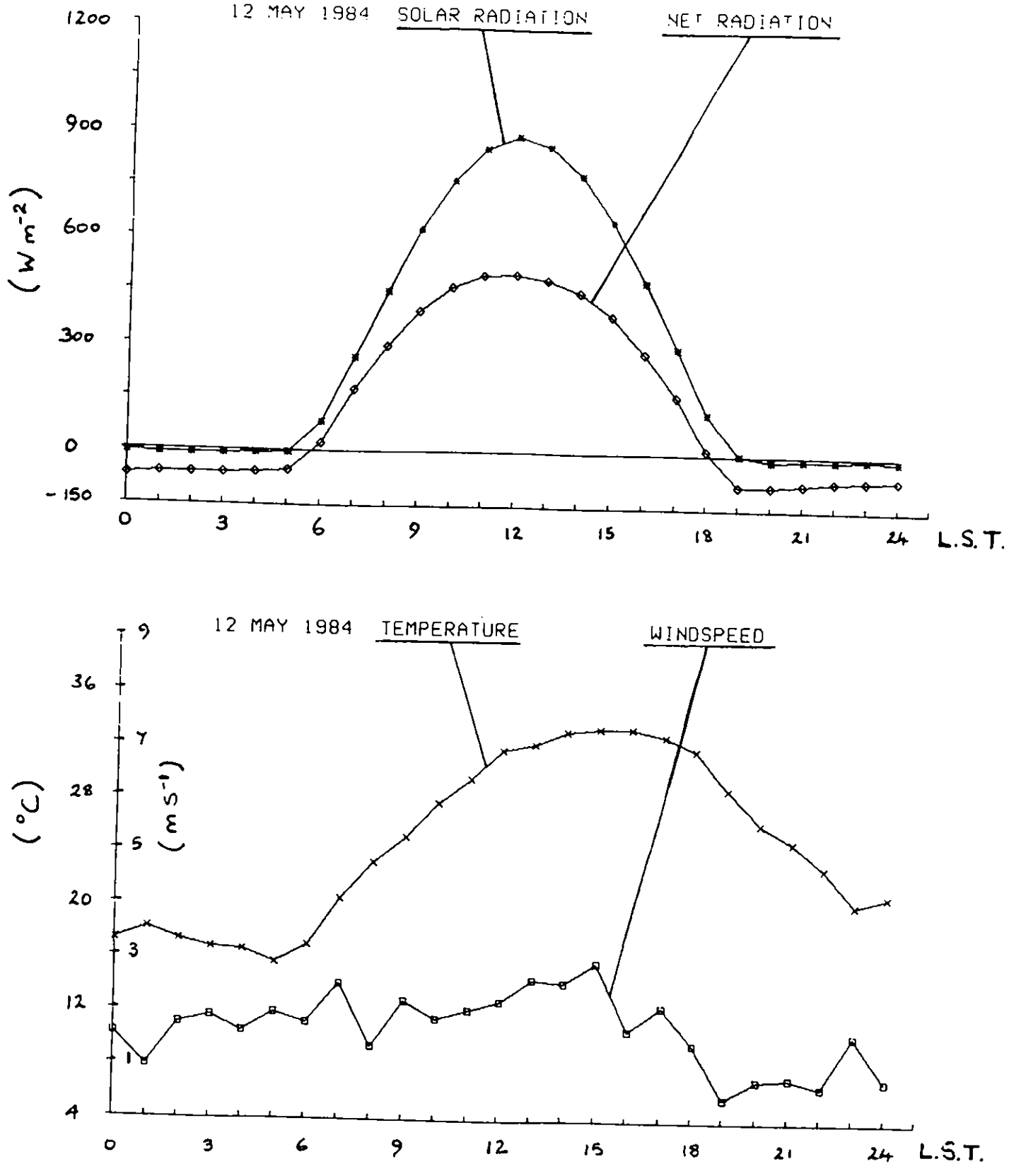

Figure 18. An example of the computer plotted weather data from 12 May 1984. In practice four different colours can be used (black, blue, red and green).

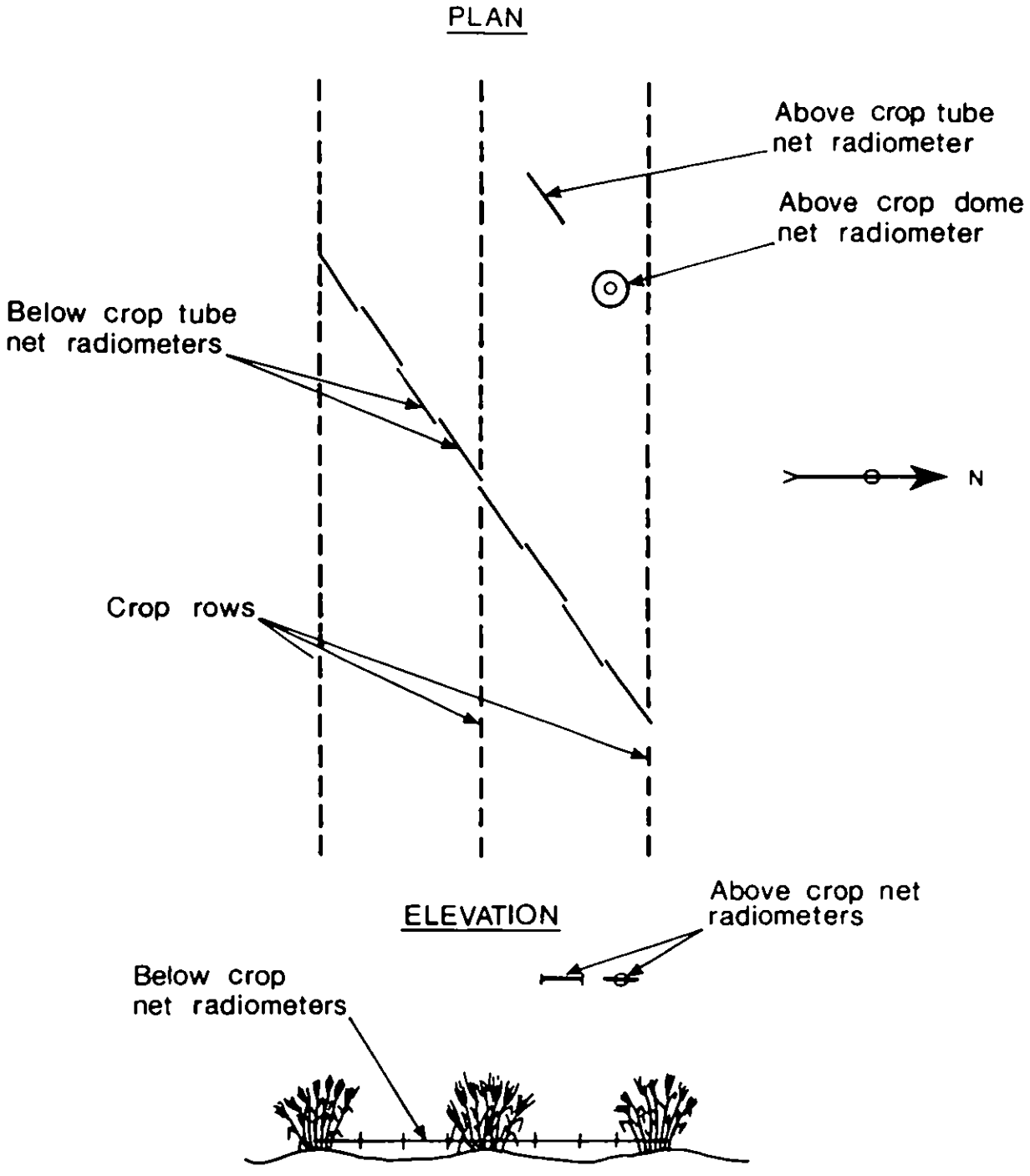

Figure 19. Schematic diagram showing the arrangement of radiometers used to measure net radiation interception (not to scale).

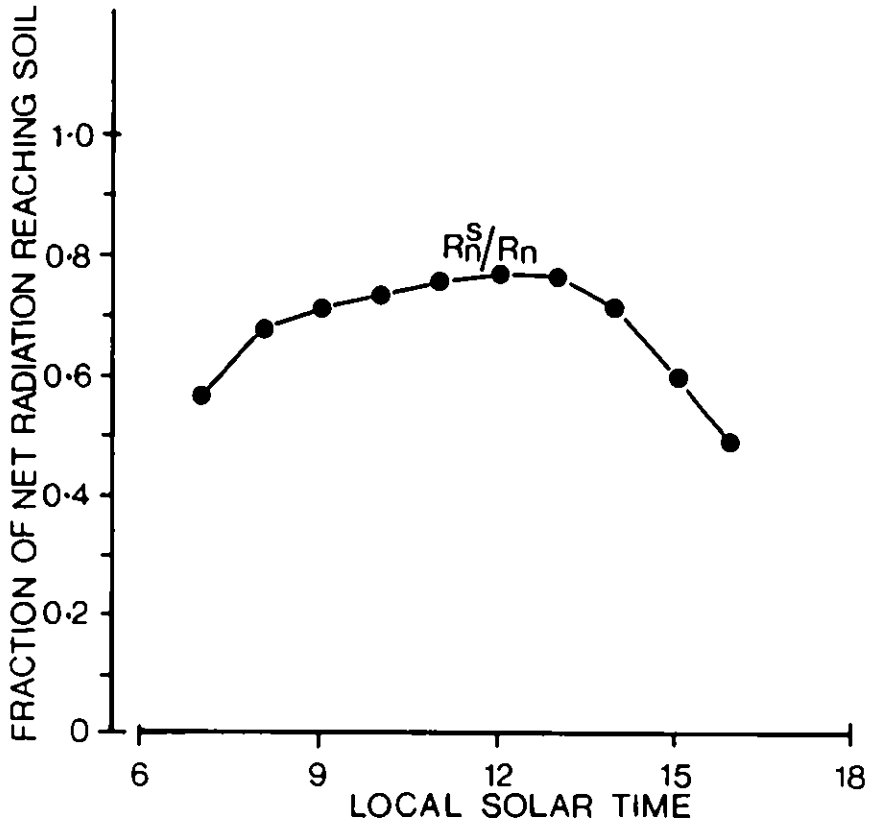

Figure 20. The mean fraction of net radiation reaching the soil (R_n^s/R_n) during three cloudless days before harvest. (1, 5 and 6 May 1984).

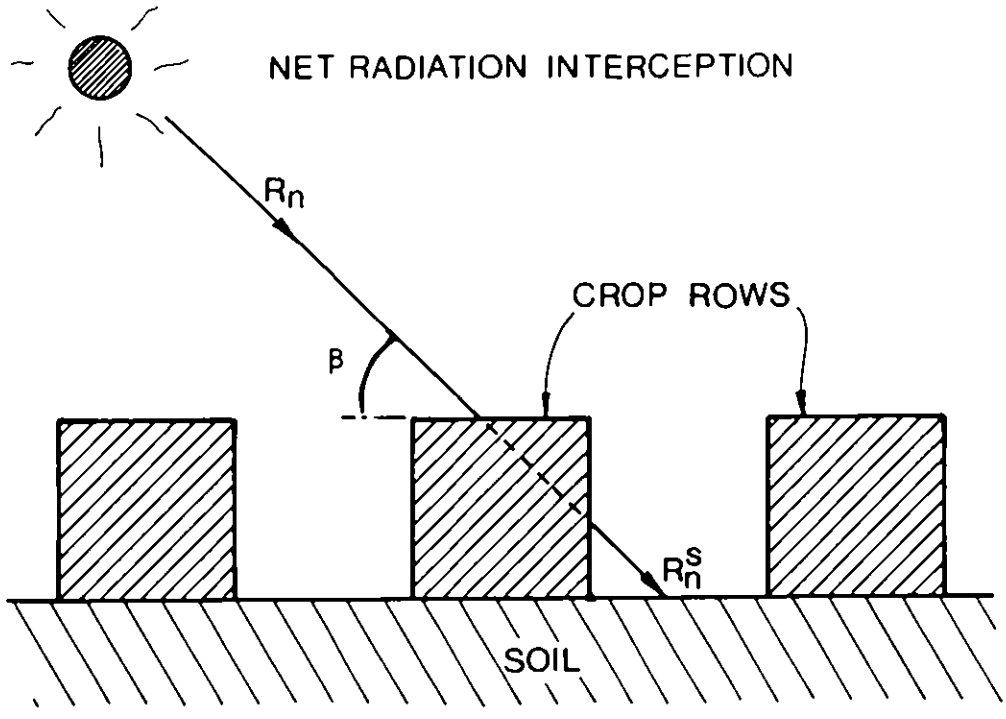

$$R_n^s = R_n \exp(-K L)$$

where, L is the leaf area index and

K is the extinction coefficient, given by

$$K = K_{min} / \sin\beta$$

β is the solar altitude.

Figure 21. Schematic representation of net radiation interception in a crop with rows orientated East-West.

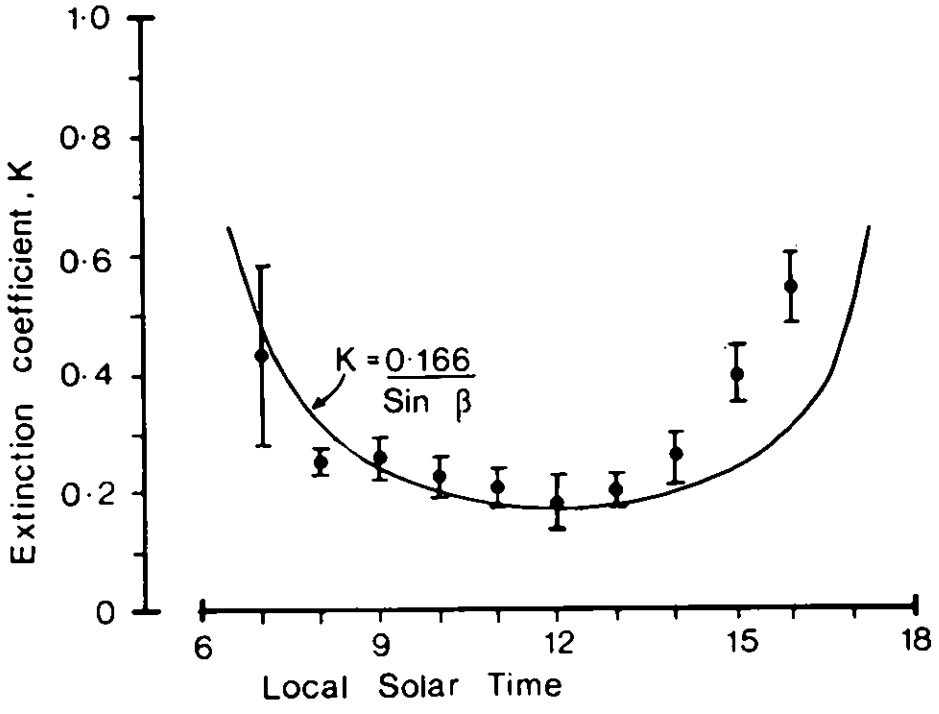

Figure 22. Diurnal variation in the net radiation extinction coefficient, K. The solid line is the relationship predicted from the variation in optical path length through the crop with solar zenith angle, β.

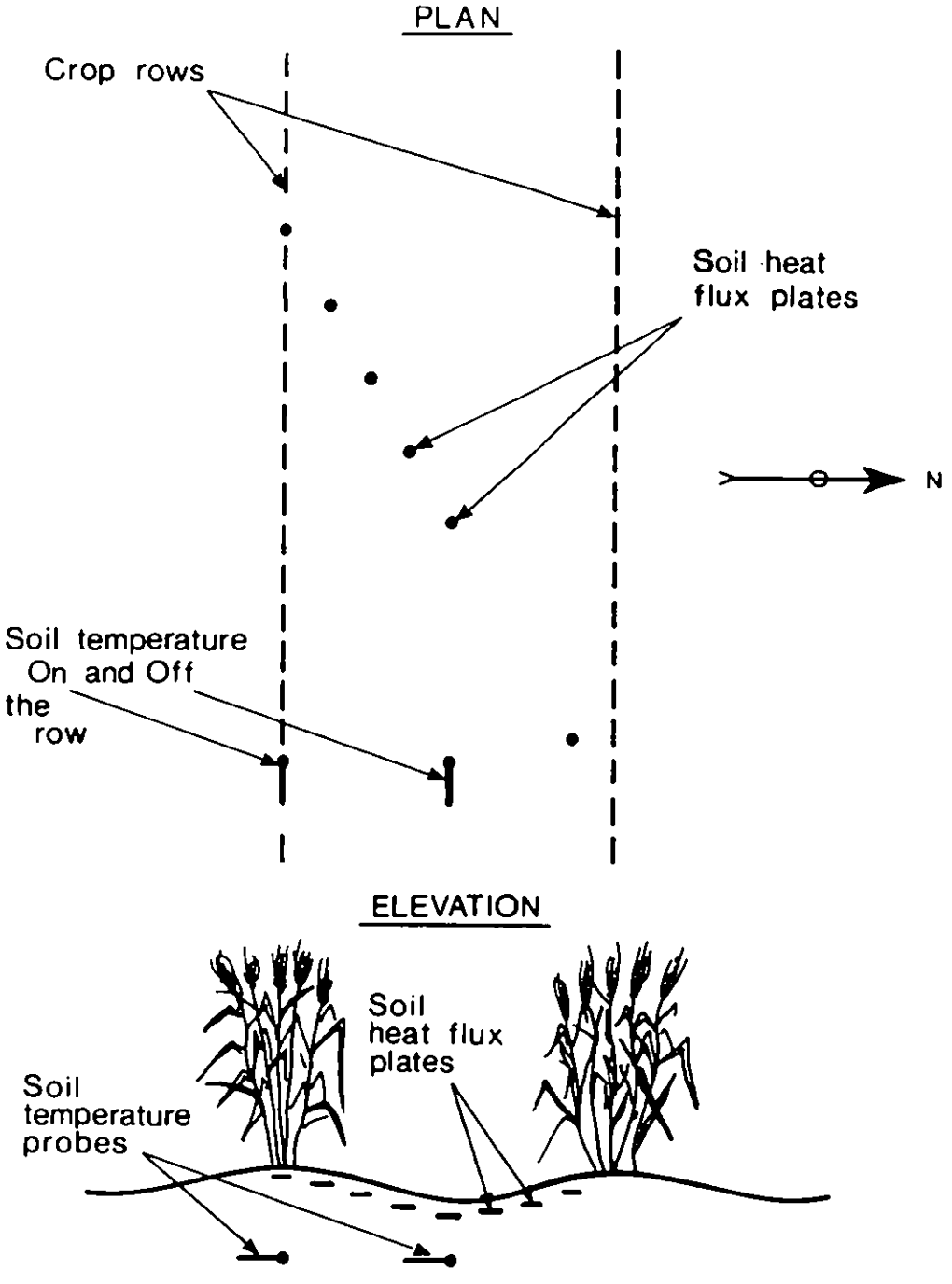

Figure 23. Schematic diagram showing the location of the soil heat flux plates and temperature probes (not to scale.).

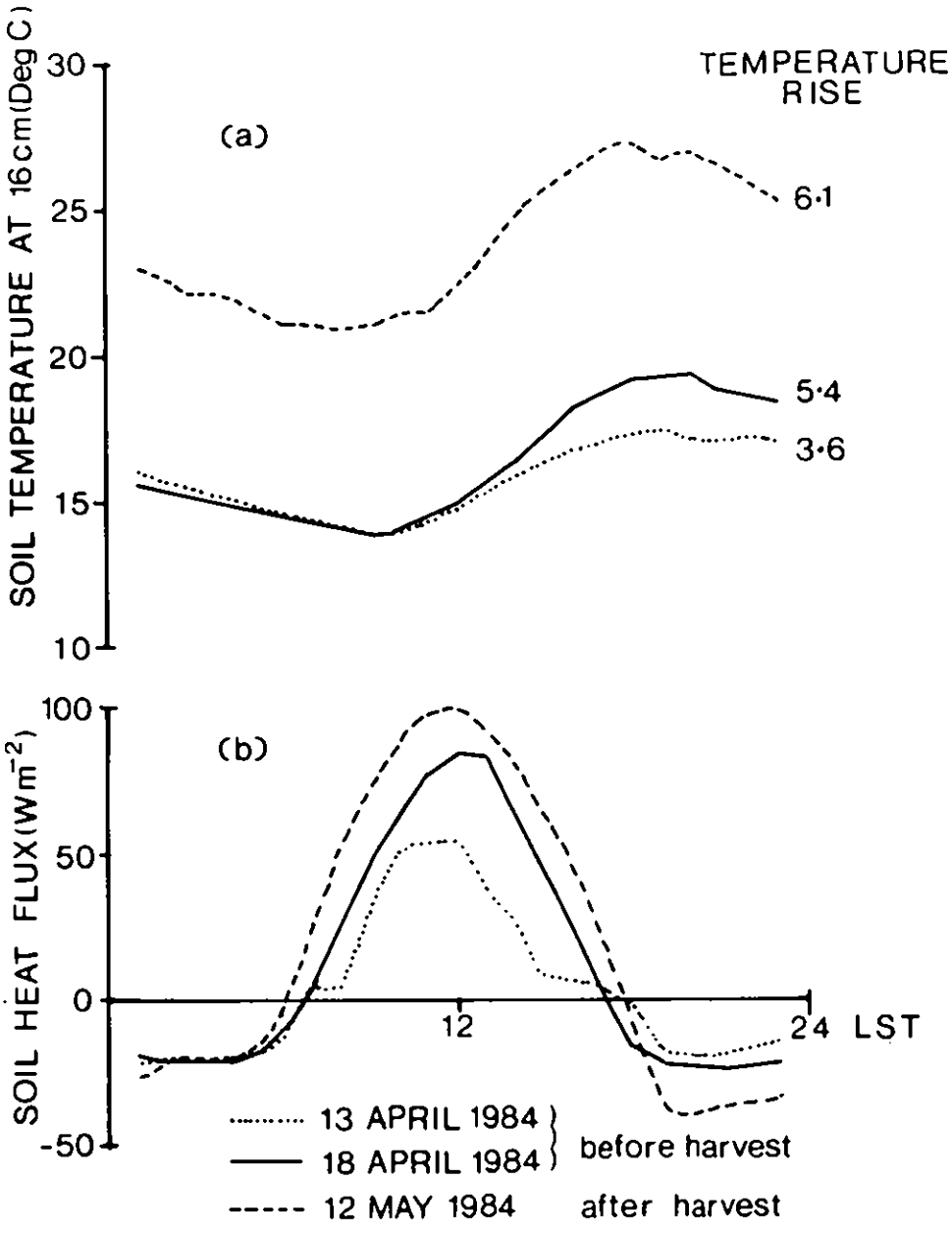

Figure 24. Three examples of the diurnal change in soil (a) temperature and (b) heat flux.

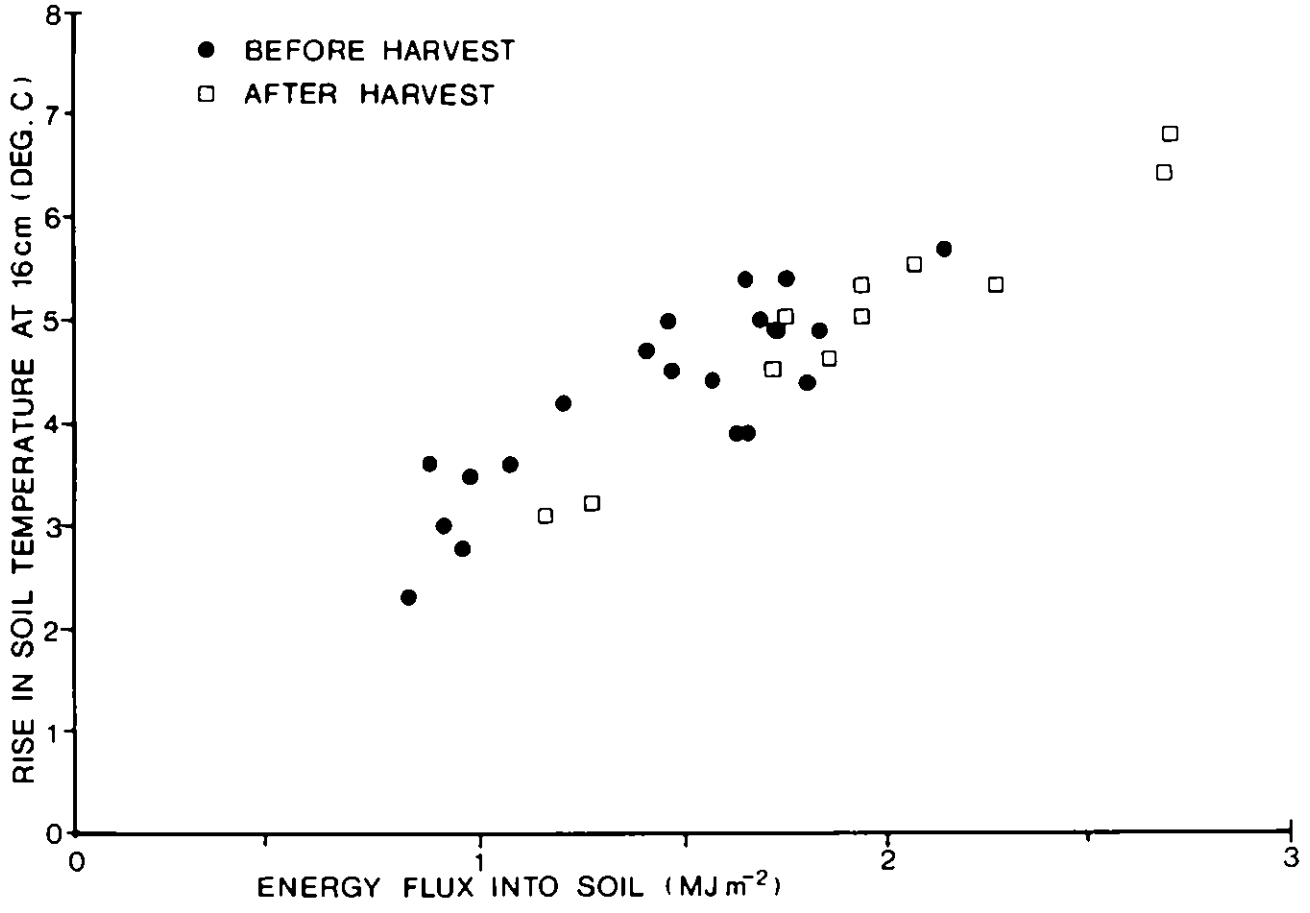

Figure 25. A plot of the rise in soil temperature at 16 cm against total energy flux into the soil for a number of days before and after harvest.

9. APPENDIX I. THEORETICAL ESTIMATES OF THE SAMPLING ERROR IN THE MICROMETEOROLOGICAL MEASUREMENTS AT TEL HADYA

INTRODUCTION

In common with most agricultural research stations the plots at Tel Hadya are not of a size that would normally be considered adequate for micrometeorological measurements. Although the maximum fetch, some 400 m, would probably be thought sufficient; for wind directions other than along the long length of the plot rectangle the fetch must become increasingly marginal as the wind blows over shorter distances of the crop under study. This note attempts to quantify the sampling error involved in the Hydra measurements by application of the recently developed effective fetch theory (Gash, 1985). This theory, by treating water vapour as a passive contaminant to the flow, applies diffusion equations to estimate the effect upwind sample of a point evaporation measurement. The theory contains simplifying assumptions, which have previously been estimated to result in errors of the order of ±20 per cent in the calculated distances. The theory is also restricted to conditions of neutral atmospheric stability (i.e., no temperature gradient) and changes in surface roughness are not accounted for. The results of this analysis should therefore be treated as an approximate guide rather than accurate predictions.

THEORETICAL BACKGROUND

The F per cent effective fetch is defined for an infinite fetch, as the distance upwind of the point of measurement from which F per cent of the water vapour molecules responsible for the measured flux are evaporated. The derivation is too lengthy to be repeated here, but the result is given by the relationship:

$$x_F = \frac{\ln(z_M/z_o) - 1 + z_o/z_M}{k^2 \ln (F/100)} \qquad (A1)$$

k = von karman's constant, taken as 0.41

x_F = the F per cent effective fetch

z_o = the roughness length

z_M = the height of measurement above the zero plane displacement.

Suppose the fetch is not infinite, but that the distance beyond x_F is comprised of vegetation evaporating, not at the rate of the crop under study, E, but at a rate CE. Then if there is only negligible change in the aerodynamic roughness of the surface at the interface, the fractional "error" in the measurement resulting from having an inadequate fetch is given by

$$\frac{E_{meas}}{E} = C + (1 - C)\, e^{z_M\,(\ln(z_M/z_o) - 1 + z_o/z_M)/k^2\; x_F} \qquad (A2)$$

where E_{meas} is the evaporation as measured by the instrument.

RESULTS

Equation (A1) has been evaluated for the following conditions:

i. z_M = 3.0 m, assuming an actual measurement height of 3.4 m above ground and a zero plane displacement of 0.4 m, approximately three quarters of the crop height at maturity, 0.55 m.

ii. z_o = 0.055 m, assuming the roughness length is 10 per cent of the crop height at maturity.

The results are shown in Figure (A1) as isopleths of F for both the instruments at Tel Hadya. This figure shows the sample the instruments would have if there were an infinite fetch of barley.

In practice as the fetch is limited we invoke Equation (A2), with the assumption that the change in roughness at the edge of the plot can be neglected. Table (A1) shows the result of evaluating Equation (A2) with the same values of z_M and z_o as used previously, and for C = 1.2 or 0.8 ($C > 1$ results in a positive error; $C < 1$ a negative error). These values of C are considered likely to be typical.

DISCUSSION

It can be seen from Table (A1) that for wind directions between 270° through north to 30° for Hydra S and for 270° through south to 150° for Hydra N, the theory predicts a sampling error of less than 5 per cent, under the conditions specified. An error of 9 per cent or less is obtained for all wind directions from one or other instrument and a maximum error of 13 per cent is estimated for the shortest fetch. The measurement error of the Hydra should be in the range 5 to 15 per cent. The sampling error for the 240° sector centred on the prevailing westerly wind direction should therefore be less than the measurement error and probably can be considered negligible. Some care should be taken in interpreting the results for sector from 30° to 150°.

REFERENCES

Gash, J.H.C. 1985. A simple method for estimating the effective fetch of micrometeorological evaporation measurements. Submitted to Boundary-layer Meteorology.

Table A1 **The change in fetch and error in evaporation with wind direction for the two Hydras at Tel Hadya.**

Wind direction (degrees)		Fetch over barley	Error for C=1.2 or 0.8
Hydra S	Hydra N	(m)	(%)
270	270	410	2
290	250	436	2
310	230	311	3
330	210	231	4
350	190	203	5
10	170	203	5
30	150	180	5
50	130	117	7
70	110	96	9
90	90	90	9
110	70	96	9
130	50	78	10
150	30	58	12
170	10	51	13
190	350	51	13
210	330	58	12
230	310	65	11
250	290	146	6
270	270	410	2

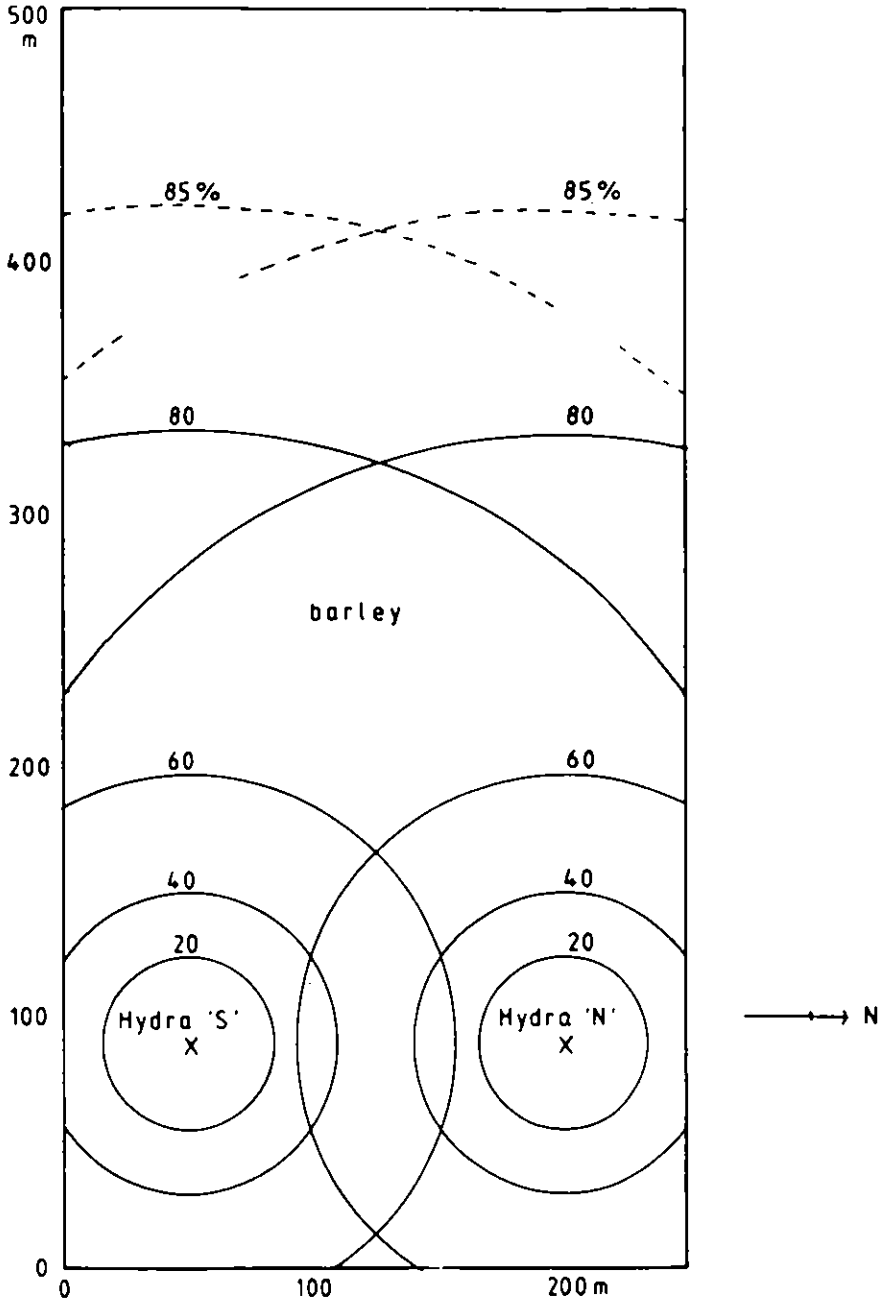

Figure A1.1 Isopleths of % effective fetch for the two instrument positions, Hydra S and Hydra N, in the Tel Hadya barley field, 1984.

10. APPENDIX II. "ARMA Constants : their consequence on frequency attenuation in eddy correlation flux calculations, and flux contamination through correlated sensor drift

This note reports calculations with programs which simulate those which are (or could be) carried out in the on-line Hydra software. They follow the description given by Lloyd et.al. (1984), except in the case of certain calculations made with a 'w prefilter'. In this case the vertical windspeed, w, supplied to the standard set of flux calculations is obtained from the observed vertical windspeed, w_{OB}, by the following procedure

$$w = w_{OB} - \langle w_{OB} \rangle \qquad \text{(AII.1)}$$

where $\langle w_{OB} \rangle_i = \langle w_{OB} \rangle_{i-1} + (1-a)\, w_{OB}$ (AII.2)

The ARMA constant, a, is given in this and other calculations by the expression

$$a = \exp(-\Delta t/\tau) \qquad \text{(AII.3)}$$

where Δt is the 'coupling frequency' used to input values to the calculations and τ is the time constant studied.

(i) Frequency Attenuation of Calculated Eddy Fluxes

Simulated inputs of vertical windspeed, temperature and (in effect) humidity were created with the following form

$$a \sin\left(\frac{2\pi t}{T}\right) \qquad (m\ s^{-1}) \qquad \text{(AII.4)}$$

$$T_p = 18 + b \sin\left(\frac{2\pi t}{T}\right) \qquad (^{\circ}C) \qquad \text{(AII.5)}$$

$$8.5 \left[1 + c \sin\left(\frac{2\pi t}{T}\right)\right] \quad \text{(Volts)} \qquad \text{(AII.6)}$$

Here w is vertical windspeed, T_p is temperature, V is the voltage given by the hygrometer ($\frac{\Delta V}{V} \propto \Delta q$), t is the time, and T the period of the simulated oscillation. These inputs generate fluxes of sensible heat (H) and latent heat (λE) when passed through the ARMA eddy correlation analysis, and test the sensitivity of this analysis at a frequency which is <u>twice</u> that of the basic inputs i.e. $H \propto (wT_p) \propto (\sin^2 wt) \propto 1/2\ (1 - \cos 2wt)$. Calculations for a given value of T are providing information on attenuation for fluxes with a period (T/2).

Calculations were made with samples made 60l times per hour and were allowed to proceed for 10 hours. The average flux given over the last four hours was used. (<u>Note</u> With low frequency inputs hourly average fluxes are sometimes 'noisy' from one hour to the next). The flux obtained in this way was normalized by that calculated at high frequency (T = 0.5 min) to obtain the flux attenuation as a function f, of the oscillation period present in the artificial flux.

The results are shown in Figure AII.1(a) for sensible heat (H) and latent heat (λE), and for two ARMA time constants 18.25 and 6.25 minutes. This illustrates that the ARMA eddy flux calculation provides fluxes with an acceptance which does not fall off exponentially with a time constant τ, (as expected by some Hydra users). The primary observations are

(a) The acceptance for latent and sensible heat are different (presumably related to the fact that we make a 'double' ARMA in calculating latent heat).

(b) The acceptance falls off much more slowly than might be expected. They fall to 37 per cent of their initial values in about 2.5 τ for latent heat and 3.5 τ for sensible heat.

(c) The form of the function is not a decaying exponential. The behaviour down to f = 0.5 is in fact quite well described by a 'Gaussian' of the form

$$f = \exp\left\{-\frac{1}{2}\left(\frac{T}{\sigma}\right)^2\right\} \qquad \text{(AII.7)}$$

where $\sigma = 1.72\,\tau$ for λE (AII.8)

and $\sigma = 2.5\,\tau$ for H (AII.9)

These are the broken lines shown in figure AII.1(a). For longer periods (lower frequency) flux contributions, the fall in F is much slower than this and has a long 'tail' to low frequency. The presence of this tail gives rise to drift generated flux contamination which is discussed in a later section.

An interesting consequence of incorporating the 'w prefilter', specified by equations AII.1 and AII.2, is that the acceptance functions for sensible heat and latent heat become identical and virtually identical to that for latent heat without a w prefilter. The resulting acceptance functions are shown in Figure AII.1(b). The dotted lines are given by equation AII.7 with $\sigma = 1.72\,\tau$.

(ii) Drift Contamination of Flux and Deviations

The experimental data obtained in Syria was extremely useful in drawing attention to the very real possibility that fluxes and standard deviations calculated using the on-line Hydra software can be contaminated in the presence of correlated drifts in the sensors. The experimental situation there is such that rather large drifts in the outputs of the existing hygrometer and sonic anemometer are generated by the daily temperature cycle, exacerbated by radiation loading on the sensors. In this section we illustrate the problem using data drawn from one particular day (9/5/84) and synthesize the low frequency response of the on-line software using the measured variation in temperature and apparent affect in vertical windspeed. A synthetic hygrometer response to temperature variation is created using the assumption that the voltage output increases by that one per cent per degree. Such a response is consistent with that observed in the field, and is now confirmed in the environment chamber.

Samples of these input functions were taken, one every minute, and calculations made using the standard Hydra software with different time constants, with and without a 'w prefilter' (viz Equations AII.1 and AII.2). The input functions were linear interpolations between hourly mean values which were taken from the raw data, but were 'sharpened' to take out the effect of averaging (Appendix AII.1), and 'advanced' to compensate for the ARMA induced delay. This dual process ensures that the mean values generated by the present ARMA analysis reproduces the mean values observed in the field. The resulting variations in temperature and vertical windspeed are illustrated in Figures AII.2(a) and AII.2(b). Figure AII.2(c) shows the synthetic 'F' function ($F = \left[\frac{V}{\langle V \rangle} - 1\right]$ generated from the assumed relationship with temperature, with ARMA time constants of 18.75 and 6.25 minutes.

Figure AII.3(a) and AII.3(b) illustrate the synthetic or 'pseudo' fluxes of latent and sensible heat generated on this day (9/5/84) as a result of this long term sensor drift. Figure AII.3(c) and AII.3(d) show the 'pseudo' standard deviations in temperature and humidity. All calculations in this figure are made using a time constant of 18.75 minutes, the value used in the field. The dotted lines in Figures AII.3(a) and AII.3(b) illustrate the effect of including a 'w' prefilter in the calculation.

Figure AII.4 illustrates the pseudo fluxes and standard deviation which would have occurred had we used a time constant of 6.25 minutes in the on-line calculations. There is an obvious and dramatic reduction in contamination introduced by correlated sensor drifts with a shorter time constant; including a 'w prefilter' essentially removes the flux contamination altogether in this case.

(iii) Flux Contamination due to Sensor Correlation at Higher Frequency

The previous section investigates flux contamination generated by large cycles of long (daily) duration, but the possibility exists that some contamination of calculated fluxes may occur due to correlations in sensor drift at higher frequencies. To investigate this we assume correlations typical of those observed (in Syria) at the daily time scale also exist at shorter time scales, and set

$$W = A + 0.025\ T_p \qquad (m\ s^{-1}) \qquad \text{(AII.10)}$$

$$V = 8.5\ (1 + 0.01\ T_p)\ \text{(Volts)} \qquad \text{(AII.11)}$$

We pass these through an analysis identical to that described in section (i), using a temperature input function

$$T_p = 0.5 \sin\left(\frac{2\pi t}{T}\right) \qquad \text{(AII.12)}$$

and study the amount of 'pseudo' flux generated as a function of the period of input temperature cycle.

Calculations are made with an ARMA time constant of 18.25 minutes. The results are shown in Figures AII.5(a) and AII.5(b) for two situations: the full line represents the response for sensors with no thermal inertia; the dotted line for windspeed and humidity sensors with the thermal time constants of 5 and 8 minutes respectively. In effect the calculated fluxes are those which would be generated for a standard deviation in temperature of 0.35°C if all the temperature oscillations occurred with a particular oscillation period T, or at a particular frequency (1/T). The fluxes fall off more slowly than the acceptance function described in section (i) because these 'pseudo' fluxes occur at a frequency which is twice that of the driving temperature oscillation.

The quantitative interpretation of Figure AII.5 is difficult because we have no real knowledge of the frequency distribution of the temperature fluctuations. Clearly the presence of finite thermal time constants in the sensors helps significantly, as would the reduction (or removal) of temperature correlated drift in the vertical windspeed and humidity sensors. The figure is more of a warning that a worry, but none-the-less implies that we cannot rule out systematic shifts in measured fluxes in the existing Syrian data, which are related to the standard deviation of temperature. For σ_T = 0.35°C, the shift in sensible heat could be + 2 W m^{-2} (maximum + 4 W m^{-2}), and that in latent heat - 5 W m^{-2} (maximum - 15 W m^{-2}). These sound small, but it should be remembered that a mean daily latent heat flux of + 14 W m^{-2} corresponds to an evaporation of 0.5 mm/d, about the evaporation rate we observed towards the end of the season in Syria.

Shortage of time means we have not been able to complete the analysis of this effect with a shorter ARMA constant, but it is clear that reducing the envelope of the full line curves in Figure AII.5 by a factor of three will greatly improve the situation and reduce the pseudo fluxes generated, particularly for sensors with finite thermal time constants.

(iv) Concluding Remarks

This note is meant to generate discussion rather than reach firm conclusions, but certain observations are apparent. Clearly, the exploration of flux and standard deviation presented here, stimulated and supported by the field observations made in Syria, strongly suggest the use of as short a time constant in the ARMA analysis as possible. It does not necessarily follow that τ = 6.25 min is the best choice in all situations, and further parallel logging experiments with different time constants is called for next year.

The inclusion of a 'w prefilter' in the Hydra program before flux calculation has the effect of generating identical acceptance functions for the sensible and latent heat fluxes, (which is a more elegant), and the practical effect of significantly improving the drift contamination problems. At the same time we have not explored any negative consequences. Parallel logging experiments with and without this feature are also called for.

The hardware changes, presently in hand, to reduce temperature/radiation correlated drift in the vertical windspeed and humidity sensors should considerably improve the quality of measurements given by the Hydra; but, on the basis of this report, a few fairly simple changes in the Hydra software could be of equal or even greater benefit.

(Note. The program 'HYDRA-DRIFT' through which we are presently passing Hydra data attempts to correct for the effects in sections (ii) and (iii) of this note. It synthesises and then subtracts 'pseudo fluxes' generated by long term drift (but using the measured values of F, rather than the synthetic ones used here). It also provides two alternative corrections in line with section (iii) viz.

$$\begin{pmatrix} H' \\ \lambda E' \end{pmatrix} = \begin{pmatrix} H \\ \lambda E \end{pmatrix} + \begin{pmatrix} 2 \\ 5 \end{pmatrix} (\sigma_T/0.351)$$

and

$$\begin{pmatrix} H' \\ \lambda E' \end{pmatrix} = \begin{pmatrix} H \\ \lambda E \end{pmatrix} + \begin{pmatrix} 4 \\ -10 \end{pmatrix} (\sigma_T/0.351)$$

The value of σ_T used in these is itself 'drift' corrected. In practice the second correction is quite small).

Appendix AII.1

'Sharpening' Measured Variations in T, w and F

The process of calculating mean values smooths the apparent variations in experimental values. We obviously cannot recreate the original function which gave rise to the observed hourly mean values, but it is possible to adjust the individual values so that linear interpolation between these values, when passed through an averaging process recreates the observed hourly mean values. Consider three successive hours with average values $\bar{y}_{n-1}$, $\bar{y}_n$ and $\bar{y}_{n+1}$ and assume the input function which generated these was a linear interpolation between the values y_{n-1}, y_n and y_{n+1} and assume the input function which generated these was a linear interpolation between the values y_{n-1}, y_n and y_{n+1} thus:

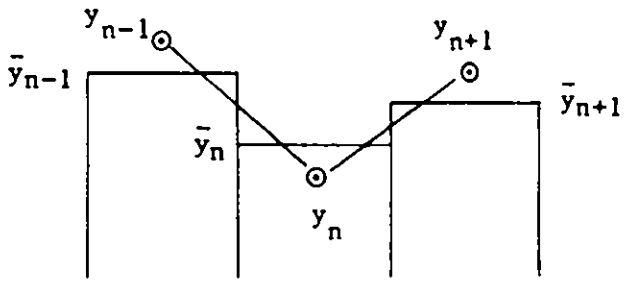

The value of $\bar{y}_n$ is in this case given by

$$\bar{y}_n = \frac{1}{2}\left[\frac{y_n + \frac{y_{n+1} + y_n}{2}}{2} \qquad \frac{y_n + \frac{y_{n-1} + y_n}{2}}{2}\right]$$

$$\frac{y_n}{4} + \frac{y_{n+1}}{8} + \frac{y_n}{8} + \frac{y_n}{4} + \frac{y_{n-1}}{8} + \frac{y_n}{8} \qquad \text{(AII.13)}$$

$$\bar{y}_n = \frac{3}{4} y_n + \frac{y_{n+1}}{8} + \frac{y_{n-1}}{8} \qquad \text{(AII.14)}$$

$$y_n = \frac{4}{3} \bar{y}_n - \frac{1}{6} y_{n+1} - \frac{1}{6} y_{n-1} \qquad \text{(AII.15)}$$

In principle we can calculate the 'sharpened' set of y_n from the available values of $\bar{y}_n$ providing we have limiting values y_0 and y_N, using an iterative procedure. In practice we set $y_0 = \bar{y}_0$ and and $y_N = \bar{y}_N$ using data on either side of the 24 hours of current interest and iterate first forwards and then backwards using equation AII.15 until stability is achieved. In practice 3 double-iterations is enough. The program looks like this:

```
11500 FORK=1TO27:Z2(K)=Z1(K):NEXTK
11502 FORI=1TO3
11510 FORK=2TO26STEP 1
11512 Z2(K)=4/3*Z1(K)-Z2(K-1)/6-Z2(K+1)/6
11516 NEXTK
11520 FORK=26TO2STEP-1
11522 Z2(K)=4/3*Z1(K)-Z2(K-1)/6-Z2(K+1)/6
11526 NEXTK
11530 NEXTI
11599 RETURN
```

Z1 is the original array of hourly average values (with data on either side of the 24 hours of interest) and Z2 is the 'sharpened' values returned to generate the time series supplied to the ARMA analysis.

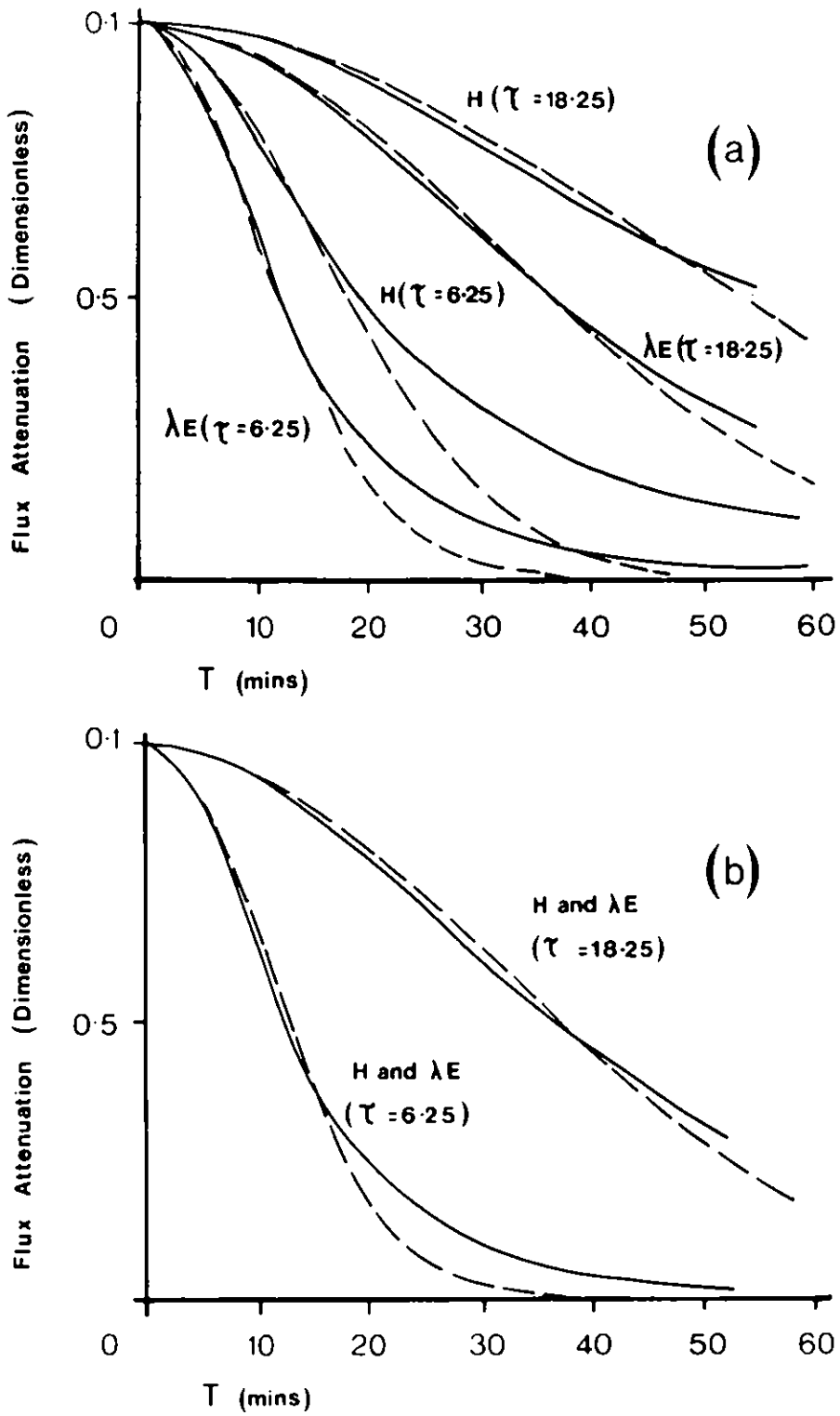

Figure AII.1 (a) The attenuation of sensible (H) and latent heat (λE) fluxes for two ARMA time constants, 18.25 and 6.25 minutes. The dashed lines are Gaussian functions of the form of equation AII.7.

(b) As for (a) but with the 'w prefilter' specified by equations AII.1 and AII.2.

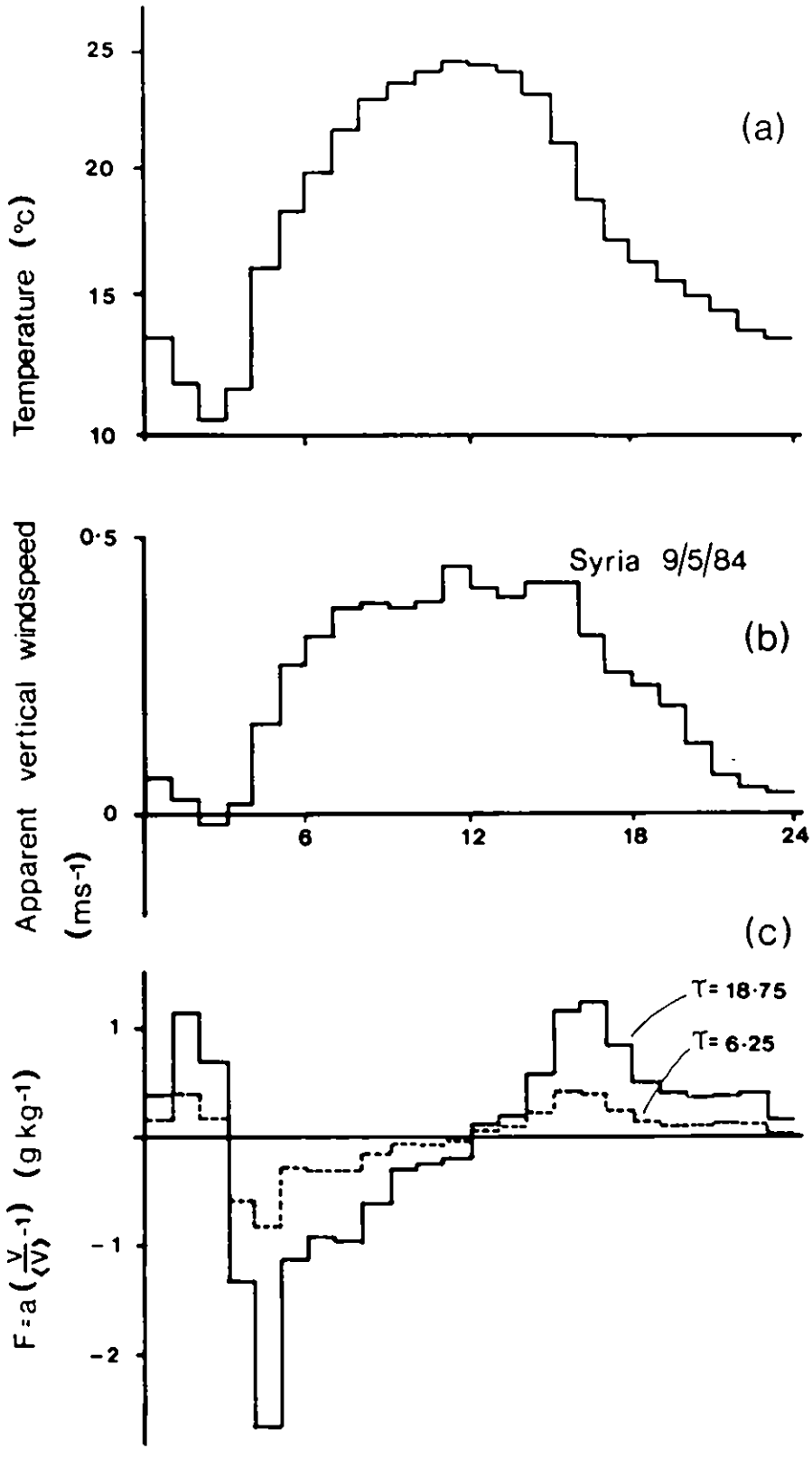

Figure AII.2 The variations in (a) measured temperature (b) apparent vertical windspeed and (c) calculated hygrometer 'F' function ($= \frac{V}{\langle V \rangle} - 1$) on 9 May 1984.

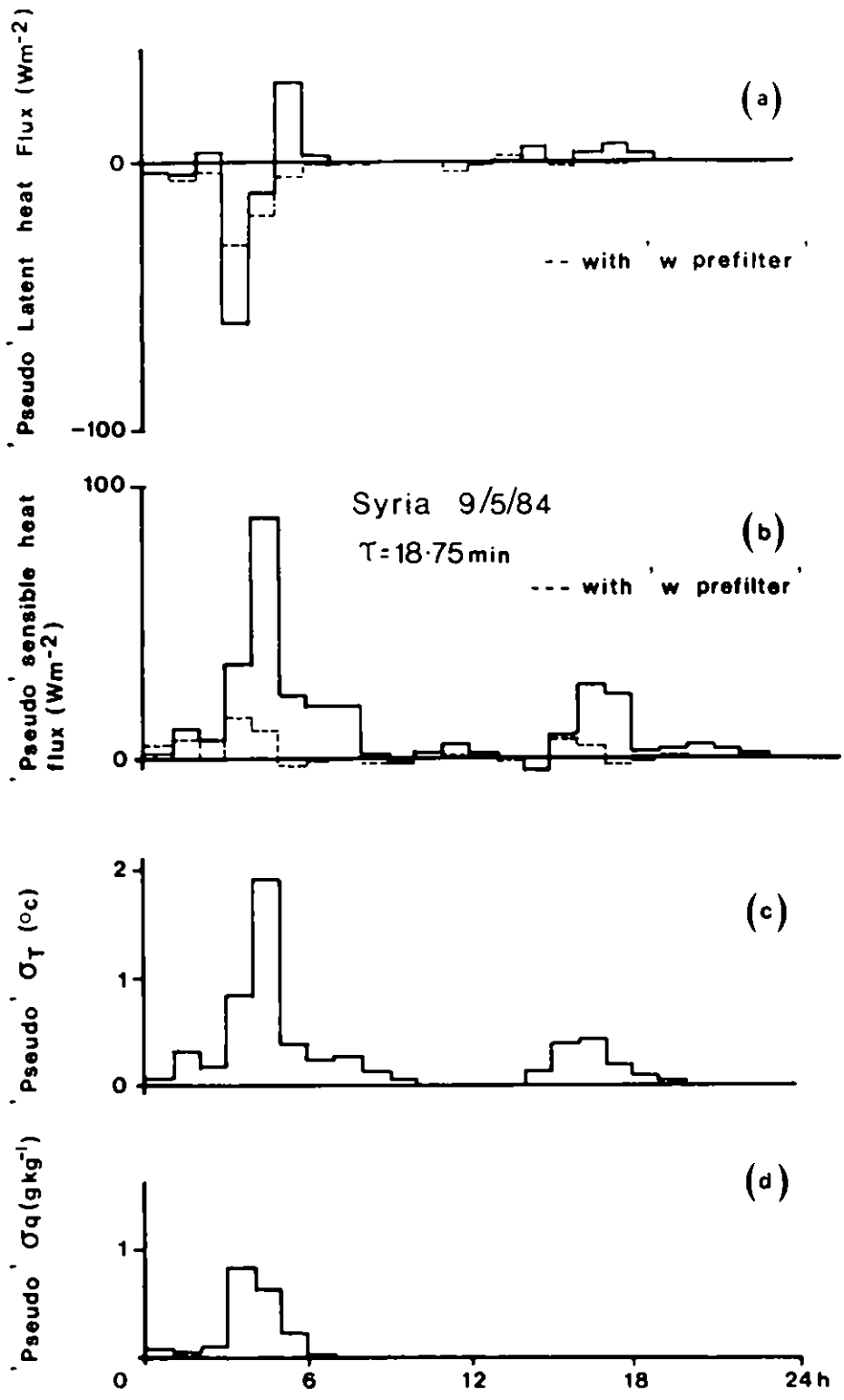

Figure AII.3 Pseudo fluxes of (a) latent and (b) sensible heat as a result of the long term sensor drifts (specified in Figure AII.2) with a time constant τ = 18.25 mm. Pseudo standard deviations in (c) temperature and (d) humidity are also shown.

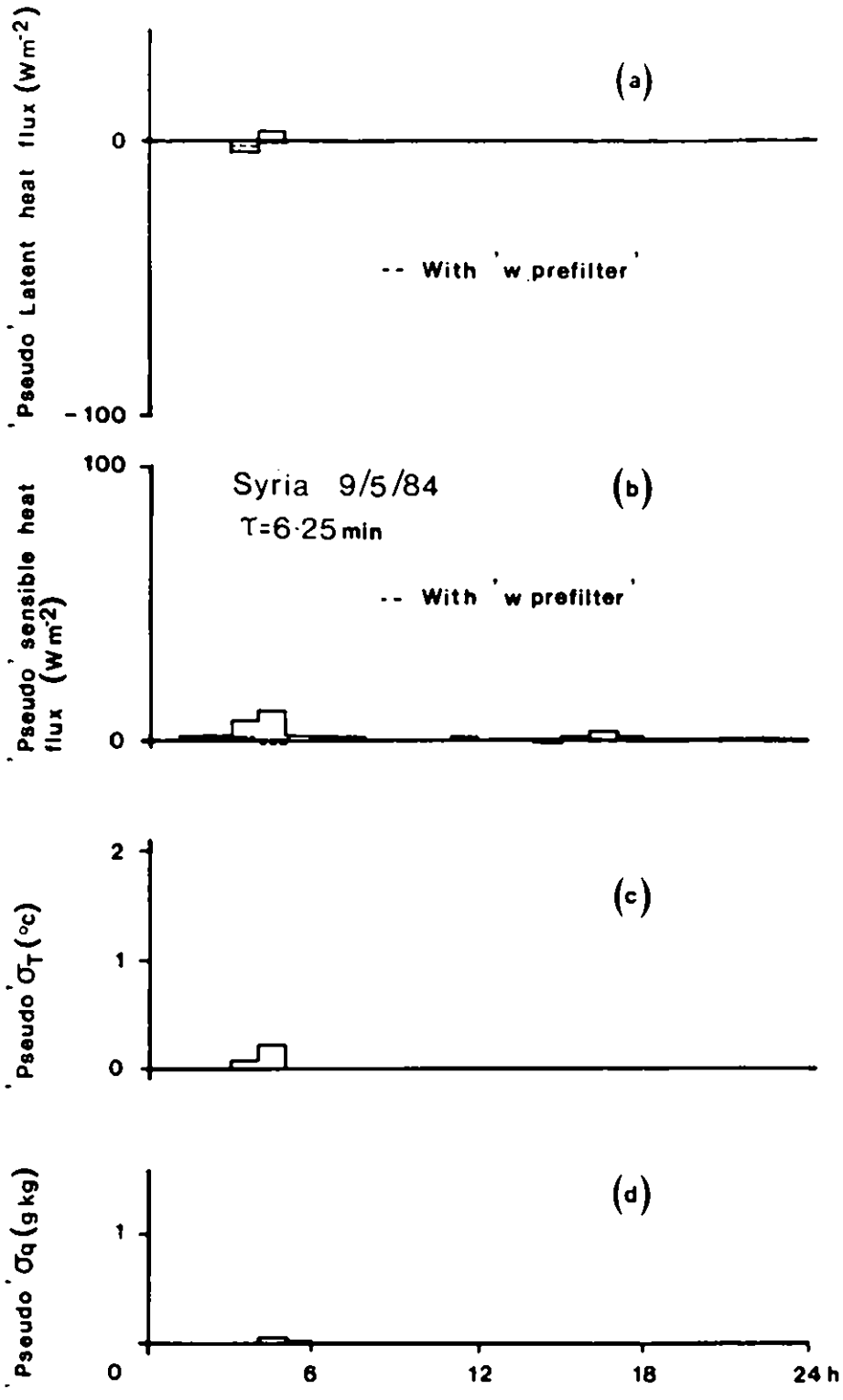

Figure AII.4 Psuedo fluxes of (a) latent and (b) sensible heat as a result of the long-term sensor drift (specified in Figure AII.2) with a time constant τ = 6.25 min. Pseudo standard deviations in (c) temprature and (d) humidity are also shown.

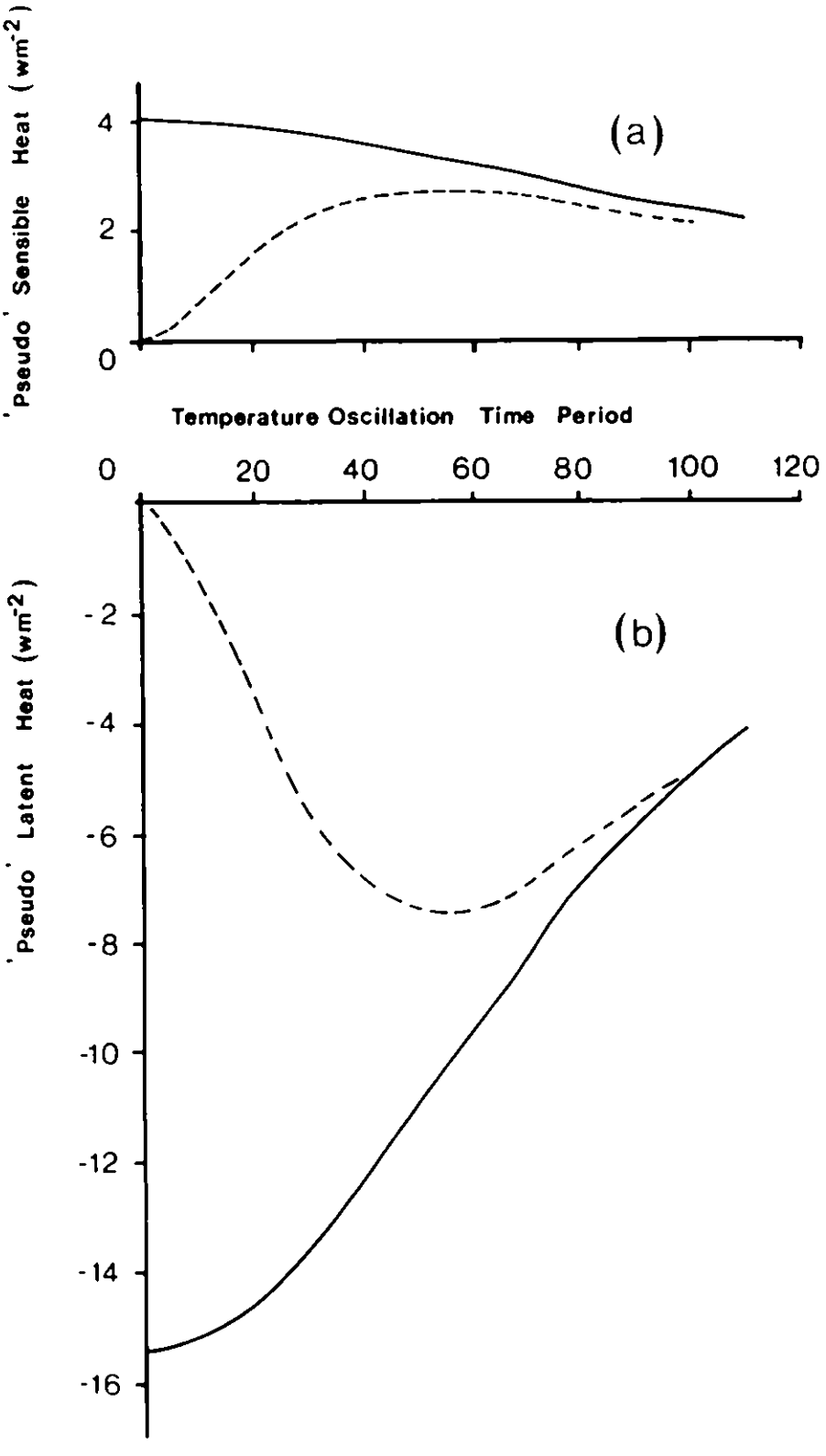

Figure AII.5 Calculated pseudo fluxes of (a) sensible and (b) latentheat generated as a function of the period of the input temperature cycle with an ARMA time constant of 18.25 minutes. The dotted and full lines represent the response for sensors with and without thermal inertia repsectively.

11. APPENDIX III. ANALYSIS OF THE FREQUENCY RESPONSE OF THE HYDRA SYSTEM

INTRODUCTION

Measurement of the fluxes of sensible heat, latent heat and momentum using the eddy correlation technique imposes certain requirements on the sensors and on-line data acquisition and analysis system. In particular, the complete eddy correlation system must be capable of obtaining, and subsequently analysing, signals corresponding to the whole frequency range of atmospheric turbulence in the form of temperature, humidity and wind velocity fluctuations.

In reality, no sensor or system can respond perfectly to all the frequencies encountered in the atmosphere; in many cases other design criteria reduce the frequency response of sensors to a point where significant underestimation of fluxes can occur. Besides obvious characteristics such as the sensor time constant, many other factors must be taken into account. Those include sensor size, or path length; sensor separations; height of exposure; windspeed and atmospheric stability. The frequency response of each of the components of the HYDRA system is described and quantified in sections 3 to 6 where each factor effecting the frequency responses is discussed and quantified.

To determine the underestimation in measured fluxes ('flux loss') it is necessary to know how the contribution of turbulence to transport of the fluxes in the real atmosphere is distributed over frequency. Such cospectra for sensible heat, latent heat, and momentum are described in section 2 where we have made great use of the data obtained in the Kansas Great Plain experiment (of Kaimal et al., 1972).

Finally 'flux loss' is estimated by convoluting the response functions with the appropriate cospectra. Chapter 7 describes this process in more detail and gives results for a number of particular situations.

ATMOSPHERIC CO-SPECTRA

Although a large number of atmospheric spectra and co-spectra have been reported in the literature, it is common to use those reported by Kaimal et al. (1972) for modelling purposes. Even if these do not represent 'universal' spectra, they are almost 'universally' accepted as such. All the spectra presented in this section are from Kaimal et al. (1972).

2.1 Co-spectra for Sensible Heat Flux

2.1.1 Stable Conditions

The W-T cospectra, $S_{WT}(f)$, for stable stratification is given by

$$fS_{WT}(f) = \frac{A_1(f/f_o)}{1 + 1.5\ (f/f_o)^{2.1}} \qquad z/L > 0 \qquad \text{(AIII.2.1)}$$

where the frequency, f , is given by

$$f_o = 0.23\ (\frac{u}{z})\ \ (1 + 6.4\ \frac{z}{L}\ )^{0.75} \qquad z/L > 0 \qquad \text{(AIII.2.2)}$$

and u = windspeed, z = height above zero-plane displacement and L = Obukhov's length. The parameter A_1 is chosen such that

$$\int_o^\infty S_{WT}(f)\ df =$$

$$A_1 = \left[\int_o^\infty \frac{dx}{1 + 1.5\ x^{2.1}} \right] \qquad 0.808$$

2.1.2 Unstable Conditions

The structure of the low frequency eddies in unstable conditions is not well defined. As shown by Kaimal et al. (1972), the low frequency position of the spectra and co-spectra will fall within an envelope defined by the two spectral functions, $S^u_{WT}(f)$ and $S^n_{WT}(f)$ which represent the co-spectra for the stability limits of Z/L = - 2 and Z/L = 0 respectively.

Fitting functions to the curves given by Kaimal et al. (1972) gives for the unstable bound

$$f\,S^{u}_{WT}(f) = \begin{cases} \dfrac{A_2\, f_n}{(1 + 32.26\, f_n)^{1.6}} & f_n < 0.2 \\ \dfrac{A_3\, f_n}{(1 + 3.8\, f_n)^{2.4}} & f_n > 0.2 \end{cases}$$

where $f_n = fz/u$. Matching at $f_n = 0.2$ and a unity co-spectral integral gives $A_2 = 20.208$ and $A_3 = 3.156$.

The neutral bound is given by

$$f\,S^{n}_{WT}(f) = \begin{cases} \dfrac{A_4\, f_n}{(1 + 5.5\, f_n)^{2.4}} & f_n < 0.2 \\ 0.0337\, A_4 & 0.2 < f_n < 0.461 \\ \dfrac{A_5\, f_n}{(1 + 3.8\, f_n)^{2.4}} & f_n > 0.461 \end{cases} \qquad \text{(AIII.2.4)}$$

With $A_4 = 6.673$ and $A_5 = 5.538$

2.2 Co-spectra for Latent Heat Flux

Without any suitable co-spectra data available, it is assumed that the co-spectral forms for sensible and latent heat fluxes are identical, and equations (AIII.2.1) to (AIII.2.4) are used for the w-q co-spectra, $S_{wq}(f)$

2.3 Co-spectra for Momentum

2.3.1 Stable Conditions

The u-w co-spectrum, $S_{uw}(f)$, for stable stratification is given by

$$f.S_{uw}(f) = \frac{B_1(f/f_o)}{1 + 1.5(f/f_o)^{2.1}} \qquad z/L > 0 \qquad \text{(AIII.2.5)}$$

$$f_o = 0.10 \left(\frac{u}{z}\right) \left(1 + 7.9 \frac{z}{L}\right)^{0.75} \qquad z/L > 0$$

Normalising the integral of the co-spectrum to unity also gives $B_1 = 0.808$

2.3.2 Unstable Conditions

As in section 2.1.2, it is found that u-w co-spectra in unstable conditions fall within an envelope defined by the spectral functions $S^u_{uw}(f)$ and $S^n_{uw}(f)$, corresponding to the limits of the stability range $z/L = -2$ and $z/L = 0$ respectively.

Fitting functions to the curves given by Kaimal et al. (1972) gives the unstable bound as

$$f\, S^u_{uw}(f) = \begin{cases} \dfrac{B_2\, f_n}{(1 + 32.0\, f_n)^2} & f_n < 0.5 \\ \dfrac{B_3\, f_n}{(1 + 9.6\, f_n)^{2.4}} & f_n > 0.5 \end{cases} \qquad \text{(AIII.2.6)}$$

where matching at 0.5 and unity integral gives $B_2 = 32.357$ and $B_3 = 7.608$. The neutral bound is described by

$$f\, S^n_{uw}(f) \qquad \text{(2.7)}$$

$$\begin{cases} \dfrac{B_4\, f_n}{(1 + 7.1\, f_n)^{2.4}} & f_n < 0.5 \\ \dfrac{B_5\, f_n}{(1 + 9.6\, f\,)^{2.4}} & f_n > 0.5 \end{cases} \qquad \text{(AIII.2.7)}$$

where $B_4 = 10.009$ and $B_5 = 17.922$.

3. SENSOR RESPONSES

3.1 Temperature Sensor

The temperature sensor used in the HYDRA system is a fast respone Chromel-constantan (Ch-Co) thermocouple. In common with most temperature sensors used in eddy correlation instrumentation, it behaves as a simple first order system with response, H(f), and gain, G(f), functions system with response, H(f), and gain, G(f), functions given by

$$H(f) = \left[1 + 2\pi i f\tau\right]^{-1} \qquad \text{(AIII.3.1)}$$

$$G(f) = \left[1 + (2\pi f\tau)^2\right]^{-1/2} \qquad \text{(AIII.3.2)}$$

where f = frequency (Hz) and τ = time constant (secs).

3.1.1 Time constant

Consider a small length, δx, of the thermocouple, represented by a cylinder of diameter, d, specific heat/unit volume, c_v, and temperature, T. A small gain of heat from the air, δq, will produce a temperature rise in the thermocouple, such that

$$\delta_q = \pi d.\ \delta x.\ h.\ (T_a - T) = \frac{\pi d^2}{4}.\ \delta x.\ c_v.\ \frac{\delta T}{\delta t}$$

where h = coefficient for heat transfer between the thermocouple and the air at temperature T_a. This equation can be simplified and solved to give

$$T(t) = T_a + (T(o) - T_a)_e^{-t/\tau}$$

$$\text{where } \tau = \frac{dc_v}{4h} \qquad \text{(AIII.3.3)}$$

3.1.2 Heat Transfer Coefficient

The heat transfer coefficient, h, can be described by

$$h = \frac{k\ Nu}{d} \qquad \text{(AIII.3.4)}$$

where k = thermal conductivity of air, and Nu is the Nusselt number. Expressions for the Nusselt number for heat transfer between cylinders and air have been developed for various ranges of the Reynold's number, Re = ud/ν where u = windspeed and ν = kinematic viscosity of air. The expression

$$Nu = 0.24 + 0.56\ (Re)^{0.45} \qquad Re < 44 \qquad \text{(AIII.3.5)}$$

(Duchan, 1964) is suitable for the range of Reynolds numbers encountered by a fine wire thermocouple in the atmosphere.

Combining equations (AIII.3.3) and (AIII.3.5) therefore gives

$$= \frac{c_v\ d^2}{4k\ [0.24 + 0.56\ (ud/\nu)^{0.45}]} \qquad \text{(AIII.3.6)}$$

3.1.3 Numerical Values

For a Ch-Co wire and air, the values of the relevant quantities are:

c_v = 3.75×10^6 J m^{-3} $^oK^{-1}$

= 0.024 W m^{-3} $^oK^{-1}$

1.5×10^{-5} m^2 sec^{-1}

If u has units [m sec^{-1}] and d has [m] then equation (26) becomes

$$\tau_T = \frac{0.47 \times 10^6\ d^2}{0.0029 + (ud)^{0.45}} \qquad \text{(AIII.3.7)}$$

with association gain function, $G_T(f)$, given by equation (3.2). If d is specified in thou [inches], remember that d[m] ≡ 25.4×10^{-6} d [thou].

3.2 Humidity Sensor

The humidity sensor used in the HYDRA system is a single-beam infra-red hygrometer (Hyson and Hicks, 1974; Moore, 1983). The high frequency limit of the 'sensor' is only limited by the chopping of the infra-red light beam, and

this is typically about 300 Hz. In practice, the signal from the sensor passes through electronic circuits which includes low-pass filters that smooth the pulse-like signal and remove signals at frequencies above the Nyquist frequency that might cause aliasing problems. Such a low-pass filter effectively defines the high frequency response of the humidity sensor.

3.2.1 Low-pass Electronic Filter

The low-pass filter used in the output stage of the humidity sensor is shown in Fig. AIII.1. Analysis shows that such a circuit has a response function given by

$$H(f) = \frac{1}{1 - (\frac{f}{f_o})^2 + 2\zeta\, i\, (\frac{f}{f_o})} \qquad \text{(AIII.3.8)}$$

and a gain function,

$$G(f) = \left[(1 - (\frac{f}{f_o})^2)^2 + 4\zeta^2(\frac{f}{f_o})^2\right]^{-1/2} \qquad \text{(AIII.3.9)}$$

Where $f_o = \left[4\pi^2 R_1 R_2 C_1 C_2\right]^{-1/2}$ and $\zeta = \frac{1}{2}\left[(\frac{R_2C_2}{R_1C_1})^{1/2} + (\frac{R_1C_2}{R_2C_1})^{1/2}\right]$.

The damping factor ζ is chosen to be 'critical', such that $\zeta = 2^{-1/2}$. Also, it is common practice to simplify calculation by setting $R_1 = R_2$. This leads to $C_1 = 2C_2$, a requirement that can only be approximately satisfied in practice. If $\zeta_1 = (C_2/C_1)^{1/2}$ then $f_o = (2\pi\, \zeta_1\, RC_1)^{-1}$.

3.2.2 Numerical Values

The circuit has component values

$R_1 = R_2 = 220$ KΩ

$C_1 = 100$ nF $= 10 \times 10^{-8}$ F

$C_2 = 47$ nF $= 47 \times 10^{-8}$ F

Thus $\zeta_1 = 0.6855$ and $f_{oq} = 10.55$ Hz and the gain, using equation (AIII.3.9) is

$$G_q(f) = \left[(1 - (\frac{f}{f_{oq}})^2)^2 + 1.88 (\frac{f}{f_{oq}})^2 \right]^{-1/2} \qquad \text{(AIII.3.10)}$$

3.3 Vertical Wind Velocity Sensor

The HYDRA incorporates a sonic anemometer developed at the Institute of Hydrology (Shuttleworth et al., 1982) for measuring the vertical wind velocity component. High frequency measurements using this sensor is limited by the switching frequency, about 40 Hz, between each transducer transmitting and receiving. As in the case of the infra-red hygrometer, however, the signal is passed through a low-pass filter to remove the switching frequency components of the signal, and which effectively defines the high-frequency response of the sensor.

3.3.1 Low-pass Electronic Filter

The low-pass filter used in the output stage of the vertical wind velocity sensor is identical to that shown in Fig. AIII.1, and has frequency response identical to that described in section 2.2.1.

3.3.2 Numerical Values

For the sonic anemometer, the circuit has component values,

$R_1 = R_2 = 100$ kΩ

$C_1 = 0.22 \times 10^{-6}$ F

$C_2 = 0.1 \times 10^{-6}$ F

Thus $\zeta_1 = 0.6742$ and $f_{ow} = 10.73$ Hz and the gain is

$$G_w(f) = \left[(1 - (\frac{f}{f_{ow}})^2)^2 + 1.82 (\frac{f}{f_{ow}})^2 \right]^{-1/2} \qquad \text{(AIII.3.11)}$$

3.4 Horizontal Wind Velocity Sensor

The horizontal wind velocity sensor used in the earlier HYDRA system was a Gill helicaid propeller anemometer pair, mounted at 90° to each other, and exposed such that the bi-secting angle corresponded to the mean wind direction whenever possible. The Gill propeller anemometer response can be described by a simple first-order system with frequency response and gain functions given by equations (AIII.3.1) and (AIII.3.2) respectively.

3.4.1 Time Constant

Rather than a simple time constant, the response of the Gill anemometer is specified by a response length, L, which is independent of windspeed, but which depends on angle of attack, θ, between the wind vector and the shaft of the anemometer. The time constant, τ, is related to response length as

$$= \frac{L(\theta)}{u} = \frac{L_a(\theta)}{u \cos \theta}$$

where L_a is response length referred to the axial velocity component. Hicks (1972) and others have shown from wind tunnel experiments that

$$L_a(\theta) = L_a(o)\cos^{1/2} \theta$$

giving

$$= L_a(o)/u \cos^{1/2}\theta \qquad \text{(AIII3.12)}$$

Brook (1977) combined the response of two orthogonally mounted anemometers and showed that

$$1 < \frac{\tau U}{L_a(o)} < 1.19$$

with the upper limit corresponding to wind approaching both anemometers at 45°, the preferred orientation in the case of the HYDRA system. Since it also represents a 'worst case', the time constant used in the gain equation (AIII.3.2) for the Gill anemometer pair is therfore

$$\tau_a = 1.19 \; L_a(o)/u \qquad \text{(AIII.3.13)}$$

$L_a(o)$, the response length when the wind is blowing along the anemometer shaft has a value $L_a(o) \simeq 1.0$ m. The gain function, $G_u(f)$, is then given by

$$G_u(f) = \left[1 + (2\pi f \tau_u)^2\right]^{-1/2}$$

4. SENSOR LINE AVERAGING

4.1 Line Averaging a Scalar

Expressions for the effect of line averaging a scalar quantity such as temperature or humidity have been given by Gurvich (1962) and Silverman (1968) as a spectrum transfer function $T(f) = S_{\alpha\alpha}(f)/S_{\alpha\alpha}(f)$ where $S_{\alpha\alpha}$ and $S_{\alpha\alpha}$ represent measured and actual spectra of quantity α. Silverman (1968) gives

$$T(\xi,\theta) = \frac{5/\Gamma(4/3)}{6\Gamma(11/6)\pi^{3/2}} \quad \frac{I(\xi,\theta)}{\xi \sin\theta} \qquad \text{(AIII.4.1)}$$

$$\text{and} \quad I(\xi,\theta) = \int_{-\infty}^{\infty} \{1 + [\frac{\frac{x}{\pi\xi} - \cos\theta}{\sin\theta}]^2\}^{4/3} \quad (\frac{\sin x}{x})^2 \quad dx,$$

where the normalized frequency $\xi = fs/u$, s = path length and θ = angle between the wind vector and the axis of the path.

4.1.1 Line Averaging of the Hygrometer

In the earlier versions of the HYDRA, the hygrometer path was horizontal to the ground, which meant that the mean wind vector could have an angle from 0° to 360° to the path axis. In later versions, with a vertical path, the angle between wind vector and path axis is always close to 90°. Given that, in the earlier versions, the probability that the average of θ was closer to 90° than 0° or 360°, the form of equation (AIII.4.1) with $\theta = 90^\circ$ (corresponding to the Gurvich function) was adopted to describe the hygrometer line average.

This function $T(\xi, \pi/2)$ is shown in Fig. AIII.2 together with simplified, fitted functions. These allow the effective gain function $G_{\ell q}(\xi) = T^{1/2}(\xi,\pi/2)$ to be described by

$$G_{\ell q}(\xi) = \begin{cases} (1 + \xi)^{-1/2} & \xi < 0.21 \\ [\dfrac{0.569}{\xi + 0.452} - 0.032]^{1/2} & \xi > 0.21 \end{cases} \qquad \text{(AIII.4.2)}$$

4.2 Line Averaging of Vector Wind

Line averaging by sonic anemometers has been described by Kaimal et al. (1968) and Horst (1973). They both derive th e spectral transfer function $T_\beta(\xi)$ for the β-wind velocity component from

$$T_\beta(2\pi\xi) = \frac{\int\int_{-\infty}^{\infty} \left[\frac{\sin(\underline{k}.\underline{s}/2)}{\underline{k}.\underline{s}/2}\right]^2 \phi_{\beta\beta}(\underline{k})\, dk_2\, dk_3}{\int\int_{-\infty}^{\infty} \phi_{\beta\beta}(\underline{k})\, dk_2\, dk_3} \qquad \text{(AIII.4.3)}$$

where ϕ_{ij} is the spectral density tensor. For further details, see the above references.

4.2.1 Line Averaging of the Sonic Anemometer

In the HYDRA, the vertical wind velocity component is measured with a single path sonic anemometer designed at the Institute of Hydrology (Shuttleworth et al., 1982). The spectral transfer function $T_3(\xi)$, $\xi = fs/u$ where s is the path length, has been obtained from equation (AIII.4.3) (Kaimal et al., 1968; Horst, 1973 and is shown plotted in Fig. AIII.3, together with fitted functions.

The effective gain $G(\xi) = T_3^{1/2}(\xi)$ for the vertical sonic anemometer due to line averaging can be described by

$$G_{\ell w}(\xi) \begin{cases} \left[1 + \xi^{1.4}\right]^{-1/2} & \xi < 0.25 \\ \left[0.465 - 0.297 \ln \xi\right]^{1/2} & \xi > 0.25 \end{cases}$$

where $\xi = fs_{\ell w}/u$ and $s_{\ell w}$ = length of the sonic path.

4.2.2 Line Averaging of the Gill Anemometers

Although Gill propellor anemometers do not measure wind velocity over a path, some averaging must occur over the scale of eddies in the order of the size of their propellors. Also separation of the propellers measuring u_A and u_B (from which the horizontal, u, and transverse wind component, v, are calculated) has an important effect on the spectral transfer function.

Analysis should include both effects, as shown by Kaimal et al. (1968) but this is very complex and, at present, there is nothing published for the case of two orthoganol Gill anemometers. For the moment, it is assumed that the effect of line averaging by each Gill anemometer can be described by $G_{\ell u}(\xi)$ to to a sufficient accuracy, where $G_{\ell u}(\xi)$ is given by equation (AIII.4.4) with $\xi = f\, s_{\ell u}/u$, where $s_{\ell u}$ is the propeller diameter. The effect of separation is given in Section 5.3.3.

5. SENSOR SEPARATION

In general, the effect of sensor separation cannot be treated in the same way as line averaging, described in section 4. Except when considering the wind components derived from separated sensors (cf Kaimal et al., 1968), the effect of sensor separation of less than say, 1 m, on spectra is nil since the atmosphere is generally specially homogeneous at such small wavelengths. However, separation of sensor α from sensor β will effect the cross-spectrum $C_{\alpha\beta}(f)$ in a way which will depend on the wind direction.

Consider the case when two identical sensors measure the same quantity α or α' at points A and A' in space while a third sensor measures quantity β at point A. A co-spectral transfer function $T_{\alpha\alpha'}$ could be defined such that

$$S_{\alpha'\beta} = T_{\alpha\alpha'}(f). \; r_{\alpha\beta} \; (S_{\alpha'\alpha'} \; S_{\beta\beta})^{1/2} \qquad \text{(AIII.5.1)}$$

where $S_{\alpha'\beta}$ is the co-spectrum of α' and β, $S_{\alpha'\alpha'}$ and $S_{\beta\beta}$ are the spectra of α' and β respectively. The correlation coefficient $r_{\alpha\beta}$ is defined by

$$S_{\alpha\beta} = r_{\alpha\beta}(S_{\alpha\alpha} \; S_{\beta\beta})^{1/2}$$

Since $S_{\alpha\alpha} = S_{\alpha'\alpha'}$ then

$$T_{\alpha\alpha'}(f) = S_{\alpha'\beta}/S_{\alpha\beta} = S_{\alpha'\alpha}/S_{\alpha\alpha} \qquad \text{(AIII.5.2)}$$

Note that coherency Coh(f) is usually defined as

$$Coh_{\alpha\beta}(f) = \frac{|C_{\alpha\beta}(f)|^2}{S_{\alpha\alpha} \; S_{\beta\beta}} \qquad \frac{S_{\alpha\beta}^2 + Q_{\alpha\beta}^2}{S_{\alpha\alpha} \; S_{\beta\beta}}$$

If the quadrature spectrum, $Q_{\alpha\beta}$, of α and β is negligible compared to the co-spectrum $S_{\alpha\beta}$, then it follows that

$$T_{\alpha\alpha'}(f) \approx Coh_{\alpha\alpha'}^{1/2}(f) \qquad \text{(AIII.5.3)}$$

5.1 Lateral Separation

Since the effect of sensor separation on the fluxes of sensible and latent heats and momentum can be ascribed to a translation of the vertical wind velocity, w, sensor, it is therefore only necessary to consider this component. Both Irwin (1979) and Kristensen and Jensen (1979) present an analysis of lateral coherence (i.e. separation of points A and A' perpendicular to the mean wind) of wind velocity components in isotropic turbulence. Using different approaches they imply that

$$T_{ww'}(\xi) \simeq \frac{2^{1/6}}{\Gamma(5/6)} \left[2\pi\xi\right]^{5/6} K_{5/6}(2\pi\xi) \qquad \text{(AIII.5.4)}$$

where $\xi = fs/u$ as before and $K_{5/6}$ is a modified Bessel function of the second kind. Using the table of weighted Bessel functions in Irwin (1979), $T_{ww'}(\xi)$ was plotted as shown in Fig. AIII.4, together with a fitted function approximating $T_{ww'}(\xi)$, and given by

$$T_{ww'}(\xi) \simeq e^{-9.9\xi^{1.5}} \qquad \text{(AIII.5.5)}$$

5.2 Longitudinal Separation

Providing that s/u is small compared to the mean eddy lifetime, then separation of sensors in the direction of the mean wind will introduce a phase shift related to s/u in the cross-spectrum. As shown by Kristensen and Jensen (1979), the cross-spectrum becomes

$$C_{\alpha'\beta}(f) = e^{-2\pi i fs/u} C_{\alpha\beta}(f) \qquad \text{(AIII.5.6)}$$

but in this case, the coherency is not effected (increase in quadrature is balanced by decrease in co-spectra) and equation (AIII.5.3) is not useful. However by expanding equation (AIII.5.6) it follows that

$$T_{\alpha\beta}(f) = \frac{S_{\alpha'\beta}}{S_{\alpha\beta}} = \cos(2\pi fs/u) + \sin(2\pi fs/u) \frac{Q_{\alpha\beta}(f)}{S_{\alpha\beta}(f)} \qquad \text{(AIII.5.7)}$$

Assuming that the quadrature is small, a first approximation (cf Hicks, 1972) may be

$$T_{\alpha\beta}(\xi) = \cos(2\pi\xi) , \quad \xi = fs/u \qquad \text{(AIII.5.8)}$$

and this is also shown plotted in Fig.AIII.3. However, as $\cos(2\pi\xi)$ decreases to zero it would be expected that the quadrature term in equation (AIII.2.5) must become significant, and equation (AIII.2.6) would no longer be valid.

Inspection of Fig. AIII.4, indicates that the lateral co-spectral transfer function and equation (AIII.2.6) are not significantly different with both losing about the same 50% "cut-off" frequency. For the purpose of investigating flux loss from the HYDRA system, this suggests that equation (AIII.5.4), via equation (AIII.5.5) would be sufficiently accurate for longitudinal separations, although it is recognized that a small over-estimate in flux loss may result. Also, adopting the one expression for longitudinal and lateral separation simplifies analysis of flux loss, since it is then independent of wind direction.

5.3 Separation of Specific Sensors

5.3.1 Sensible Heat Measurements

If $S = S_{WT}$, the separation of the thermometer and centre of the vertical sonic anemometer path, then the co-spectral transfer function for sensible heat measurements can be obtained from equation (AIII.5.5) and written

$$T_H(\xi) = \exp[-9.9\xi^{1.5}] , \xi = f\, S_{WT}/u \qquad \text{(AIII.5.9)}$$

5.3.2 Latent Heat Measurements

In this case, let $S = S_{QT}$ the separation of the mid points of the hygrometer and sonic anemometer paths. The co-spectral transfer function for latent heat measurements is then

$$T_E(\xi) = \exp[-9.9\,\xi^{1.5}] , \quad \xi = f\, S_{QT}/u \qquad \text{(AIII.5.10)}$$

5.3.3 Momentum Measurements

As mentioned in section 4.2.2, the effect on momentum flux measurements due to propeller separation in the Gill anemometer pair cannot easily be determined accurately. If u_A, v_A and u_B, v_B are the instantaneous, wind velocity components incident or propeller A and B respectively, as shown in Fig AIII.5, then it can be shown (cf Kaimal et al., 1968) that the measured wind velocity components are

$$u_m = 1/2 \quad (u_A + u_B + v_B - v_A)$$

$$v_m = 1/2 \quad (v_A + v_B + u_B - u_A)$$

It follows that measurem,ent of shear stress, $\overline{u'w'}$, by correlating the vertical wind velocity component, w, with the horizontal wind velocity component u_m obtained from the propeller anemometer pair has components given by

$$\overline{u_m'w'} = 1/2 \quad \left[\overline{u_A'w'} + \overline{u_B'w'} + \overline{v_B'w'} - \overline{v_A'w'}\right] \qquad \text{(AIII.5.11)}$$

In terms of co-spectra this can be written

$$S_{u_m w} = 1/2 \quad \left[S_{u_A w} + S_{u_B w} + S_{v_B w} - S_{v_A w}\right]$$

$$1/2 \quad (T_{ww_A} + T_{ww_B})\, S_{uw} + 1/2 \quad (T_{ww_B} - T_{ww_A})\, S_{vw}$$

or if the net co-spectral transfer function is T_m, then

$$T_m = 1/2 \quad (T_{ww_A} + T_{ww_B}) \qquad \text{(AIII.5.12)}$$

It is a reasonable assumption that the term $(T_{ww_B} - T_{ww_A})S_{vw}$ can be neglected. T_m therefore reduces to a simple average of the transfer functions between the w-sensor and each propeller. If s_{WA} and s_{WE} are the respective distances then

$$T_m(f) = 1/2\left[\exp(-9.9\,\xi_1^{1.5}) + \exp(-9.9\,\xi_2^{1.5})\right] \qquad \text{(AIII.5.13)}$$

where $\xi_1 = fS_{WA}/u$ and $\xi_2 = fS_{WB}/u$.

6. FREQUENCY RESPONSE OF DATA ACQUISITION AND ANALYSIS SYSTEM

6.1 Discrete Sampling

A signal representing the discrete sampling of a continuous time series $x(t)$ can be regarded as the product of $x(t)$ and a train of delta functions $\delta(t-n\Delta)$, where Δ is the time interval between samples. The frequency response function $G_s(f)$ resulting from sampling can therefore be given by

$$G_s(f) = \frac{\Delta \int_{-\infty}^{\infty} x(t)\,\delta(t-n\Delta)e^{-2\pi ift}dt}{\int_{-\infty}^{\infty} x(t)e^{-2\pi ift}}$$

The solution (Jenkins and Watts, 1969) is

$$G_s(f) = \begin{cases} f < 1/2\Delta \\ \\ f > 1/2\Delta \end{cases} \qquad \text{(AIII.6.1)}$$

6.2 Signal Averaging

The reason that it is usual to take time averages of atmospheric turbulent quantities rather than spatial averages, is a result of measurements being obtained at a fixed point in space, and reflected as a time series. However, as far as atmospheric physical processes are concerned it is operations in space that are more appropriate - it is through various length scales that turbulence is best described. The use of Taylor's hypothesis, $x = ut$ allows transformation from spatial to temporal scales to be made, and although this generally works well, it is only an approximation.

Therefore consider first, the spatial average of an atmospheric quantity, s, at any given moment, t. If a tilde ($\tilde{}$) represents a spatial average then we can define

$$\tilde{s}(t) = 1/2 \int_0^L s(x,t)dx$$

where s is averaged along a horizontal line between points $x = 0$ and $x = L$ and parallel to the mean wind direction. If the mean wind speed over $x = 0$ to $x = L$ is $\tilde{u}$ then a parcel of air will take a time $\tau = L/\tilde{u}$ to travel the

distance L. Therefore an equivalent time average, represented by an over bar ($\bar{}$), to s(t) would be $\bar{s}(t+\tau)$, obtained, say, by a sensor fixed at x = L.

The spatial average of s a small instant, δt, later can be given by

$$\tilde{s}(t + \delta t) = \left[\tilde{s}(t) - \frac{\tilde{u}\,\delta t}{L}\, s(L,t)\right] + \frac{\tilde{u}\,\delta t}{L}\, s(0,t+\delta t)$$

The equivalent time average immediately follows thus,

$$\bar{s}\,(t + \tau + \delta t) = \left[\bar{s}(t + \tau) - \frac{\delta t}{\tau}\, s(L,t)\right] + \frac{\delta t}{\tau}\, s(L,\, t + \tau + \delta t)$$

This equation can be reduced to a discrete form. If s_{i+1} represents s at an instant $i + 1 = t + \tau + \delta t$ and s_i represents s at an instant $i = t + \tau$ then

$$\bar{s}_{i+1} = (\bar{s}_i - \alpha S_{i-k}) + \alpha\, S_{i+1} \qquad \text{(AIII.6.2)}$$

where $\alpha = \delta t/\tau$ and $k = \tau/\delta t$.

6.2.1 Recursive Low Pass Filter

Equation (AIII.6.2) represents a temporal process that corresponds to a linear unweighted spatial average of some atmospheric quantity s. It has the form of a simple digital recursive low-pass filter,

$$\bar{s}_i = a\, \bar{s}_{i-1} + (1-a)s_i \qquad \text{(AIII.6.3)}$$

if $a = (1 - \alpha)$ and $s_{i-k}/\bar{s}_i = 1$. Provided that the turbulent intensity of s, $s(\sigma_s/\bar{s})$, is small then the second condition can approximately be met. The response function of such a filter is given (cf Jenkins and Watts, 1969) by

$$H_{d\ell}(f) = \frac{1-a}{1 - a\, e^{-2\pi i f \Delta}} \qquad \text{(AIII.6.4)}$$

and gain

$$G_{d\ell}(f) = \frac{1 - a}{(1 + a^2 - 2a \cos 2\pi f \Delta)} \qquad \text{(AIII.6.5)}$$

If f_o is the 3dB cut-off frequency and $\tau = (2\pi f_o)^{-1}$ is the associated time constant then the parameter a has the value

$$a = 2 - \cos\frac{\Delta}{\tau} - (\cos^2\frac{\Delta}{\tau} - 4\cos\frac{\Delta}{\tau} + 3)^{1/2}$$

$$1 - \frac{\Delta}{\tau} + 1/2\ (\frac{\Delta}{\tau})^2 \quad \text{if} \quad \tau >> \Delta.$$

6.2.2 Recursive High Pass Filter

In obtaining fluctuation signals for eddy correlation analysis, it is more usual to extract the mean component of each signal. Thus, if $s' = s - \bar{s}$ then from equation (AIII.6.3)

$$S_i' = S_i - \bar{S}_i$$

$$a\ (S_i - S_{i-1}) + a\ S'_{i-1} \qquad \text{(AIII.6.6)}$$

This has the frequency response function

$$H_{dh} = \frac{a(1 - e^{-2\pi i f\Delta})}{1 - ae^{-2\pi i f\Delta}} - H_{dl} \qquad \text{(AIII.6.7)}$$

with a gain of

$$G_{dh} = a\left[\frac{2(1 - \cos 2\pi f\Delta)}{1 + a^2 - 2a\cos 2\pi f\Delta}\right]^{1/2} \qquad \text{(AIII.6.8)}$$

Note that because of limited precision of some computers, for small $f\Delta (< 10^{-5}$, say) equation (AIII.6.8) should be calculated using

$$G_{dh} = \left[\frac{1}{a} + (\frac{1-a}{2\pi f\Delta a})^2\right]^{-1} = \frac{x^2}{1 + x^2}\ ,\ x = \frac{2\pi f\Delta a}{1-a} \qquad \text{(AIII.6.9)}$$

If the time constant $\tau >> \Delta$ then the parameter a is given by

$$a = 1 - \frac{\Delta}{\tau} + \frac{3}{2}\ (\frac{\Delta}{\tau})^2$$

ESTIMATION OF MEASUREMENT ERRORS

7.1 Sensible Heat Flux

The w-T co-spectrum, $S_{wT}(f)$ was defined in section (2). By convoluting this co-spectrum with the net system co-spectral transfer function, T_l, an estimate of the sensible heat flux loss, ΔH, due to frequency response can be determined from

$$\frac{\Delta H}{H} = 1 \quad \frac{\int_o^\infty T_l \, S_{wT}(f) \, df}{\int_o^\infty S_{wT}(f) \, df}$$

where H is the actual sensible heat flux. This equation can be reduced to

$$\frac{\Delta H}{H} = 1 - \int_o^\infty T_l \, S_{wT}(f) \, df \qquad \text{(AIII.7.1)}$$

If the co-spectrum is suitable normalized, as shown in Section 2.1.1.

The transfer function, T_l, consists oif the following factors;

$$T_l(f) = G_T(f, \tau_T) . \, G_w(f, f_{ow}) . \, G_{\ell w}(f \, s_{ew}/u) .$$

$$T_H(f \, s_{wT}/u) . \, G_s(f,\Delta) . \, G^2_{dh}(f,a) \qquad \text{(AIII.7.2)}$$

Here

$G_T(f,\tau_T)$ = thermocouple gain; τ_T = time constant.

$G_w(f,f_{ow})$ = Sonic anemometer output filter gain; f_{ow} = cut-off frequency

$G_{\ell w}(f \, s_{\ell w}/u)$ = Line average 'gain' of the sonic path of length $s_{\ell w}$.

$T_H \, (f \, s_{wT}/u)$ = Sensor separation transfer function for w and T, and s_{wT} is separation distance.

$G_s(f, \Delta)$ = response due to discrete sampling; Δ = sampling interval.

$G_{dh}(f, a)$ = effective high-pass gain of the digital filter; a is related to the time constant.

7.2 Latent Heat Flux

The latent heat flux loss, $\Delta\lambda E$, due to frequency response can be determined using an expression similar to equation (A.III.1), viz

$$\frac{\Delta \lambda E}{\lambda E} = 1 - \int_0^\infty T_2 \, S_{wQ}(f) \, df \qquad \text{(AIII.7.3)}$$

where λE = actual latent heat flux, $S_{wQ}(f)$ = w-q co-spectrum, which in practice is assumed identical to $S_{wT}(f)$, and T_2 is the net co-spectral transfer function, composed of the following factors;

$$T_2(f) = G_q(f, f_{oq}).\ G_w(f, f_{ow}).\ G_{\ell q}(f\ s_{\ell q}/u).$$

$$G_{\ell w}(f\ s_{ew}/u).\ T_E(f\ s_{wq}/u).\ G_s(f, \Delta).\ G^2_{dh}(f, a) \qquad \text{(AIII.7.4)}$$

Here,

$G_q(f, f_{oq})$ = gain of hygrometer output filter; f_{oq} = cut-off frequency.

$G_w(f, f_{ow})$ = gain of sonic anemometer output filter; f_{oq} = cut-off

$G_{\ell q}(f\ s_{\ell q}/u)$ = line average 'gain' of the hygrometer path of length $s_{\ell q}$

$G_{\ell w}(f\ s_{\ell w}/u)$ = line average 'gain' of the sonic path of length $s_{\ell w}$.

$T\ (f\ s_{wq}/u)$ = sensor separation transfer function for w and q, and s_{wq} in the separation distance.

$G_s(f, \Delta)$ = response due to discrete sampling; Δ = sampling interval

$G_{dh}(f, a)$ = effective high pass gain of the digital filter; a is related to time constant.

7.3 Momentum Flux

The momentum flux loss, $\Delta(u^{*2})$, expressed in terms of friction velocity, u^*, due to frequency response can be determined using an expression similar to equation (AIII.7.1), viz

$$\frac{\Delta(u^{*2})}{u^{*2}} = 1 - \int_o^\infty T_3 \; S_{uw}(f) \; df \qquad \text{(AIII.7.5)}$$

where u^{*2} is the actual momentum flux, $S_{uw}(f)$ is the momentum co-spectrum an T_3 is the net system transfer function consisting of the following factors;

$$T_3(f) = G_w(f, f_{ow}).\; G_{\ell w}\, f\, s_{\ell w}/u).\; G_u(f, L_a).$$

$$G_{\ell n}(f\, s_{\ell n}/u).\; T_M(f(s_{wA} + s_{wB})/2u).$$

$$G_s(f, \Delta).\; G^2{}_{dh}(f, a) \qquad \text{(AIII.7.6)}$$

Here

$G_w(f, f_{ow})$ = gain of sonic anemometer output filter; f_{ow} = cut-off frequency

$G_{\ell w}(f\, s_{ew}/m)$ = line average 'gain' of the sonic anemometer path of length $s_{\ell w}$

$G_n(f, L_a)$ = Propeller anemometer gain; L_a = axial response length.

$G_{\ell a}(f\, s_{\ell u}/u)$ = Effective line average 'gain' due to diameter, $s_{\ell u}$, of the propellers.

$T_M(fS_{wA} + S_{wB})/2u)$ = Sensor separation response function for w and u.

(S_{WA} and S_{WB} are the W - propellor A and w - propellor B separation distances respectively).

$G_s(f, \Delta)$ = Response due to discrete sampling; Δ = sampling interval.

$G_{dh}(f, a)$ = coeffective high pass gain of the digital filter; is related to time constant.

REFERENCES

Brook, R.R., 1977: Effective dynamic response of paired Gill anemometers. Boundary-Layer Meteorol., 11, 33-37.

Duchon, C.E., 1964: Estimates of the infra-red radiation temperature correction for cylindrical temperature sensors. J. Appl. Meteorol., 3, 327-335.

Gurvich, A.S., 1962: The pulsation spectra of the vertical component of wind velocity and their relations to the micrometeorological conditions. Izv. Atmos. Oceanic Phys., 4, 101-136.

Hicks, B.B., 1972: Propellor anemometers as sensors of atmospheric turbulence. Boundary-Layer Meteorol., 3, 214-228.

Horst, T.W., 1973: Spectral transfer functions for a three-component sonic anemometer. J. Appl. Meteorol., 12, 1072-1075.

Hyson, P. and Hicks, B.B., 1975: A single-beam infrared hygrometer for evaporation measurement. J. Appl. Meteorol., 14, 301-307.

Irwin, H.P.A.H., 1979: Cross-spectra of turbulence velocities in isotropic turbulence. Boundary-Layer Meteorol., 16, 237-243.

Jenkins, G.M. and Watts, D.G., 1969: Spectral Analysis and its applications. Holden-Day Inc., San Francisco. 525pp.

Krtistensen, L. and Jensen, N.O., 1979: Lateral coherence in isotropic turbulence and in the natural wind. Boundary-Layer Meteorol., 17, 353-373.

Kaimal, J.C., Wyngaard, J.C., and Haugen, D.A., 1968: Deriving power spectra from a three-component sonic anemometer. J. Appl. Meteorol., 7, 827-834.

Kaimal, J.C., Wyngaard, J.C., Izumi, Y. and Cote, O.R., 1972: Spectral characteristics of surface layer turbulence. Quart. J.R. Meteorol. Soc., 98, 563-589.

Moore, C.J., 1983: On the calibration and temperature behaviour of single-beam infrared hygrometers. Boundary-Layer Meteorol., 25, 245-269.

Shuttleworth, W.J., McNeil, D.D. and Moore, C.J., 1982: A switched continous-wave sonic anemometer for measuring surface heat fluxes. Boundary-Layer Meteorol., 23, 425-448.

Silverman, B.A., 1968: The effects of spatial averaging on spectrum estimation. J. Appl. Meteorol., 7, 168-172.

Low pass active filter

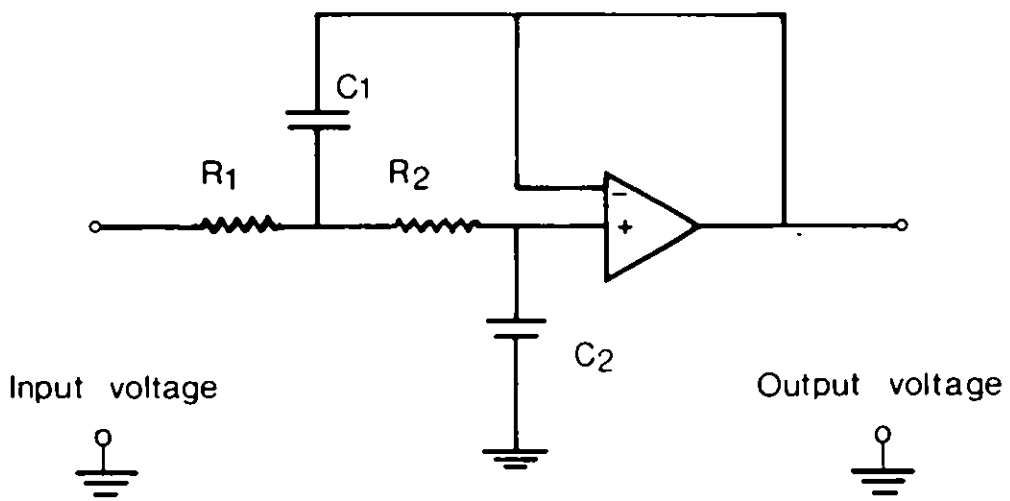

Figure AIII.1 Circuit diagram of the low pass active filter typically used for the removal of high frequency noise from sensor signals.

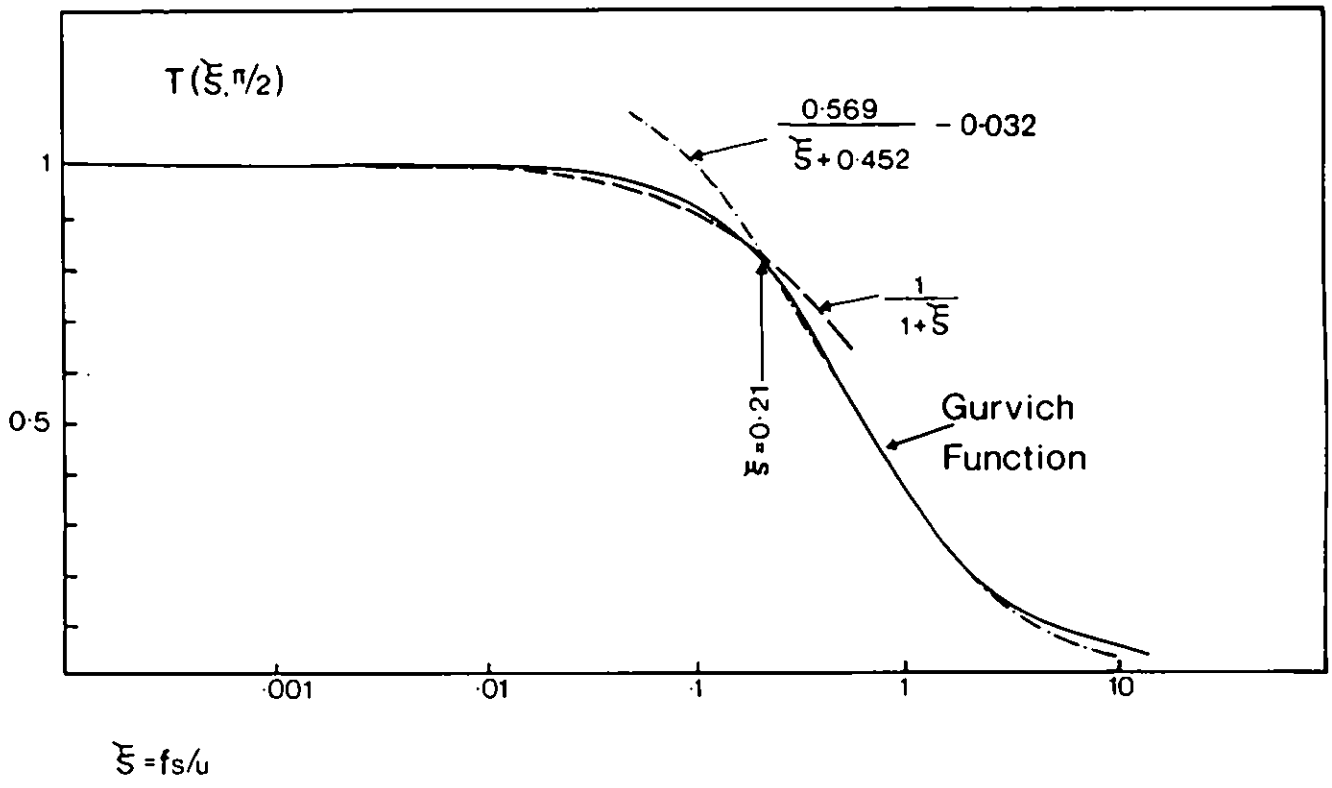

Figure AIII.2 Spectral transfer function, T, associated with the measurement of a scalar quantity averaged over a finite path length, shown as a solid curve plotted against normalized frequency $\xi = fs/u$. Fitted functions approximating this curve are also shown.

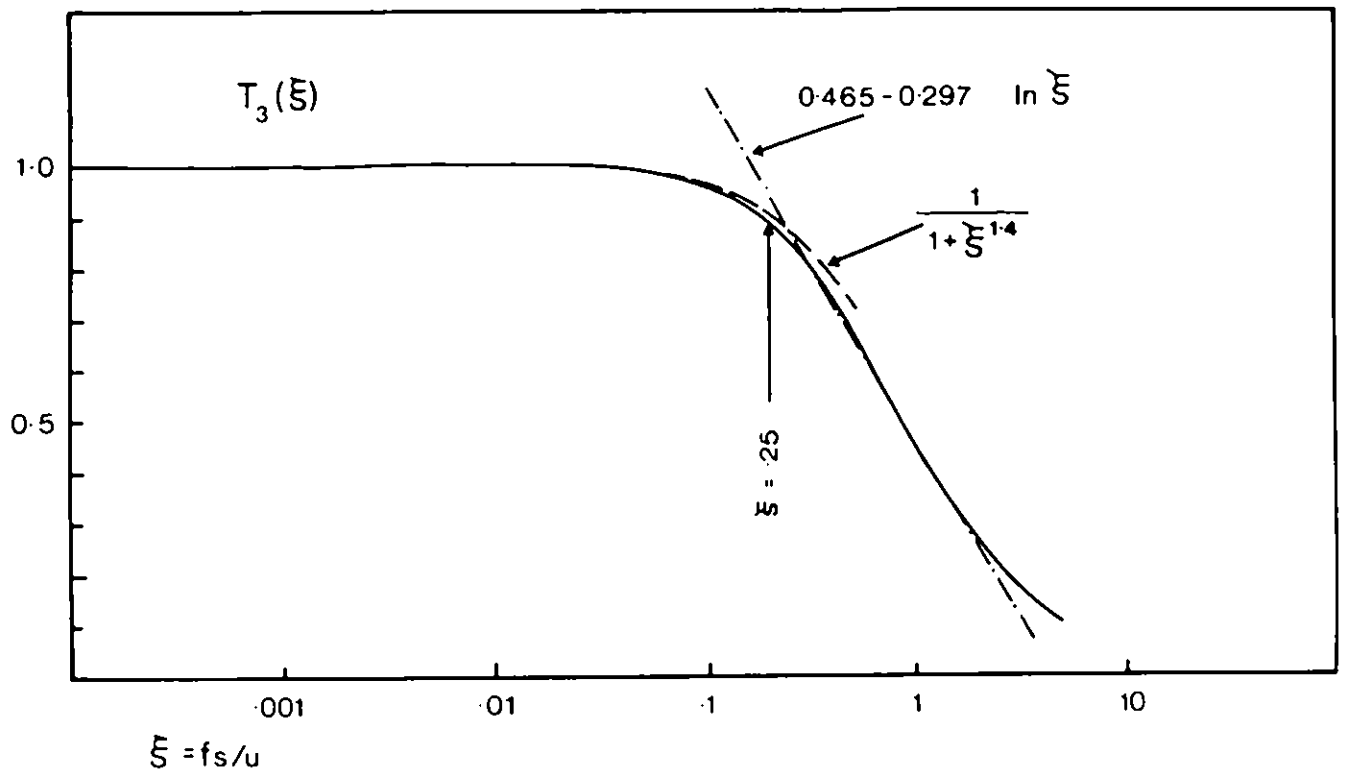

Figure AIII.3 Spectral transfer function, T_3, associated with the measurement of vertical wind velocity averaged over a finite path length, shown as a solid curve plotted against normalized frequency $\xi = fs/u$. Fitted functions approximating this curve are also shown.

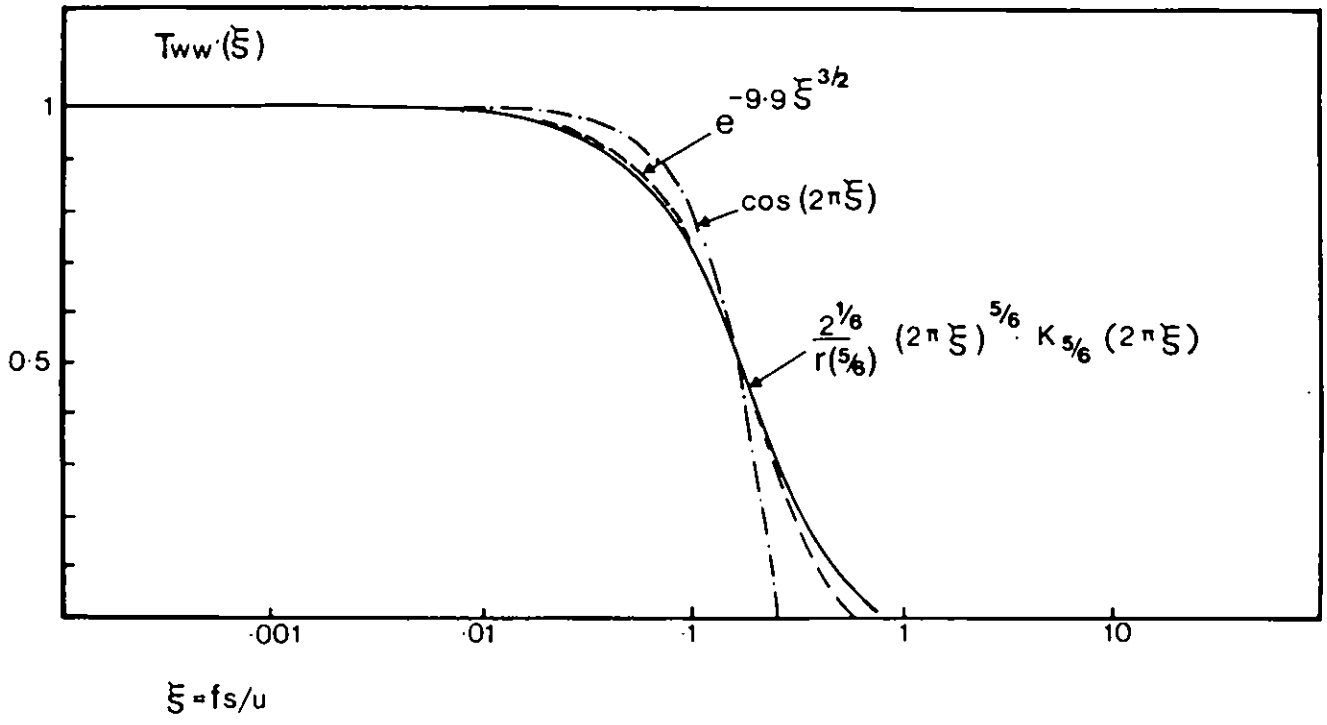

Figure AIII.4 Cospectral transfer function $T_{ww'}$, associated with the measurement of vertical wind velocity component at two positions separated laterally to the mean wind flow by a distance s, as shown by the solid curve plotted against normalized frequency ξ = fs/u. Fitted functions approximating this curve are also shown.

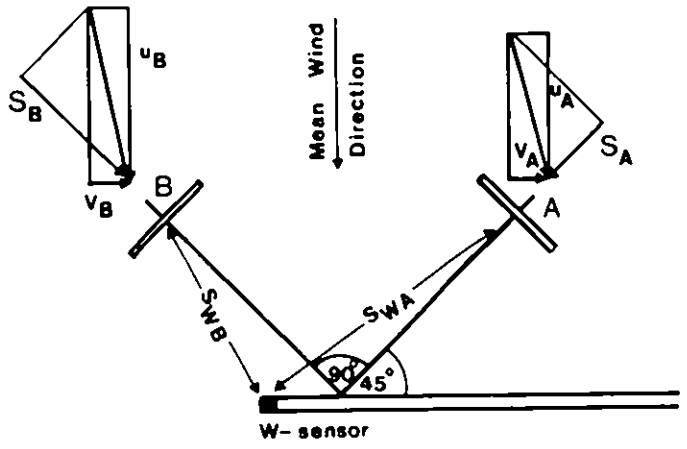

$$S_A = \frac{1}{\sqrt{2}} (u_A - v_A)$$

$$S_B = \frac{1}{\sqrt{2}} (u_B + v_B)$$

Measured wind speed u_m and v_m given by

$$u_m = \frac{1}{\sqrt{2}} (S_A + S_B)$$

$$v_m = \frac{1}{\sqrt{2}} (S_B - S_A)$$

$$\text{Thus } u_m = \frac{1}{2} [(u_A + u_B) + (v_B - v_A)]$$

$$\text{and } v_m = \frac{1}{2} [(v_A + v_B) + (u_B - u_A)]$$

Figure AIII.5 Schematic of the wind vector components incident on two horizontal propellor anemometers (A and B) mounted orthogonally into the mean wind flow. Derivation of the measured wind components is shown.

12. Appendix IV: EVAPORATION FROM SPARSE CROPS - AN ENERGY COMBINATION THEORY*

by

W. James Shuttleworth and J.S. Wallace

(Institute of Hydrology, Wallingford, Oxon., U.K.)

*To be published separately in the Quarterly Journal of the Royal Meteorological Society (July 1985).

SUMMARY

A one dimensional model is adopted to describe the energy partition of sparse crops. Theoretical development of this model yields a combination equation which describes evaporation in terms of controlling resistances associated with the plants, and with the soil or water in which they are growing. The equation provides a simple but physically plausible description of the transition between bare substrate and a closed canopy. Although the aerodynamic transfer resistances for incomplete canopies have, as yet, no experimental justification, typical values, appropriate to a specimen agricultural crop and soil, are shown to have limited sensitivity in the model. Processes which require further study if the equation is to be used to calculate evaporation throughout a crop season are also discussed.

INTRODUCTION

Previous steps in the development of a physically based model of the vegetation-atmosphere interaction (e.g. Shuttleworth, 1976; 1978) explicitly treat the vegetation as a closed, stable canopy of uniform structure. They emphasize the interaction of the vegetation, with fluxes arising at the soil surface introduced as an unspecified, and implicitly small, input to the model (Shuttleworth, 1979). In this paper this theoretical work is reinterpreted and developed into the situation of sparse crops, where the use of a one-dimensional model has less obvious justification. In describing such crops the soil and plant components must carry equal status, since they can be of similar size and their relative importance can change significantly with crop cover.

The philosophy of this paper is to make minimum concession to the more obvious three dimensional structure of sparse and row crops. Accordingly a one dimensional model of the interaction is adopted to derive a combination equation, which can provide a physically plausible transition between the bare substrate and closed canopy limits. The equation is expressed in terms of conceptual resistances now familiar to the micrometeorologist and plant physiologist, canopy resistance and boundary layer resistance etc; it also requires the less familiar concept of a surface resistance for bare soil (Monteith, 1981). In the later sections of the paper typical values of these resistances are used to illustrate how energy partition varies between crops of the same height, but with different leaf areas.

THE ONE DIMENSIONAL MODEL

The problem of sparse crops is approached using the knowledge that the two asymptotic limits (bare substrate and a closed canopy) can both be represented by a one dimensional model. Moreover it is acknowledged that, in describing the closed canopy situation, models which represent the canopy interaction as occurring as a single source (Monteith, 1965) have increasing acceptance. Such models represent a practical compromise between physical rigour and field application. The basic assumption, that there is numerical similarity between bulk stomatal resistance and an integration of component stomatal resistances in dry conditions (Monteith, 1965), has been tested experimentally (Black et.al., 1970; Szeicz et.al., 1973; Tan and Black, 1976), numerically (Sinclair et.al., 1971) and explored theoretically (Shuttleworth, 1976).

Implicit in this successful assumption is the idea that the real three dimensional nature of a crop can be ignored in terms of its practical consequences. It is also assumed that aerodaynamic mixing within the crop is sufficiently good to allow the hypothetical existence of a 'mean canopy airstream' (Thom, 1972) which can be described by meteorological parameters such as temperature, humidity and windspeed. These assumptions are necessary if progress is to be made towards providing a description which is general (in the sense that it is not merely a description of a particular crop at a particular time). Previous models based on these assumptions have been proposed and tested (Black et.al., 1970; Szeicz et.al., 1973) even in closed canopies, where the aerodynamic interaction within the canopy is minimized.

The degree of aerodynamic mixing in sparse and row structured crops is likely to be greater than that in closed canopies. Adopting the Monteith assumption for such crops is therefore arguably more plausible in terms of mixing in the vertical. It does however require a reconsideration of the scale relevant to the horizontal averaging process, and will involve additional uncertainty regarding the consequences of persistent features within the aerodynamic mixing pattern in the horizontal plane (see, for example, Arkin and Perrier, 1974).

Any one dimensional description assumes horizontal uniformity, but in practise recognisable three-dimensional features of the crop (individual plants and rows, and persistent aerodynamic mixing features) are always present. If a description of the Monteith type is to be used it is necessary that the elements of which the model is composed (e.g. energy fluxes, stomatal resistance etc) are defined as horizontal averages over area scales in which persistent features occur in sufficient numbers to allow such averaging. A one dimensional description is clearly not relevant to horizontal scales less than this.

In this study a simple two component structure is maintained and energy partition treated as occurring at 'the crop' and 'the soil'. This simplification appears particularly arbitrary in the case of row crops since it involves, for instance, no distinction between soil beneath the vegetation and that between the rows. The presence of a defined three dimensional structure clearly cannot be totally ignored in certain aspects of the interaction. For example, in the case of interception of solar radiation, row orientation may affect the effective absorption coefficient relevant at the scale of the horizontal averaging. The diurnal cycle in solar altitude reduces the distinction between the daily total absorption by such organized structures and that of randomly distributed sparse vegetation. None-the-less, the realistic philosophy in dealing with row crops is to treat separately such aspects of the problem, but then to return to an averaging scale over which a one dimensional model is assumed to apply.

The model adopted and developed in this paper is illustrated in Figure 1. It incorporates the now familiar concept of a bulk stomatal resistance for the vegetation, r_s^c, but also the less familiar concept of a surface resistance at the substrate surface, r_s^s.

The physical origin of this surface resistance is less obvious for soil than it is for vegetation but its mathematical definition is precise. Its presence reflects the fact that the layer of air adjacent to the soil surface is not necessarily saturated unless the soil surface is wet. If soil evaporation is λE_s, and the temperature and vapour pressure at the soil surface T_s and e_s respectively, then the surface resistance of the soil is defined by the equation

$$r_s^s \quad \frac{\rho c_p}{\gamma} \quad \frac{[e_w(T_s) - e_s]}{\lambda E_s} \qquad (1)$$

where $e_w(T_s)$ is the saturated vapour pressure at temperature T_s and the other quantities are defined in section 3(a). Monteith (1981) interprets this resistance in conceptual terms by describing evaporation from a drying soil as occurring from wet soil below a dry soil layer of increasing thickness, treated as isothermal. This provides a description qualitatively consistent with observation. Although this obvious over-simplification leads to problems in physical interpretation (Fuchs and Tanner, 1967), Equation (1) defines an entity which can form the subject of empirical models. Such modelling is not discussed further in the present paper.

The model described in Figure 1 adopts the concept of a bulk boundary layer resistance, r_a^c, which controls transfer between the surface of the vegetation and the canopy air stream (Thom, 1972). Vertical transport is controlled by two further aerodynamic resistances. The first, r_a^a, is the transfer resistance between the hypothetical mean canopy flow and the reference height, κ, above the crop. The second, r_a^s, is the aerodynamic resistance encountered by the energy fluxes leaving the substrate before they are incorporated into the mean canopy flow. For simplicity in this analysis it is assumed that the various aerodynamic resistances are identical for sensible and latent heat. Making this assumption simplifies the formalism but does not alter the derivation in any fundamental way.

It is worth remembering at this point that the so called 'aerodynamic resistance' generally employed when describing energy partition with a combination equation (Monteith, 1965) is obtained by the addition of the component resistances described in the previous paragraph. In this way the aerodynamic resistance used in a combination equation describing a closed canopy (with no soil evaporation) is $(r_a^a + r_a^c)$, while that which would be used to describe evaporation from the substrate is $(r_a^a + r_a^s)$. The relevant 'surface' resistances in these two situations are r_s^c and r_s^s. The objective in the following sections is to derive a combination equation, descriptive of both plant and substrate evaporation, but which asymptotes towards simpler combination equations involving the aerodynamic and surface resistances relevant in limiting situations.

THEORETICAL DEVELOPMENT

(a) Nomenclature

Total energy flux leaving the complete crop as sensible and latent heat per unit ground area ($W\ m^{-2}$)

A_s Total energy flux leaving the substrate as sensible and latent heat per unit ground area ($W\ m^{-2}$)

Extinction coefficient of the crop for net radiation (dimensionless)

c_p Specific heat at constant pressure ($J\ kg^{-1}\ K^{-1}$)

Zero plane displacement of crop with complete canopy cover (L=4) (m)

Vapour-pressure deficit at reference height $[e_w(T_x) - e_x]$ (mb)

D_o Vapour-pressure deficit at canopy source height $[e_w(T_o) - e_o]$ (mb)

Vapour-pressure at canopy source height (mb)

Vapour-pressure at the soil surface (mb)

Vapour-pressure at reference height (mb)

$e_w(T)$ Saturated vapour pressure at temperature T ($T = T_x$, T_o, T_s) (mb)

Soil heat flux ($W\ m^{-2}$)

Crop height (m)

Sensible heat flux from the complete crop ($W\ m^{-1}$)

H_s Sensible heat flux from the substrate ($W\ m^{-1}$)

Von Karman's constant (dimensionless)

Eddy diffusion coefficient ($m^2\ s^{-1}$)

K_h Eddy diffusion coefficient at top of canopy ($m^2\ s^{-1}$)

Projected area of leaf per unit ground area (Leaf Area Index) (dimensionless)

Eddy diffusivity decay constant in a crop with complete canopy cover (L=4) (dimensionless)

Biochemical storage of energy in the crop below reference height ($W\ m^{-2}$)

r_a^a Aerodynamic resistance between canopy source height and reference level ($s\ m^{-1}$)

r_a^c Bulk boundary layer reistance of the vegetative elements in the canopy ($s\ m^{-1}$)

r_a^s Aerodynamic resistance between the substrate and canopy source height ($s\ m^{-1}$)

Mean boundary layer resistance per unit area of vegetation ($s\ m^{-1}$)

r_s^c Bulk stomatal resistance of the canopy ($s\ m^{-1}$)

r_s^s Surface resistance of the substrate ($s\ m^{-1}$)

r_{ST} Mean stomatal resistance ($s\ m^{-1}$)

$r_a^a(0)$ Value of r_a^a for bare substrate ($s\ m^{-1}$)

$r_a^a(\alpha)$ Value of r_a^a for crop with complete canopy cover (L=4) ($s\ m^{-1}$)

$r_a^s(0)$ Value of r_a^s for bare substrate ($s\ m^{-1}$)

$r_a^s(\alpha)$ Value of r_a^s for crop with complete canopy cover (L=4) ($s\ m^{-1}$)

R_n Net radiation flux into the complete crop ($W\ m^{-2}$)

R_n^s Net radiation flux into the substrate ($W\ m^{-2}$)

Physical storage of energy in the atmosphere and crop below reference height ($W\ m^{-2}$)

T_o Air temperature at canopy source height (^oC)

T_s Temperature of the substrate surface (^oC)

T_x Air temperature at reference height (^oC)

Windspeed at the reference height ($m\ s^{-1}$)

Friction velocity ($m\ s^{-1}$)

Reference height above the crop where meteorological measurements are available (2 m in this analysis)

height (variable) (m)

Roughness length of crop with complete canopy cover (L=4) (m)

z_o' Roughness length of the bare substrate (m)

Mean rate of change of saturated vapour pressure as a function of temperature, $[e_w(T_x) - e_w(T_o)]/[T_x - T_o]$ (mb $^oC^{-1}$)

Psychrometric 'constant' (mb $^oC^{-1}$)

λE Latent heat flux from the complete crop (W m^{-2})

λE_c Latent heat flux from the plant canopy (W m^{-2})

λE_s Latent heat flux from the substrate (W m^{-2})

Density of air (kg m^{-3})

(b) The Energy Budget

All combination equations rely on drawing up an energy budget between the outward fluxes of sensible and latent heat and the energy available in other forms. In this problem two budgets are drawn up, one at the substrate surface and one for the complete crop. The sum of the above canopy fluxes of sensible heat, H, and latent heat, λE, is the available energy, A, and is given by

$$A = \lambda E + H \quad (2)$$

$$= R_n - S - P - G \quad (3)$$

where R_n is the incoming net radiation, S and P are the physical and biochemical energy storage terms, and G is the heat conduction into the substrate. In a similar way, the energy available at the substrate, A_s, is given by

$$A_S = \lambda E_s + H_s \quad (4)$$

$$R_n^s - \quad (5)$$

where R_n^s is the net radiation at the substrate surface.

In drawing up such energy budgets it is clearly necessary to consider average values of the several components defined over horizontal scales which involve significant numbers of the identifiable crop and soil features. In general R_n^s is less than R_n and A_s less than A. In the limit of bare substrate A and A_s are equal.

(c) In Canopy Deficit

By analogy with Ohm's Law for the electrical analogue shown in Figure 1, the difference in vapour pressure deficit and temperature between the level of mean canopy flow and reference height can be written in terms of resistance and flux as

$$e_x - e_o = \frac{\lambda E \, r_a^a \, \gamma}{\rho c_p} \tag{6}$$

$$\text{and } T_x - T_o = - \frac{H \, r_a^a}{\rho c_p} \tag{7}$$

Introducing the definition of Δ into the expression for the vapour pressure deficit at the canopy source height, D_o, gives

$$D_o = e_w(T_x) - [e_w(T_x) - e_w(T_o)] - e_o$$

and substituting equations (7), (6) and (2), yields a relationship between D_o and D such that

$$D_o \quad D + [\Delta A - (\Delta + \gamma) \, \lambda E] \, \frac{r_a^a}{\rho c_p} \tag{8}$$

(d) The Sparse Crop Combination Equation

In the model illustrated (Figure 1), the evaporation from the substrate, λE_s, and plants in the canopy, λE_c, can be separately calculated from equations of the Penman-Monteith type, thus

$$\lambda E_s = \frac{\Delta A_s + \rho c_p D_o / r_a^s}{\Delta + \gamma(1 + r_s^s / r_a^s)} \tag{9}$$

$$\lambda E_c = \frac{\Delta (A - A_s) + \rho c_p D_o / r_a^c}{\Delta + \gamma(1 + r_s^c / r_a^c)} \tag{10}$$

The total evaporation from the crop, λE, is the sum of these two, and it can be shown (see Appendix) that D_o can be eliminated and the resultant equation arranged in the form

$$\lambda E = C_c PM_c + C_s PM_s \tag{11}$$

where PM_c and PM_s are terms each similar to the Penman-Monteith combination equations which would apply to evaporation from a closed canopy and from bare substrate respectively. They have the form

$$PM_c = \frac{\Delta A + [\rho c_p D - \Delta r_a^c A_s]/(r_a^a + r_a^c)}{\Delta + \gamma [1 + r_s^c/(r_a^a + r_a^c)]} \tag{12}$$

$$PM_S = \frac{\Delta A + [\rho c_p D - \Delta r_a^s (A - A_s)]/(r_a^a + r_a^s)}{\Delta + \gamma [1 + r_s^s/(r_a^a + r_a^s)]} \tag{13}$$

The coefficients C_c and C_s are given by the expressions

$$C_c = \left[1 + \frac{R_c R_a}{R_s (R_c + R_a)}\right]^{-1} \tag{14}$$

$$\text{and } C_s = \left[1 + \frac{R_s R_a}{R_c (R_s + R_a)}\right]^{-1} \tag{15}$$

$$\text{where } R_a = (\Delta + \gamma) r_a^a \tag{16}$$

$$R_s = (\Delta + \gamma) r_a^s + \gamma\, r_s^s \tag{17}$$

$$R_c = (\Delta + \gamma) r_a^c + \gamma\, r_s^c \tag{18}$$

It can be easily seen that equation (11) has correctly defined asymptotic limits. If there is no substrate evaporation, r_s^s and hence R_s are infinite, PM_s is zero in Equation (11), and C_c is unity. If, in addition, there is no sensible heat flux from the substrate, H_s and hence A_s are zero, and equation (11) reduces to the conventional Penman-Monteith equation describing closed canopy evaporation with no substrate interaction. In a similar way, if there is no canopy present r_s^c and hence R_c are infinite, and $A = A_s$. Equation (11) reduces to a conventional form, describing substrate evaporation with the Penman-Monteith equation involving a surface resistance applicable to the substrate.

In the more general intermediate situation, when both substrate and canopy evaporation occur, equation (11) provides a physically plausible description of the total evaporation λE. Once calculated, this can be substituted into Equation (8) to compute D_o, and in this way the component fluxes λE_c and λE_s calculated from Equations (9) and (10) if required.

(c) The leaf area dependence of surface resistance

The assumptions and observations made in Shuttleworth (1979) and associated papers (Shuttleworth, 1976; 1978) are implicit in Equation (11). In the context of the present problem a point of particular relevance is the fact that the mean boundary layer resistance of the canopy, r_a^c, and the bulk stomatal resistance of the canopy, r_s^c, are both 'surface' resistances, influenced by the surface area of the vegetation present. They vary inversely with the total leaf area of the vegetative elements present (Shuttleworth, 1976). This is important when considering the effect of changes in leaf area index on energy partition and it is convenient in this case to rewrite these two surface resistances in the form

$$r_s^c = \frac{r_{ST}}{2L} \tag{19}$$

$$r_a^c \quad \frac{r_b}{2L} \tag{20}$$

where r_{ST} is the mean stomatal resistance (of amphistomatous leaves) and r_b the mean boundary layer resistance, both expressed per unit surface area of vegetation. L is the leaf area index of the canopy, i.e. the projected area of the vegetation per unit ground area. In this way these two resistances are high in very sparse canopies and, all other things being equal, decrease inversely as the area of vegetation per unit ground area increases. In practice this is just a first approximation since r_b may itself be influenced by changes in mean canopy windspeed, and r_{ST} may change in response to differences in shading.

The resistance r_s^s is also a surface resistance and should therefore be divided by the area of exposed substrate per unit ground area. In practice the area occupied by plant stems is likely to be a small fraction of ground area. Any litter present on the ground can be regarded as part of the substrate.

VEGETATION DENSITY VARIATIONS

In this section the response of equation (11) is explored when applied to crops of the same height but with different leaf areas, which are subject to a specified atmospheric demand. For the purposes of comparison, calculations are carried out assuming measured meteorological variables are available above the crops at a height, x, of 2 m. In this way it is assumed that any density related interaction between the crop and the meteorological variables, e.g. albedo changes, can be treated separately (we return to this point later). Calculations are made for soil and water substrates, using a specification of the component resistances drawn from the literature, and taken as applying to a 'typical' agricultural crop.

(a) Model specification

(i) Available Energy

The physical and biochemical storage terms, S and P, are ignored in equation (3). Since net radiation during daylight hours is primarily determined by direct radiation, it has been found experimentally (e.g. Ross, 1981) that the radiation reaching the soil surface, R_n^s, can be calculated using a Beer's Law relationship of the form

$$R_n^s = R_n \exp(-CL) \qquad (21)$$

where C is the extinction coefficient of the crop for net radiation, chosen arbitrarily as 0.7 (see for example Monteith, 1973). It is convenient here to ignore variations in C which may occur in response to structural differences in crops of different density, although this could (if known) be included in specific cases. In the present calculation the heat conduction into the substrate, G, is arbitrarily set to 20 per cent of the radiation received at the substrate surface, R_n^s, and therefore G also changes with crop density.

(ii) Mean Stomatal Resistance

The mean stomatal resistance, r_{ST}, is taken as 400 s m^{-1}. It follows from Equation (19) that, for a leaf area index, L, of 4, the bulk stomatal resistance, r_s^c, is 50 s m^{-1}. This value is typical

of a fully grown agricultural crop (see Wallace et.al., 1981).

(iii) Mean Boundary Layer Resistance

Measurements of mean boundary layer resistance, r_b, generally have significant scatter and exhibit some dependence on in-canopy windspeed. The value of r_b for stands of vegetation of different density is therefore uncertain. Typical values measured in the field are in the order 25 s m^{-1} (see Denmead. 1976; Uchijima. 1976) and this value is assumed here. The corresponding bulk boundary layer resistance is 3 s m^{-1} for a leaf area index of L=4. In practice this resistance is only significant in equation (11) when acting in combination with the much larger bulk stomatal resistance; errors in its assumed value are shown later to be of limited numerical importance.

(iv) Surface Resistance of the Substrate

The description of substrate evaporation in terms of a surface resistance is somewhat novel in this paper, and, in consequence, typical values are difficult to specify. Calculations are performed for three values of r_s^s, viz 0, 500 and 2000 s m^{-1}. The first value (r_s^s=0) corresponds to a substrate of wet soil or free water, whilst the last (r_s^s=2000) is arguably typical of fairly dry soil - theoretically, it corresponds to molecular diffusion through a 1.5 cm thick layer of dry sandy soil (Fuchs and Tanner, 1967). The third value (r_s^s=500) is chosen merely as an intermediate value; on a unit area basis it is in the same order as that of dry vegetation.

(v) Eddy Diffusion Resistances

Clearly crop density affects the size of the aerodynamic resistances r_a^a and r_a^s, but the quantitative response of within canopy aerodynamic transfer to differing leaf area index is perhaps the least understood aspect of micrometeorology, and likely to remain so in the foreseeable future. In these circumstances we have assumed the simplest possible model in which r_a^a and r_a^s vary

linearly with leaf are index between the values associated with their two limits, namely bare substrate and a complete canopy cover (which we arbitrarily assume corresponds to L=4). In fact, as we demonstrate later, the quantative effect of this simple treatment has a limited effect on component and total evaporation fluxes.

In crops with complete cover the effective source, at which mean canopy air stream conditions are assumed to apply, is defined to occur at a height $(d+z_o)$ in the crop where d is zero plane displacement and z_o is crop roughness length. Monteith (1973) relates d and z_o to crop height for the fully developed crop through the expressions

$$= 0.63\ h$$

$$z_o = 0.13\ h \qquad (22)$$

In sparser crops we assume that the effective source height remains fixed at this fraction of crop height. It follows that in this exercise, where crop height is held constant, the effective height at which the plant components of sensible and latent heat arise is assumed to be independent of crop density. For simplicity stability effects are ignored here and the eddy diffusion coefficients describing the vertical movement of heat and water vapour are equated to those for momentum.

Above the fully developed crop ($L \gtrsim 4$), the eddy diffusion coefficient, K, is given by

$$K = k\ u_* (z - d) \quad (z > h) \qquad (23)$$

where k is Von Karman's constant, z is height and u_* is the friction velocity, which, in conditions of neutral atmospheric stability, is given by the expression,

$$= k\ u\ /\ \ln ([x - d]/z_o) \qquad (24)$$

where u is the windspeed at the reference height x. It is also assumed that, in the closed canopy, the eddy diffusion coefficient decreases expontentially with height, thus

$$= K_h \exp\left[-n\ \left(1 - \frac{z}{h}\right)\right] \qquad (25)$$

where K_h is the value of K at the top of the crop ($K_h = ku_*[h-d]$); we use a value of n = 2.5 which is typical of the agricultural crop being specified (Monteith, 1973). Using these several assumptions and performing an integration over the height ranges 0 to $(d + z_o)$ and $(d + z_o)$ to x respectively, it is possible to write

$$r_a^s(\alpha) = \frac{\ln([x - d]/z_o)}{k^2 u} \frac{h}{n(h-d)} \left\{ \exp(n) - \exp\left(n\left[1 - \frac{d + z_o}{h}\right]\right) \right\} \quad (26)$$

$$r_a^a(\alpha) = \frac{\ln([x - d]/z_o}{k^2 u} \left[\ln(x - d]/[h - d] \right.$$

$$\left. \frac{h}{n(h-d)} \left\{ \exp\left(n\left[1 - \frac{d + z_o}{h}\right]\right) - 1 \right\} \right] \quad (27)$$

For a crop height (h) of 0.3 m and windspeed (u) of 2 m s^{-1}, this gives $r_a^s(\alpha)$ = 128 s m^{-1} and $r_a^a(\alpha)$ = 42 s m^{-1}.

With a bare substrate, computation is simpler. Here the aerodynamic resistances are given by

$$r_a^s(0) = \frac{\ln(x/z_o') \ln([d + z_o]/z_o')}{k^2 u} \quad (28)$$

$$r_a^a(0) = \frac{\ln^2(x/z_o')}{k^2 u} r_a^s(0) \quad (29)$$

where z_o' is the effective roughness length of the substrate. For bare soil z_o' is commonly taken as 0.01 m (see Van Bavel and Hillel, 1976) and for simplicity here differences in the surface roughness between wet soil and free water substrates are neglected. The values of these resistances in the present situation with u=2 m s^{-1} are $r_a^s(0)$ = 49 s m^{-1} and $r_a^a(0)$ = 34 s m^{-1} respectively.

Since we do not yet know exactly how r_a^a and r_a^s will vary, we assume they have a linear relationship between their asymptotic limits. Thus

$$\left.\begin{aligned} r_a^a &= \frac{L}{4}\, r_a^a(\alpha) + \frac{(4 - L)}{4}\, r_a^a(0) \\ r_a^s &= \frac{L}{4}\, r_a^s(\alpha) + \frac{(4 - L)}{4}\, r_a^s(0) \end{aligned}\right\} \quad 0 \leq L \leq 4 \qquad (30)$$

$$\left.\begin{aligned} r_a^a &= r_a^a(\alpha) \\ r_a^s &= r_a^s(\alpha) \end{aligned}\right\} \quad L > 4 \qquad (31)$$

It is shown later that the exact form of these relationships are usually of limited numerical importance in calculations of evaporation. Implicit in the above equations is the assumption that the roughness length and zero plane displacement of crops with intermediate cover ($0 < L < 4$) vary between the values appropriate to complete cover (z_o and d) and bare soil (z_o' and zero) and are therefore <u>not</u> a fixed fraction of crop height. However, the effective source height of the energy fluxes from the vegetation (mean canopy flow) <u>is</u> a fixed fraction of crop height.

(b) Model predictions

Calculations are carried out for the following meteorological conditions

$$R_n = 400 \text{ W m}^{-1}$$

$$D = 0, 10, 20 \text{ mb}$$

$$T_x = 25\ ^{o}C$$

and u 2 m s^{-1}

Such meteorological conditions might be considered typical for midday in the middle of a growing season at a subtropical site. However, the objective is not to make detailed predictions for particular meteorological conditions, it is rather to illustrate the general features of the theoretical treatment described.

(i) Free Water Substrate

The situation in which $r_s^s = 0$ is in some regards a particular case. It might be considered to represent the behaviour of paddy rice or crops which are (over) watered by trickle irrigation. Results for this situation are illustrated in Figure 2.

Figure 2(a) illustrates total crop evaporation rates for the meteorological conditions specified above, for crops of different density, defined by their leaf area index. These rates are compared with the energy available to the whole crop, and that available to the substrate. The energy available to the system increases slightly with crop cover, while that of the substrate falls monotonically. This behaviour merely reflects the assumptions regarding G and R_n^s made in section 4(a)(i). The total evaporation rate varies considerably with vapour pressure deficit, but for a given atmospheric demand is fairly independent of crop cover (± 9 per cent). The rate dips around L = 1 when radiation capture by the plants is significant, but their bulk stomatal resistance is still quite large.

Figure 2(b) illustrates the fraction of the available energy partitioned by the vegetation, $(A - A_s)/A$, and the fractional contribution made to total evaporation by the plants, $\lambda E_c/\lambda E$,

for different atmospheric deficits. The fraction of the total evaporation generated by the crop is fairly insensitive to deficit and noticeably less than the fraction of radiation intercepted.

(ii) Substrate Resistance Dependence

Figure 3 illustrates the effect of changes in the surface resistance of a soil substrate for crops of different density. Calculations are presented for an atmospheric vapour pressure defict of 20 mb; the effect at different deficits is qualitatively similar, although the actual value of the evaporation rate changes.

The total evaporation rate of sparse crops is significantly altered by the condition (i.e. surface resistance) of the soil substrate (Figure 3a). The contribution to total evaporation made by plants is also sensitive to r_s^s, and can easily exceed the fraction of energy intercepted by the canopy when leaf area index is low ($L < 2$) and soil surface resistance high. In this situation some of the energy incident on the soil is transferred as sensible heat to the canopy and utilized there for transpiration.

(c) Model sensitivity

In this section the sensitivity of the calculations made using the sparse crop combination equation (Equation (11)) to the assumptions made in section 4(a) is explored when the model is used with surface resistances appropriate to sparse crops growing in soil.

(i) The Parameterization of Aerodynamic Resistance

Calculations of evaporation rate and the fraction of evaporation arising in the crop are presented in Tables 1 and 2 respectively. The values presented are for a vapour pressure deficit of 20 mb, a stomatal resistance of 400 s m^{-1} and a soil surface resistance of 500 m s^{-1} with the assumptions made in 4(a), except that extreme changes are made in the parameterization of aerodynamic resistance.

Table 1(a) and 2(a) illustrates the effect of halving and doubling the assumed value of mean boundary layer resistance. Clearly the model, and the physical process it describes, is rather insensitive to the value of r_b: changing the value by a factor two changes λE and $(\lambda E_c/\lambda E)$ by 2 per cent or less.

The effect of halving and doubling the constant n, which describes the exponential decay in eddy diffusivity through a fully developed crop, Equation (25), is illustrated in Table 1(b) and 2(b). The magnitude of the response is in the order of 5 per cent, the proportionately largest effect in sparse canopies.

Table 1(c) and 2(c) test the sensitivity of the model to extreme changes in the parameterization of r_a^a and r_a^s as a function of the leaf area index, L, given in Equation (30) and (31). Calculations are made with these aerodynamic resistances held at their complete cover and bare substrate limits. Again the magnitude of the response is typically in the order of 5 per cent. The effect on total evaporation rate of using the complete cover resistance in bare substrate conditions is greater than this, 21.5 per cent, but corresponds to miscalculating the aerodynamic resistance by a factor of two in conditions of high vapour pressure deficit.

Net Radiation Absorption

Table 3 presents calculations of (a) evaporation rate and (b) the fraction of evaporation originating from the crop for D = 20 mb, r_{ST} = 400 s m^{-1} and r_s^s = 500 s m^{-1}, with other parameters as in section 4(a) except that C is alered. Calculations are made for C = 0.7, as elsewhere in the analysis, and for C = 0.5 and C = 0.9. Such a range in radiation absorption coefficient is not atypical of that found for real crops. With these assumptions the response of total evaporation rate to changes in C is small, less than 1 per cent; that in the plant fraction of this evaporation is larger, 5-10 per cent.

Some care is necessary in interpreting these particular results. The calculations presented in Table 3 represent the behaviour of sparse crops growing in soil with a surface resistance r_s^s = 500 s m^{-1} and a stomatal resistance r_{ST} = 400 s m^{-1} (consistent with the rest of this section). However in this situation we get a minimal response of evaporation to changes in C. This parameter directly controls the fractional absorption of radiation by the plants and is therefore a driving mechanism in the initial routing of energy for partition by the surface resistances of the plants and soil. In this calculation r_s^s and r_{ST} are in the same order and this tends to supress the response of the total evaporation rate to changes in C. Changes in the fraction of evaporation originating from the plants are more affected by changes in C.

(iii) Mean Stomatal Resistance

Figure 4 illustrate how the value of r_{ST}, and hence r_s^c, controls transpiration in crops with different density. The total evaporation rate changes significantly, though not of course proportionally, when r_{ST} is halved and doubled, and the proportion of evaporation originating at the plants also changes, especially in the sparser crops.

CONCLUDING REMARKS

The assumption (made in section 4(a) (v)) that the effective source height of the crop component of energy flux remains fixed at the value of (z_o+d) relevant to complete cover, irrespective of crop density, should not be misinterpreted as implying that z_o and d are themselves assumed constant with changing crop density. These roughness parameters do of course change in the present model and tend to the values for bare soil (z_o' and zero) in the limit. The assumption made here is, rather, that the plant components of the energy fluxes can be considered as arising at a particular fraction of the crop height (0.76 h; equation 22), which is specified by the value of (z_o+d) relevant to a closed canopy, and remains fixed at this fraction of h as vegetation density changes.

The assumption that the crop flux source height is a constant fraction of crop height involves approximation, as indeed does the additional implicit assumption that a single source level is appropriate for both heat and vapour for all crop densities, and that this is coincident with the effective sink of momentum in a closed canopy. Moreover, we have chosen to simplify the present calculations and presentation by ignoring the effect of stability in calculating components of aerodynamic resistance (although it would be fairly simple to include an iterative correction to allow for these using empirical stability functions above the crop or soil). These several approximations in the present model serve to exacerbate and illustrate a more basic lack of understanding of how aerodynamic transfer resistances evolve as crops grow. In light of this, the limited sensitivity of the present theoretical description to extreme changes in the parameterization of aerodynamic resistance (see section 4(c) (i)) is an important feature of the present paper.

The current example calculations of the variation in energy partition with crop density at fixed crop height (presented in sections 4(b) and 4(c)) should not be regarded as describing the

variation in energy partition as a crop grows; even though this may eventually be the most likely use of the model presented here. The aim of the present paper is to suggest a mathematic scheme which can be used to calculate evaporation when measurements or submodels of the crop height, leaf area, stomatal and substrate resistance, net radiation interception and soil heat flux are available. The difficulties involved in providing such crop specific submodels are not underestimated. Some are clearly interrelated, for example, leaf area influences soil heat flux and net radiation (through albedo); and, apart from the direct effect on bulk stomatal resistance, leaf area could also have indirect effects on biological control by changing the radiation loading on individual leaves. None-the-less the present paper represents an attempt to provide a framework through which such submodels may be combined to calculate energy partition. This may ultimately yield a more accurate method for calculating evaporation from sparse crops and, hence, a better understanding of how stomatal control takes over from soil conditions as crop cover increases.

REFERENCES

Arkin, G.F. and Perrier, E.R., 1974. Vorticular air flow within an open row crop canopy. Agric. Meteorol., 13, 359-374.

Black, T.A., Tanner, C.B. and Gardner, W.R., 1970. Evaporation from a snap bean crop. Agron. J., 62, 66-69.

Denmead, O.T., 1976. Temperate Cereals. In Vegetation and the Atmosphere. Vol 2. (Ed. J.L. Monteith). Academic Press, London.

Fuchs, M. and Tanner, C.B., 1967. Evaporation from drying soil. J. Appl. Meteorol., 6, 852-857.

Monteith, J.L., 1965. Evaporation and the Environment, Symp. Soc. Expl. Biol., 19, 205-234.

Monteith, J.L., 1973. Principles of Environmental Physics. Edward Arnold, London.

Monteith, J.L., 1981. Evaporation and surface temperature. Quart. J R. Met. Soc., 107, 1-27.

Ross, J. 1981. The radiation regime and architecture of plant stands. Tasks for vegetation sciences 3: (ed. Helmut Leith). Dr W. Junk Publishers. The Hague. pp 391.

Shuttleworth, W.J., 1976. A one-dimensional theoretical description of the vegetation-atmosphere interaction. Boundary-Layer Meteorol., 10, 273-302.

Shuttleworth, W.J., 1978. A simplified one-dimensional theoretical description of the vegetation-atmosphere interaction. Boundary-Layer Meteorol., 14, 3-27.

Shuttleworth, W.J., 1979. Below canopy fluxes in a simplified one dimensional theoretical description of the vegetation-atmosphere interaction. Boundary-Layer Meteorol., 17, 315-331.

Sinclair, T.R., Allen, L.H. and Stewart, D.W., 1971. A simulation model for crop environmental interactions and its use in improving crop productivity. Proc. 1971 Summer Comput. Simul. Counc., La Jolla, California.

Szeicz, G., Van Bavel, C.H.M. and Takami, S., 1973. Stomatal factor in the water use and dry matter production by sorghum. Agric. Meteorol., 12, 361-389.

Tan, C.S. and Black, T.A., 1976. Factors affecting the canopy resistance of a Douglas fir forest. Boundary-Layer Meteorol., 10, 475-488.

Thom, A.S., 1972. Momentum, mass and heat exchange of vegetation. Quart. J. R. Meteorol. Soc., 98, 124-134.

Uchijima, Z., 1976. Maize and Rice. In Vegetation and the Atmosphere, Vol.2 (Ed. J.L. Monteith). Academic Press, London.

Van Bavel, C.H.M. and Hillel, D.I., 1976. Calculating potential and actual evaporation from a bare soil surface by simulation of concurrent flow of water and heat. Agric. Meteorol., 17,453-476.

Wallace, J.S., Batchelor, C.H. and Hodnett, M.G., 1981. Crop evaporation and surface conductance calculated using soil moisture data from central India. Agric. Meteorol., 25, 83-96.

ACKNOWLEDGEMENTS

We are pleased to acknowledge the financial support of the U.K. Overseas Development Administration during the writing of this paper.

Model Change	Leaf Area Index						
	0	0.5	1.0	1.5	2.0	3.0	4.0
(a) r_b = 12.5 s m^{-1}	135	210	263	302	331	370	394
No change	135	209	261	300	329	368	392
r_b = 50 s m^{-1}	135	207	259	297	325	364	387
	(0)	(1.4)	(1.5)	(1.7)	(1.8)	(1.6)	(1.8)
(b) n = 1.25	135	207	259	299	329	370	396
No change	135	209	261	300	329	368	392
n = 5.0	135	223	270	303	328	362	382
	(0)	(7.7)	(4.2)	(1.3)	(0.3)	(2.2)	(3.6)
(c) COVER	164	221	265	299	326	365	392
No change	135	209	261	300	329	368	392
BARE	135	206	259	300	332	378	409
	(21.5)	(7.2)	(2.3)	(0.3)	(1.8)	(3.5)	(4.3)

Table 1. Calculated total crop evaporation rates (W m^{-2}) for D = 20 mb r_s^s = 500 s m^{-1} and r_{ST} = 400 s m^{-1} with changes in the parameterization of aerodynamic resistance (see text). Numbers in brackets are the full range difference in the two perturbed rates expressed as a percentage of the rate given by the unmodified model.

Model Change	Leaf Area Index						
	0	0.5	1.0	1.5	2.0	3.0	4.0
(a) r_b = 12.5 s m^{-1}	0	48.2	66.7	76.6	82.8	89.7	93.3
No change	0	47.9	66.5	76.4	82.5	89.5	93.2
r_b = 50 s m^{-1}	0	47.4	66.0	75.9	82.1	89.2	92.9
	(0)	(1.7)	(1.0)	(0.9)	(0.8)	(0.6)	(0.4)
(b) n = 1.25		48.7	67.3	76.9	82.6	88.8	92.0
No change	)	47.9	66.5	76.4	82.5	89.5	93.2
n = 5.0	0	43.3	62.5	74.4	82.3	91.2	95.4
	(0)	(11.3)	(7.2)	(3.3)	(0.4)	(2.7)	(3.6)
(c) COVER		44.4	64.6	75.7	82.4	89.7	93.2
No change		47.9	66.5	76.4	82.5	89.5	93.2
BARE	0	48.7	67.3	76.9	82.6	88.8	91.9
	(0)	(9.0)	(4.1)	(1.6)	(0.2)	(1.0)	(1.4)

Table 2. Fraction of total evaporation originating from the plants (per cent) calculated for D = 20 mb, r_s^s = 500 s m^{-1} and r_{ST} = 400 s m^{-1} with changes in the parameterization of aerodynamic resistance (see text). Numbers in brackets are the full range difference in the two perturbed values expressed as a percentage of the fraction given by the unmodified model.

Calculated Parameter	Leaf Area Index						
	0	0.5	1.0	1.5	2.0	3.0	4.0
(a) Evaporation							
= 0.5	135	208	260	298	327	366	390
= 0.7	135	209	261	300	329	368	392
= 0.9	135	209	262	301	330	369	392
	(0)	(0.5)	(0.8)	(1.0)	(0.9)	(0.8)	(0.5)
(b) Plant Fraction							
= 0.5	0.0	45.5	63.2	72.9	79.1	86.7	91.0
= 0.7	0.0	47.9	66.5	76.4	82.5	89.5	93.2
= 0.9	0.0	50.1	69.1	78.9	84.8	91.1	94.1
	(0)	(9.6)	(8.9)	(7.9)	(6.9)	(4.9)	(3.3)

Table 3. (a) Total crop evaporation rate (W m^{-2}) and (b) fraction of total evaporation originating from the plants (percent), calculated for D = 20mb, r_s^s = 500 s m^{-1} and r_{ST} = 400 s m^{-1}, for changes in the net radiation extinction coefficient C = 0.5, 0.7, 0.9. Numbers in brackets are the full range difference in the two perturbed values expressed as a percentage of those given with C = 0.7.

APPENDIX Derivation of the sparse crop combination equation

Introducing Equation (8) into Equations (9) and (10) gives

$$\lambda E_s = \frac{\Delta A_s + \frac{\rho c_p}{r_a^s}\left(D + [\Delta A - (\Delta + \gamma)\lambda E]\frac{r_a^a}{\rho c_p}\right)}{\Delta + \gamma\,(1 + r_s^s/r_a^s)} \qquad (A1)$$

$$\lambda E_c = \frac{\Delta(A - A_s) + \frac{\rho c_p}{r_a^c}\left(D + [\Delta A - (\Delta + \gamma)\lambda E]\frac{r_a^a}{\rho c_p}\right)}{\Delta + \gamma\,(1 + r_s^c/r_a^c)} \qquad (A2)$$

The total evaporation flux, λE, is given by $\lambda E = \lambda E_s + \lambda E_c$.

Adding Equations (A1) and (A2) gives

$$\lambda E = \frac{\Delta A_s\, r_a^s + \rho c_p\left(D + [\Delta A - (\Delta + \gamma)\lambda E]\frac{r_a^a}{\rho c_p}\right)}{(\Delta + \gamma)\, r_a^s + \gamma r_s^s} \qquad (A3)$$

$$+ \frac{\Delta(A - A_s)\, r_a^c + \rho c_p\left(D + [\Delta A - (\Delta + \gamma)\lambda E]\frac{r_a^a}{\rho c_p}\right)}{(\Delta + \gamma)\, r_a^c + \gamma\, r_s^c}$$

Multiplying (A3) by the product of the two denominators and collecting terms in λE gives

$$\lambda E \left\{ ([\Delta + \gamma] r_a^s \quad \gamma r_s^s)([\Delta + \gamma] r_a^c \quad \gamma r_s^c) \quad [\Delta + \gamma] r_a^a \cdot \right.$$

$$\left. ([\Delta + \gamma] r_a^c \quad \gamma r_s^c) \quad [\Delta + \gamma] r_a^a ([\Delta + \gamma] r_a^s + \gamma r_s^s) \right\} \qquad \text{(A4)}$$

$$(\Delta A_s r_a^s + \rho c_p D + \Delta A r_a^a)([\Delta + \gamma] r_a^c + \gamma r_s^c)$$

$$(\Delta [A - A_s] r_a + \rho c_p D + \Delta A r_a^a)([\Delta + \gamma] r_a^s + \gamma r_s^s)$$

If we define

$$R_s = [\Delta + \gamma] r_a^s + \gamma r_s^s \qquad \text{(A5)}$$

$$R_c = [\Delta + \gamma] r_a^c + \gamma r_s^c \qquad \text{(A6)}$$

$$R_a = [\Delta + \gamma] r_a^a \qquad \text{(A7)}$$

and substitute these into (A4) we get

$$\lambda E (R_s R_c + R_c R_a + R_s R_a) \qquad \text{(A8)}$$

$$= (\Delta A [r_a^a + r_a^s] + \rho c_p D \quad r_a^s [A - A_s]) R_c$$

$$(\Delta A [r_a^a + r_a^c] + \rho_{cp} D \quad r_a^c A_s) R_s$$

Now

$$R_s + R_a = [\Delta + \gamma] [r_a^a + r_a^s] + \gamma r_s^s \qquad \text{(A9)}$$

and $$R_c + R_a = [\Delta + \gamma] [r_a^a + r_a^c] + \gamma r_s^c \qquad \text{(A10)}$$

So we can write Equation (A8) as

$$\lambda E (R_s R_c + R_c R_a + R_s R_a)$$

$$PM_s R_c (R_s + R_a) \quad PM_c R_s (R_c + R_a) \qquad \text{(A11)}$$

where PM_s $$\frac{\Delta A + [\rho c_p D - r_a^s (A - A_s)]/[r_a^a + r_a^s]}{\Delta + \gamma (1 + r_s^s/[r_a^a + r_a^s])} \quad (A12)$$

and $$PM_c = \frac{\Delta A + [\rho c_p D - r_a^c A_s]/[r_a^a + r_a^c]}{\Delta + \gamma (1 + r_s^c/[r_a^a + r_a^c])} \quad (A13)$$

So Equation (A11) becomes

$$\lambda E = C_c PM_c + C_s PM_s \quad (A14)$$

Providing

$$C_s = \frac{R_c (R_s + R_a)}{R_s R_c + R_c R_a + R_s R_a} \left[1 + \frac{R_s R_a}{R_c (R_s + R_a)}\right]^{-1} \quad (A15)$$

$$C_s = \frac{R_s (R_c + R_a)}{R_s R_c + R_c R_a + R_s R_a} \left[1 + \frac{R_c R_a}{R_s (R_c + R_a)}\right]^{-1} \quad (A16)$$

Equation (A14) is the desired sparse crop combination equation. The contributions λE_c and λE_s can now be computed from Equations (9) and (10) with D_o given by Equation (8).

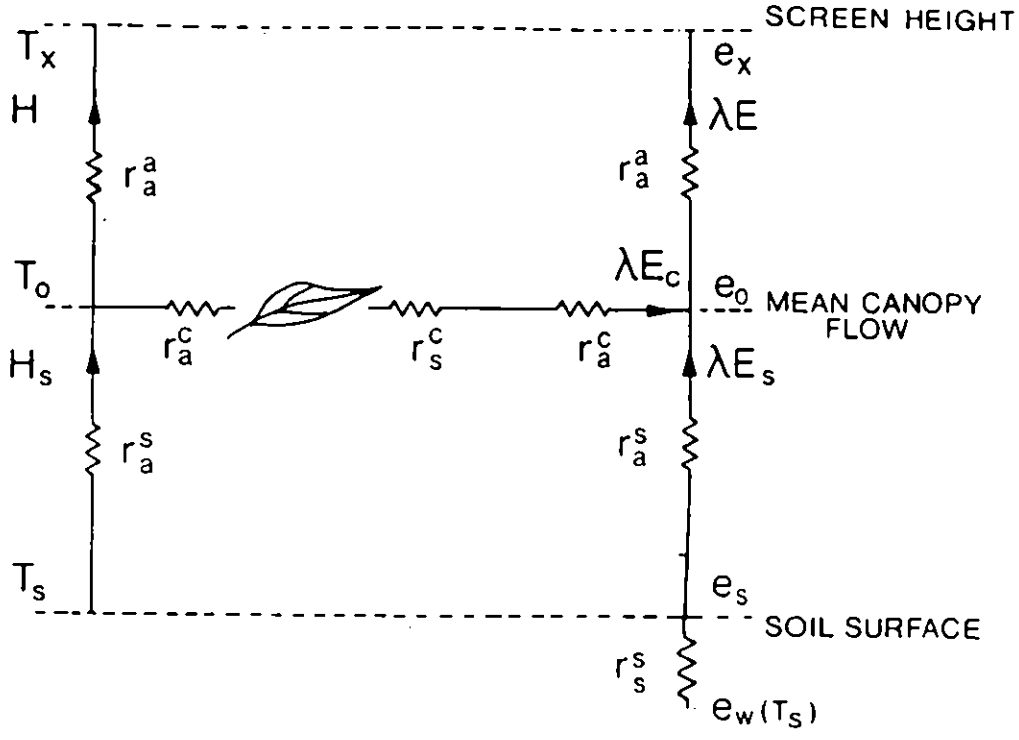

Figure 1 Schematic diagram of a one-dimensional description of energy partition for sparse crops. The nomenclature used is given in Section 3(a).

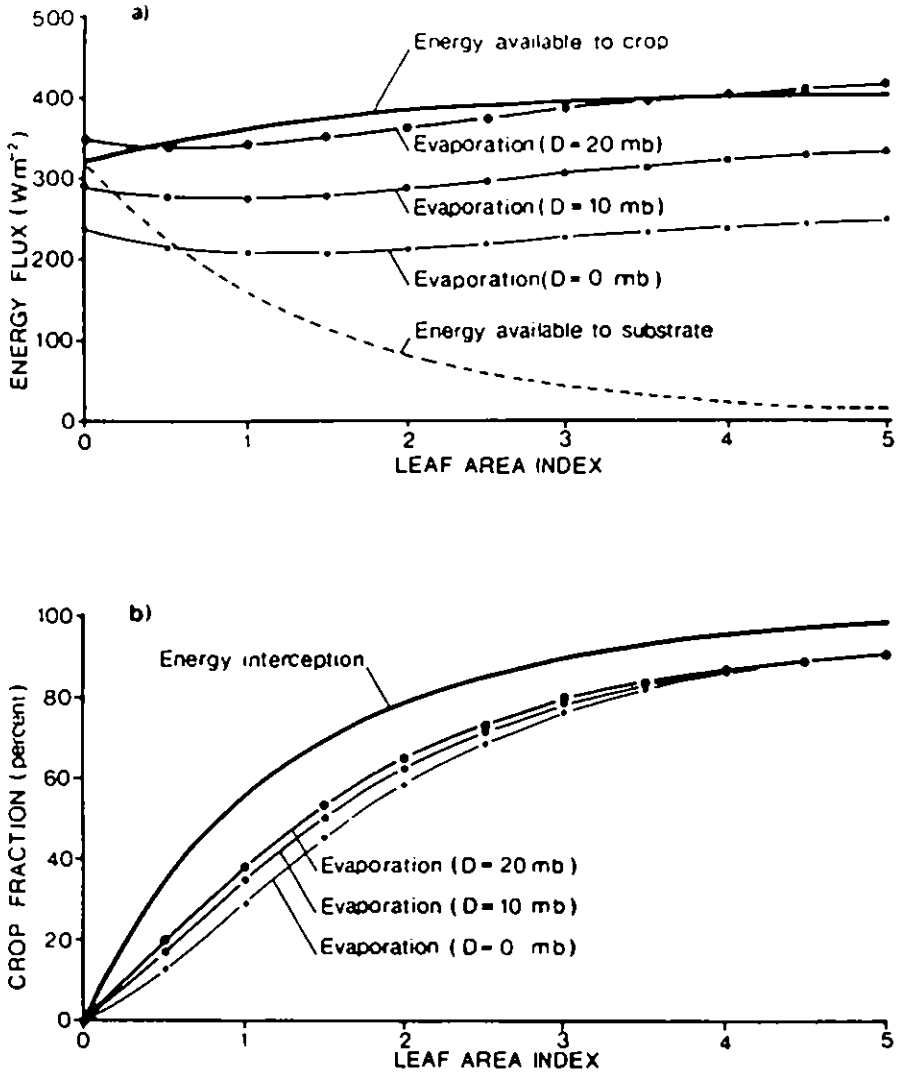

Figure 2 (a) Energy available to the crop and substrates expressed as a function of L, compared with computed total crop evaporation rates for the model and conditions described in the text, with vapour pressure deficits of 0,10 and 20 mb and a free water substrate.

(b) Fraction of total evaporation originating from the plants expressed as a function of L, computed for the model and conditions described in the text, with vapour pressure deficits of 0,10 and 20 mb and a free water substrate. The fraction of energy intercepted by the vegetation is also shown for comparison.
(R_n, T_x, u, C, n, r_s^s, r_{ST}, r_b, x, h and z_o' held constant)

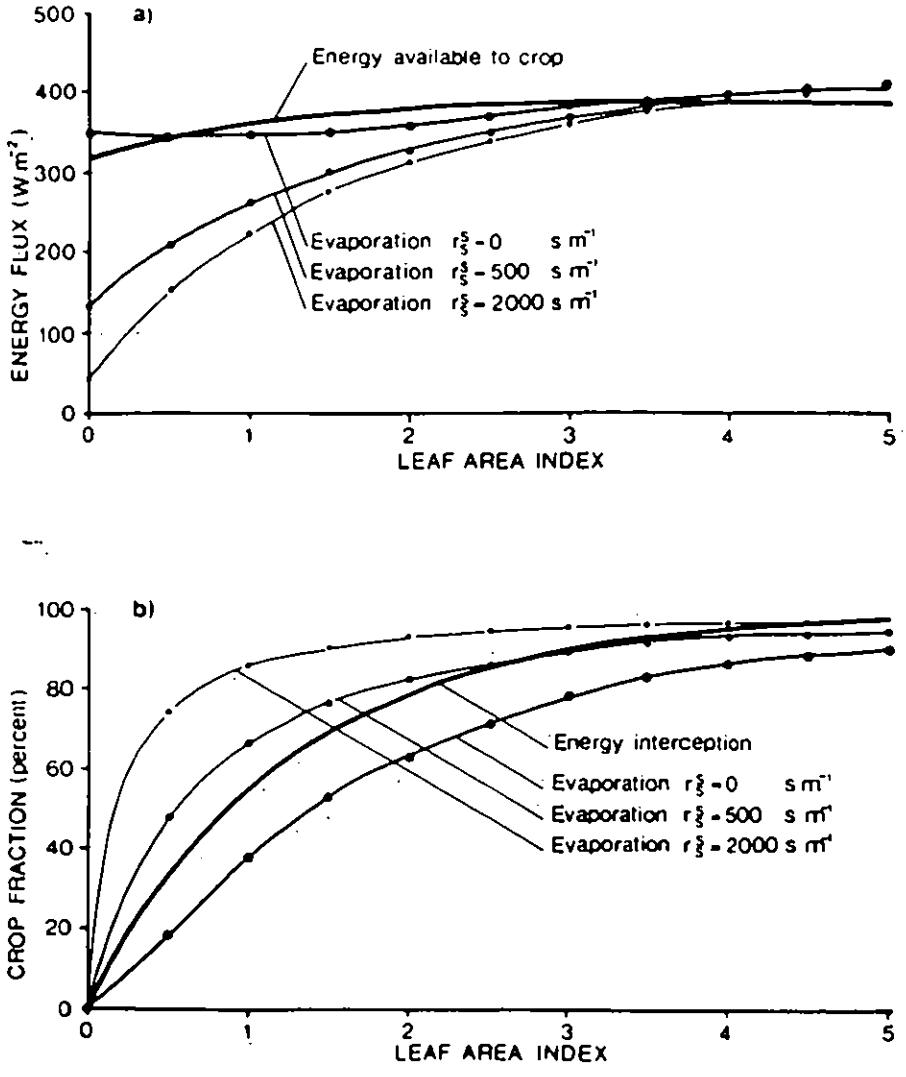

Figure 3 (a) Computed total crop evaporation rates expressed as a function of L for the model and conditions described in the text, with substrate surface resistances of 0,500 and 2000 s m^{-1}, compared with the energy available to the crop.

(b) Fraction of total evaporation originating from the plants expressed as a function of L computed for the model and conditions described in the text with substrate surface resistances of 0,500 and 2000 s m^{-1}. (R_n, T_x, u, D, C, n, r_{ST}, r_b, x, h and z_o' held constant)

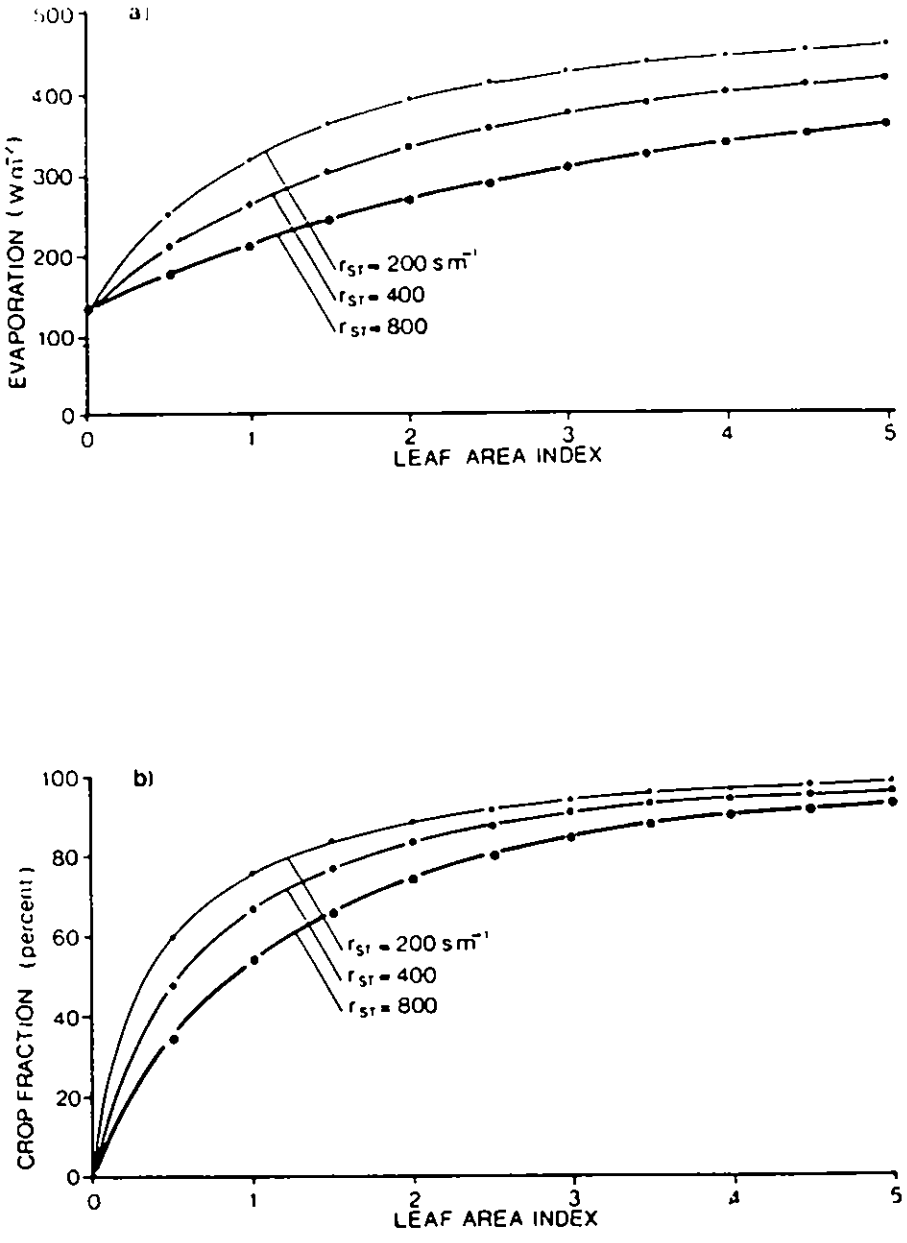

Figure 4 (a) Computed total crop evaporation rates expressed as a function of L for the model and conditions described in the text with mean stomatal resistances of 200, 400 and 800 s m^{-1}.

(b) Fraction of total evaporation originating from the plants expressed as a function of L computed for the model and conditions described in the text with mean stomatal resistances of 200, 400 and 800 s m^{-1}.
(R_n, T_x, u, D, C, n, r_s^s, r_b, x, R_n and z_o' held constant).

Institute of Hydrology Wallingford Oxfordshire OX10 8BB UK
Telephone Wallingford (STD 0491) 38800 Telegrams Hycycle Wallingford Telex 849365 Hydrol G

The Institute of Hydrology is a component establishment of the Natural Environment Research Council